Molecular Mechanism of Oxygen Photoevolution Reaction on Metal Oxide and Oxynitride Photocatalysts, Revealed by *In situ* FTIR and PL Spectroscopy

Ryuhei Nakamura

Division of Chemistry

Department of Chemical Science and Engineering

Graduate School of Engineering Science

Osaka University

2005

Contents

General Introduction

In 1972, Fujishima and Honda discovered the photoelectrochemical splitting of water into hydrogen and oxygen by a cell with a titanium dioxide (TiO_2) e1ectrode and a Pt counterelectrode.[1] This discovery marked the beginning of a new era in heterogeneous photocatalysis. Since then, photocatalytic reactions at the surfaces of TiO_2 or related metal oxides have become one of the most important research subjects not only from the point of view of basic researches but also of practical application to solar energy conversion (water splitting)[2-4], environmental cleaning (photodecomposition of waste and harmful materials)[5-8], organic photosynthesis[9-11], and photocontrol of the surface hydrophilicity[12], and thus the reactions have been attracting much attention in various fields of chemistry, electrochemistry, catalysis, surface science, surface and colloidal chemistry, organic photochemistry, photobiology, and semiconductor device physics. A serious shortcoming of large band-gaps for TiO_2 or related metal oxides is now about to be overcome by recent findings that doping with N[13,14], S[15,16], C[17-19] or other elements leads to extension of the photoactive region to the visible light and thus this research field becomes more and more attractive.

In heterogeneous photocatalytic systems, photoinduced oxidation and reduction reactions take place at the surface of semiconductor powder or films through the formation of electron-hole pairs inside the powder or films. A large number of studies have been made on the reaction products, yields, and mechanisms, in particular those for TiO_2 photocatalyst, to increase the reaction efficiencies and selectivity. However, many fundamental questions on the understanding of the photocatalytic activity have still remained unclear, most probably because of a shortage of *in situ* direct detection of active reaction intermediates by spectroscopic methods under actual reaction conditions. In addition, the difficulty of preparation of atomically well-defined and stable TiO_2 surfaces has also hindered rapid progress in the studies on the photocatalytic activity and selectivity. The elucidation of molecular reaction mechanisms by use

of *in situ* spectroscopic methods and atomically well-defined surfaces should enable us to make systematic studies on photocatalytic reactions, which will lead to rapid progress both in basic researches and application fields.

Based on these considerations, the author has made studies mainly in two directions: First, he has developed in situ FTIR spectroscopy to detect directly reaction intermediates formed at the surface of photocatalysts. He has applied a multiple internal reflection (MIR) absorption technique to in situ detection of surface intermediate species formed at a particulate TiO_2 film in contact with aqueous solutions under UV illumination. The use of a diamond or ZnSe single crystal prism as a multiple internal reflection element has enabled him to measure absorption spectra in a low frequency region from 1500 to 600 cm^{-1}, where surface intermediates of water photooxidation (oxygen photoevolution) reaction are expected to show vibrational bands. In fact, he succeeded, for the first time, in detecting directly primary intermediates of photocatalytic water oxidation and dioxygen reduction reactions at a particulate TiO_2 film in contact with aqueous solutions. The success has enabled us to clarify the detailed molecular-level mechanisms of photocatalytic reactions on TiO_2 surfaces.

Second, the author has prepared atomically well-defined n-TiO_2 (rutile) surfaces by adopting a new method of immersing commercially available single crystal wafers in 20% HF, followed by annealing at 600°C in air. The obtained surfaces were stable in aqueous solutions of pH 1 to 13, showing no change in the surface morphology on an atomic level, in contrast to atomically flat surfaces prepared by a conventional method of ion sputtering and thermal annealing under ultra high vacuum. The success in preparation of the atomically smooth and stable n-TiO_2 surfaces enabled us to reveal clear crystal-face dependences of the surface band edges (or the flat-band potential) and photocatalytic reaction mechanisms in aqueous solutions.

In addition to the above studies, the author has also studied the mechanisms for photoxidation reactions on visible-light responsive photocatalysts, in relation to those on TiO_2 photocatalysts under UV illumination.

Oxygen Photoevolution at the Surface of TiO_2 Photocatalysts

Molecular mechanisms of oxygen photoevolution (photoxidation reaction of water) at the surface of TiO_2 and related metal oxides have been studied intensively from the view point of solar energy conversion, i.e. photocatalytic water splitting. This reaction has also been studied intensively in relation with photocatalytic environmental cleaning, since the primary intermediates of oxygen photoevolution reaction have been assumed to play a crucial role in mineralization of waste materials and harmful compounds. Many efforts have, therefore, been made to clarify the reaction mechanism of water photoxidation on TiO_2 electrodes or nanoparticles, by using various spectroscopic techniques such as ESR[20-25], laser-flash photolysis[26], time-resolved absorption[27-29], FTIR absorption[30-32], and ^{1}H-NMR measurements[33,34]. To date, it has been generally assumed that the oxygen photoevolution is initiated by the formation of hydroxyl •OH radicals through the oxidation of surface Ti–OH groups by photogenerated holes.

$$Ti–OH_s + h^+ \rightarrow [Ti\ •OH]_s^+ \quad (1)$$

The •OH radicals have been accepted to be the key intermediate species in photocatalytic degradation of organic compounds. The •OH radical-driven mechanism, in fact, appears often in the literature of this research field to explain various photocatalytic reactions at the surface of TiO_2.

On the other hand, it was found in the laboratory to which the author has belonged that a photoluminescence (PL) band peaked at 840 nm was emitted from an n-TiO_2

electrode.[35-42] The later detailed studies using in-situ photocurrent and PL measurements have shown that the PL band is emitted from the (100) face of n-TiO_2 (rutile) and is assigned to an electronic transition from the conduction band to a vacant level of a "surface-trapped hole", which acts as a precursor of the oxygen photoevolution reaction.[42] The studies have also shown that the oxygen photoevolution is not initiated by reaction (1), but a nucleophilic attack of an H_2O molecule (Lewis base) to a surface-trapped hole at a surface lattice O site (Lewis acid) accompanied by bond breaking.

$$[Ti–O–Ti]_s + h^+ + H_2O \rightarrow [Ti–O\bullet \quad HO–Ti]_s + H^+ \qquad (2)$$

The key of the new mechanism is that the oxygen evolution proceeds via a Lewis acid-base-type oxidation mechanism (reaction 2), not by an electron-transfer-type oxidation mechanism (reaction 1), and therefore their energetics and kinetics are quite different from each other. The probability of occurrence for the oxygen evolution has no direct relation with the redox potential such as E^{eq}_{redox} for H_2O/•OH, in contrast to the case of the electron-transfer-type oxidation mechanism, but has a strong relation with the basicity of H_2O molecules and the Gibbs energy of formation for intermediate radicals such as $[Ti–O\bullet \quad HO–Ti]_s$. The new mechanism will be important to understand the photocatalytic activity of TiO_2 and to find new-type active materials for oxygen (photo)evolution reactions.

In the present work, the author has put an emphasis on directly detecting primary intermediates of oxygen photoevolution on TiO_2(rutile) by spectroscopic methods. The author has applied multiple internal reflection (MIR) IR absorption spectroscopy to the study of oxygen photoevolution on a particulate TiO_2(rutile) film and succeeded in detecting directly surface peroxo species, Ti-O-O-Ti and Ti-O-OH, as the primary intermediates. Isotopic labeling experiments by using $H_2{}^{18}O$ have led to the definite support to the new mechanism for oxygen evolution. The new mechanism was also confirmed by in situ PL measurements on atomically

well-defined (100) and (110) n-TiO_2 surfaces.

Oxygen Photoevolution on Visible-light-Active Photocatalysts

TiO_2 and related metal-oxide photocatalysts have strong oxidation power under UV illumination. They have, however, band gap energies too large to efficiently absorb solar light. Recently it was reported that doping of TiO_2 with other elements such as N[13,14], S[15,16], C[17-19], etc. led to an extension of the photoactivity to the visible-light region. It was also reported that another new type of photocatalysts such as $BiVO_4$[43], TaON[44], and Ta_3N_5[45] could oxidize H_2O into O_2 under visible-light irradiation at a high quantum efficiency. This research field is, therefore, taking a new turn. However, important problems of the stability and efficiency have arisen simultaneously. It has thus become more and more important to clarify the mechanisms of surface photoreactions on such visible-light active photocatalysts, compared to those on TiO_2.

In the present work, the author has investigated the mechanism of the oxygen photoevolution on N-doped TiO_2 and TaON photocatalysts. The product analysis, photocurrent measurements, and in situ FTIR absorption measurements for these materials have revealed that the oxygen photoevolution under visible-light illumination cannot proceed via the conventional mechanism of an electron-transfer-type oxidation, reaction (1), but the new mechanism proposed for TiO_2(rutile) by the laboratory to which the author has belonged, reaction (2).

Survey of Thesis

In Chapter 1, the multiple internal reflection infrared (MIRIR) absorption spectroscopy is applied to *in situ* investigations of surface intermediates of photocatalytic reduction reactions on nanocrystalline TiO_2 films in contact with aqueous solutions. UV

irradiation in the presence of dissolved O_2 caused the appearance of new bands peaked at 943, 838, and 1250-1120 cm^{-1} together with intensity changes in other bands. Investigations of influences of the solution pH, the presence or absence of hole and electron scavengers, and isotopic $H_2O \rightarrow D_2O$ exchange on the spectral changes have revealed that the primary step of photocatalytic O_2 reduction is the formation of a surface peroxo species, $Ti(O_2)$, giving the 943-cm^{-1} band, probably with a surface superoxo species, TiOO• as a precursor, in neutral and acidic solutions. The surface peroxo species is then transformed to surface hydroperoxo, TiOOH, giving the 838 and 1250-1120 cm^{-1} bands, by protonation in the dark. Based on the assignment, a possible reaction scheme for the photocatalytic O_2 reduction is proposed, which is in harmony with other spectral changes induced by the UV irradiation.

In Chapter 2, primary intermediates of oxygen photoevolution (water photooxidation) reaction at the TiO_2 (rutile)/aqueous solution interface are investigated by in situ multiple internal reflection infrared (MIRIR) absorption and photoluminescence (PL) measurements. UV irradiation of TiO_2 in the presence of 10 mM Fe^{3+} in the solution caused the appearance of a new peak at 838 cm^{-1} and a shoulder at 812 cm^{-1}. Detailed investigations of the effects of solution pH, the presence of methanol as a hole scavenger, and isotope exchange in water ($H_2{}^{16}O \rightarrow H_2{}^{18}O$) on the spectra have shown that the 838- and 812-cm^{-1} bands can be assigned to the O-O stretching mode of surface TiOOH and TiOOTi, respectively, produced as primary intermediates of the oxygen photoevolution reaction. The results have given strong support to our previously proposed mechanism that the oxygen photoevolution is initiated by a nucleophilic attack of a H_2O molecule on a photogenerated hole at a surface lattice O site, not by oxidation of surface OH group by the hole. The conclusion is supported by PL measurements. A plausible reaction scheme is proposed for the oxygen photoevolution on TiO_2 (rutile) in aqueous solutions of pH less than about 12.

In Chapter 3, atomically smooth (100) and (110) n-TiO_2 (rutile) surfaces are prepared by a method of immersion of commercially available single crystal wafers in 20% HF, followed by annealing at 600°C in air. The obtained surfaces were stable in aqueous solutions of pH 1 to 13, showing no change in the surface morphology on an atomic level, contrary to atomically flat surfaces prepared by ion sputtering and annealing under UHV. The success in preparation of the atomically smooth and stable n-TiO_2 surfaces enabled us to reveal clear crystal-face dependences of the surface band edges and hole reactivity in aqueous solutions.

In Chapter 4, the mechanisms of anodic photocurrents for a particulate N-doped TiO_2 film electrode are investigated. The N doping caused an extension of anodic photocurrents (water oxidation currents) to the visible-light region up to ca. 550 nm. Investigations of the effect of addition of reductants such as methanol, SCN^-, Br^-, I^-, and hydroquinone to the electrolyte have for the first time given clear experimental evidence to a mechanism that visible-light responses for N-doped TiO_2 arise from an N-induced mid-gap level, formed ca. 0.75 eV above the top of the (O2p) valence band. The investigations, in combination with the above mechanism, have also shown that photocatalytic oxidation of organic compounds on N-doped TiO_2 under visible illumination mainly proceed via reactions with surface intermediates of water oxidation or oxygen reduction, not by direct reactions with holes trapped at the N-induced mid-gap level.

In Chapter 5, the mechanisms of oxygen photoevolution at the surface of TaON are investigated by various methods including in photoelectrochemical and *in situ* MIR-IR absorption measurements. It was found that TaON can oxidize H_2O into O_2 under visible light irradiation ($\lambda \leq 520$ nm), but cannot oxidize reductants such as SCN^-, Br^-, and methanol. This behavior is essentially the same as that observed for N-doped TiO_2 under visible-light illumination. Since the redox potential of water oxidation (E^{eq}_{redox} for H_2O/•OH) is below (more

positive than) that of $SCN^-/SCN\bullet$ and $Br^-/Br\bullet$, it was concluded that the water oxidation on TaON cannot proceed by the conventional mechanism of an electron-transfer type oxidation, but by the new mechanism of a Lewis acid-base-type oxidation mechanism. This conclusion is supported by MIR-IR measurements for a particulate TaON film under oxygen photoevolution reactions.

References

(1) Fujishima, A. ; Honda, K., *Nature* **1972**, *238*, 37.

(2) Sato, S, and White, M. *J., Chem. Phys. Lett.,* **1980**, *72,* 83.

(3) Kato, H.; Asakura, K.; and Kudo, A. *J. Am. Chem. Soc*. **2003**, *125*, 3082.

(4) Kudo, A. Catalysis Surveys from Asia. 2003, *7*, 31.

(5) Ollis, D. S.; Al-Ekabi, H.; Eds., *Photocatalytic Purification and Treatment of Water and Air*; Elsevier, Amsterdam, **1993**.

(6) Fujishima, A.; Rao, T. N.; Tryk, D. A. *J. Photochem. Photobiol. C: Photochem. Rev.* **2000**, *1*, 1.

(7) Hoffmann, M. R.; Martin, S. T.; Choi, W.; Bahnemann, D. W. *Chem. Rev.* **1995**, *95*, 69.

(8) Linsebigler, A.; Lu, G.; Yates, J. T., Jr. *Chem. Rev.* **1995**, *95*, 735.

(9) Nishimoto, S.; Ohtani, B.; Yoshikawa, T.; Kagiya, T. *J. Am. Chem. Soc.;* **1983**; *105*, 7180.

(10) Ohtani, B.; Osaki, H.; Nishimoto, S.; Kagiya, T. *J. Am. Chem. Soc.;* **1983**; *105*, 7180.

(11) Ohno, T.; Mitsui, T.; Matsumura, M. *J. Photochem. Photobiol. A: Chemistry* **2003**, *169,* 3.

(12) Wang, R.; Hashimoto, K.; Chikuni, M.; Kojima, E.; Kitamura, A.; Shimohigashi, M.; Watanabe, T. *Nature* **1997**, *388*, 431.

(13) Sato, S., *Chem. Phys. Lett.* **1986**, *123*, 126.

(14) Asahi, R.; Morikawa, T.; Ohwaki, T.; Aoki, K.; Taga, Y. *Science* **2001**, *293*, 269.

(15) Ohno, T.; Mitsui, T.; and Matsumura, M.; *Chem. Lett.* **2003**, *32*, 364.

(16) Irie, H.; Watanabe, Y.; and Hashimoto, K.; *Chem. Lett.* **2003**, *32*, 772.

(17) Khan, S. U. M.; Al-Shahry, M.; Ingler, W. B., Jr. *Science* **2002**, *297*, 2243.

(18) Sakthivel, S.; Kisch, H. *Angew. Chem. Int. Ed*. **2003**, *42*, 4908.

(19) Irie, H.; Watanabe, Y.; and Hashimoto, K. *Chem. Lett*. **2003**, *32*, 772.

(20) Jaeger, C. D.; Bard, A. J. *J. Phys. Chem*., **1979**, *83*, 3146.

(21) Anpo, M.; Shima, T.; Kubokawa, Y. *Chem. Lett*. **1985**, 1799.

(22) Howe, R. F.; Gräetzel, M.; *J. Phys. Chem*. **1987**, *91*, 3906.

(23) Micic, O. I.; Zhang, Y.; Cromack, K. R.; Trifunac, A. D.; and Thurnauer, M. C. *J. Phys. Chem*. **1993**, *97*, 7277.

(24) Micic, O. I.; Zhang, Y.; Cromack, K. R.; Trifunac, A. D.; and Thurnauer, M. C. *J. Phys. Chem*. **1993**, *97*, 13284.

(25) Nosaka, Y.; Komori, S.; Yawata, K.; Hirakawa, T.; and Nosaka, Y. A. *Phys. Chem. Chem. Phys*., **2003**, *5*, 4731.

(26) Lawless, D.; Serpone, N.; and Meisel, D. *J. Phys. Chem.* **1990**, *94*, 331.

(27) Shkrob, I. A.; Sauer, M. C., Jr.; *J. Phys. Chem.* **2004**, *108*, 12497.

(28) Yoshihara, T.; Katoh, R.; Furube, A.; Tamaki, Y.; Murai, M.; Hara, K.; Murata, S.; Arakawa, H.; Tachiya, M. *J. Phys. Chem.* B **2004**, *108*, 3817.

(29) Tachikawa, T.; Tojo, S.; Fujitsuka, M; Majima, T. *J. Phys. Chem. B* **2004**, *108*, 5859.

(30) Szczepankiewicz, S. H.; A. Colussi, J.; Hoffmann, M. R. *J. Phys. Chem. B* **2000**, *104,* 9842.

(31) Nakamura, R.; Sato. S. *Langmuir* **2002**, *18,* 4433.

(32) Yamakata, A.; Ishibashi, T.; and Onishi. H.; *J. Mol. Cata. A.* **2003**, *199*, 85.

(33) Nosaka, A. Y.; Kojima, E.; Fujiwara, T.; Yagi, H.; Akutsu, H.; Nosaka, Y.; *J. Phys. Chem. B.* **2003**; *107*, 12042.

(34) Nosaka, A. Y.; Fujiwara, T.; Yagi, H.; Akutsu, H.; Nosaka, Y.; *J. Phys. Chem. B.* **2004**; *108*, 9121.

(35) Nakato, Y.; Tsumura, A.; Tsubomura, H. *Chem. Phys. Lett*. **1982**, *85,* 387.

(36) Nakato, Y.; Tsumura, A.; Tsubomura, H. *J. Phys. Chem.* **1983**, *87,* 2402.

(37) Nakato, Y.; Ogawa, H.; Moria, K.; Tsubomura, H. *J. Phys. Chem.* **1986**, *86,* 6210.

(38) Nakato, Y., Akanuma, H.; Shimizu, J.-I.; Magari, Y. J. *Electroanal. Chem*. **1995**, *396*, 35.

(39) Magari, Y.; Ochi, H.; Yae, S.; and Nakato, Y. *ACS Symposium Series No. 656, Solid/Liquid Electrochemical Interfaces*, The American Chemical Society, Washington, DC, **1996**, p. 297.

(40) Nakato, Y.; Akanuma, H.; Magari, Y.; Yae, S.; Shimizu, J.-I.; Mori, H. *J. Phys. Chem. B* **1997**, *101*, 4934.

(41) Tsujiko, A.; Kisumi, T.; Magari, Y.; Murakoshi, K.; and Nakato, Y. *J. Phys. Chem. B* **2000**, *104*, 4873.

(42) Kisumi, T.; Tsujiko, A.; Murakoshi, K., and Nakato, Y. J. *Electroanal. Chem*. **2003**, *545*, 99.

(43) Kudo, A.; Omori, K.; Kato, H.; *J. Am. Chem. Soc.* **1999**; *121*, 11459.

(44) Hitoki, G.; Ishikawa, A.; Takata, T.; Kondo, J. N.; Hara, M.; Domen, K. *Chem. Commun.* **2002**, 1968.

(45) Hitoki, G.; Ishikawa, A.; Takata, T.; Kondo, J. N.; Hara, M.; Domen, K. *Chem. Lett.* **2002**, 736.

Chapter 1

In Situ FTIR Studies of Primary Intermediates of Photocatalytic Reactions on Nanocrystalline TiO_2 Films in Contact with Aqueous Solutions

Introduction

Photocatalytic reactions on TiO_2 particles or thin films have been attracting much attention in view of their possible application to solar energy conversion (water splitting)[1,2] as well as photodecomposition of waste materials and harmful organic compounds[3,4]. Intensive work has been done on the reaction products, yields, and mechanisms[5-8], to increase the reaction efficiencies and selectivity, but the details of the reaction mechanisms still remain unclear, most probably because of a shortage of *in-situ* direct detection of active reaction intermediates by spectroscopic methods.

ESR spectroscopy is a useful method to investigate intermediate radicals, such as O_2^-, O^-, O_3^-, etc., formed on illuminated TiO_2 powder in air.[9-15] The method has a merit in that it can be easily applied to aqueous systems. Jaeger and Bard[16] reported long ago, using a spin-trapping method, that hydroxyl (·OH) and perhydroxyl (HO_2·) radicals were produced on illuminated TiO_2 powder in aqueous solutions. Recently, Kaise et al.[17,18] used a flow-type ESR method to detect reaction intermediates more directly and reported that methyl (CH_3·) and carboxymethyl (·CH_2COOH) radicals were formed by photocatalytic decomposition of acetic acid on TiO_2 in aqueous solutions.

Infrared (IR) spectroscopy is another powerful method to study adsorbed species on solid surfaces.[19,20] This method can give fruitful information on the molecular structure, molecular orientation, and adsorption strength of surface species. Szczepankiewicz et al. [21,22] used diffuse reflectance IR Fourier transform spectroscopy (DRIFTS) and reported a new band at 3716 cm^{-1} for UV irradiated TiO_2 powder in the gas phase in the presence of a hole scavenger. The band was assigned to OH stretching for surface Ti(3+)OH formed by electron capture at acidic Ti(4+)OH centers. They also reported another band at 3683 cm^{-1} in an oxygen atmosphere in the absence of hole scavengers and ascribed it to a surface-bound OH· radical formed by hole

capture at Ti(4+)OH centers. Recently, Sato et al.[23-25] applied surface-enhanced IR absorption spectroscopy (SEIRAS) to investigation of gas-phase photocatalytic reactions on platinized TiO_2. They succeeded in direct observation of methyl radical (CH_3·) formed by photodecomposition of acetic acid, and reported that the formation rate was significantly enhanced by Pt deposition.[23]

It is well known that the IR spectroscopy has a serious difficulty in application to aqueous systems owing to strong IR absorption of water.[19,20] The difficulty can be overcome to a large extent by using internal reflection techniques, in which evanescent IR waves penetrate only into a thin layer of an aqueous solution to the thickness of about a few micrometers from the surface of the internal reflection element (IRE), so that the IR absorption of water can be minimized.[26] A large number of work has thus been done on the internal reflection techniques of both single- and multi-reflection modes as well as their application to in situ studies of adsorbed species on thin films, as reviewed in a recent book[27]. Very recently, McQuillan et al. applied the single internal reflection (SIR) technique with a ZnSe prism as the IRE to studies of ionic surfactants[28], aromatic carboxylic acids[29], phosphates[30,31], bacteria[32], and ruthenium(II) complexes[33] adsorbed on various metal oxides such as TiO_2, ZrO_2, Al_2O_3, and Ta_2O_5 in aqueous media. Osawa applied a similar technique to electrochemical systems[35], and Baiker et al. did to heterogeneous catalytic systems[36,37]. The application of the internal reflection techniques to photocatalytic systems is, however, quite limited. Only McQuillan et al. reported[38], using the single internal reflection technique with the ZnSe IRE, that glyoxylic acid adsorbed on particulate TiO_2 in aqueous solutions was transformed to oxalate by UV irradiation.

In the present chapter, the author has applied the highly-sensitive multiple internal reflection (MIR) technique to *in-situ* studies of photocatalytic processes on the TiO_2 surface in contact with aqueous solutions. The focus was placed on the O_2 reduction by photoexcited

electrons, because active oxygen species produced by this reaction are known to be crucially important for photocatalytic oxidation of organic compounds.[39,40] We have succeeded in detecting primary intermediates of the photocatalytic O_2 reduction that have been only assumed for a long time by many workers, spectroscopically under in situ conditions.

Experimental

Two types of nanocrystalline TiO_2 particles, JRC-TIO-2 and JRC-TIO-5, were obtained from the Catalysis Society of Japan. The samples were well characterized in the Society as the reference catalysts. JRC-TIO-2 is composed of 100 % anatase with an average primary particle diameter (d_{av}) of 80 nm and a surface area of 16 m^2/g. JRC-TIO-5 is composed of 90.7 % rutile and 9.3 % anatase with d_{av} = 640 nm and a surface area of 3 m^2/g. Before experiments, the surfaces of TiO_2 particles were cleaned by heating at 500°C in an O_2 atmosphere for 5 h and UV-irradiation in O_2-saturated water for 1 h, followed by sonication for 30 min. The cleaned TiO_2 particles were, after drying, kept under vacuum (< 1×10^{-3} Torr). All chemicals, D_2O (Aldrich, 99.9 atom%), NaOH (Wako), HCl (Wako), NaOD(Aldrich, 99.9 atom%), ethanol (Wako), and $FeCl_3$ (Aldrich), were of reagent grade and used as received. All solutions were prepared using pure (Milli-Q) water with a conductivity of 18 $M\Omega^{-1}$ cm^{-1}.

The spectral cell for multiple internal reflection infrared (MIRIR) experiments is shown schematically in Figure 1. A trapezoidal-shaped ZnSe internal reflection element (IRE) (50 mm × 20 mm × 2 mm, 45° incident angle) was obtained from Pier Optics Co., Ltd. Japan. A particulate TiO_2 film was applied on one face of the IRE by a dip-coating method. Namely, the IRE was dipped in a 0.01 M TiO_2 aqueous suspension and dried in air, followed by wiping of the rear face of the IRE with a soft cloth. This procedure was repeated five times. The TiO_2

coated IRE thus obtained was set in the spectral cell made by Diflon (Figure 1). The inner volume of the cell was approximately 10 mL. The length and width of the exposed area of the IRE is 35.5 and 9.2 mm, respectively. The IR light was reflected about 9 times in the IRE with TiO_2, as calculated from the geometry of the IRE. The structure of the TiO_2 films was inspected with a Hitachi S-5000 scanning electron microscope (SEM).

The spectral cell was placed in the sample chamber of an FTIR spectrometer (Bio-Rad FTS 575C) with a deuterated triglycine sulfate (DTGS) detector. Before measurements, the sample chamber was purged with dry air and the TiO_2 film was kept in the dark for about 60 min. The IR intensity (I) vs. wavelength (λ) was obtained by averaging 100 scans at a resolution of 4 cm^{-1}, with a processing time of 1.5 min for one spectrum. All MIRIR absorption spectra were obtained in the form of absorbance, log (I_0/I), using an appropriate reference sample giving I_0. The frequency range in the present work was from 4000 to 650 cm^{-1}. The increase in the thickness and length of the TiO_2 film on the IRE reduced the total output IR intensity from the IRE in a region below 1000 cm^{-1} where TiO_2 absorbs light, making the spectrum noisy, whereas the decrease in the thickness and length weakened the signals (UV irradiation-induced spectral changes) themselves. The S/N ratio of more than 10 was obtained even at 750 cm^{-1} in the present work, by optimizing the thickness and length of the TiO_2 film.

UV illumination of the TiO_2 film in the spectral cell was performed using a 200-W Hg-Xe lamp (Hypercure 200 UV, Yamashita Denso) equipped with an optical guide. The light in wavelengths of 240 to 400 nm was chosen with a band-pass filter (Toshiba UV-D33S). A neutral density (metal net) filter and an IR-cut filter were also used to avoid cell heating. The incident UV light intensity at the position of the sample surface was approximately 20 mW cm^{-2}, as measured with a thermopile (Eppley Laboratory).

ZnSe used as the IRE is a semiconductor with a band gap of 2.7 eV and not stable in strongly

acidic and alkaline solutions. Therefore, much care was taken to prevent the occurrence of dark and photoinduced reactions at the ZnSe surface that will affect the IR spectra. We confirmed that UV irradiation of ZnSe with TiO_2 films for 30 min in aqueous solutions caused no coloring nor etching (pitting) at the ZnSe surface. Also, UV irradiation of ZnSe without TiO_2 for 30 min in aqueous solutions caused no change in the MIRIR spectrum, except a slight broad decline below 1000 cm^{-1}. Essentially the same results were obtained between the ZnSe-IRE and an IRE of germanium (Ge) with a much smaller band-gap of about 0.7 eV.

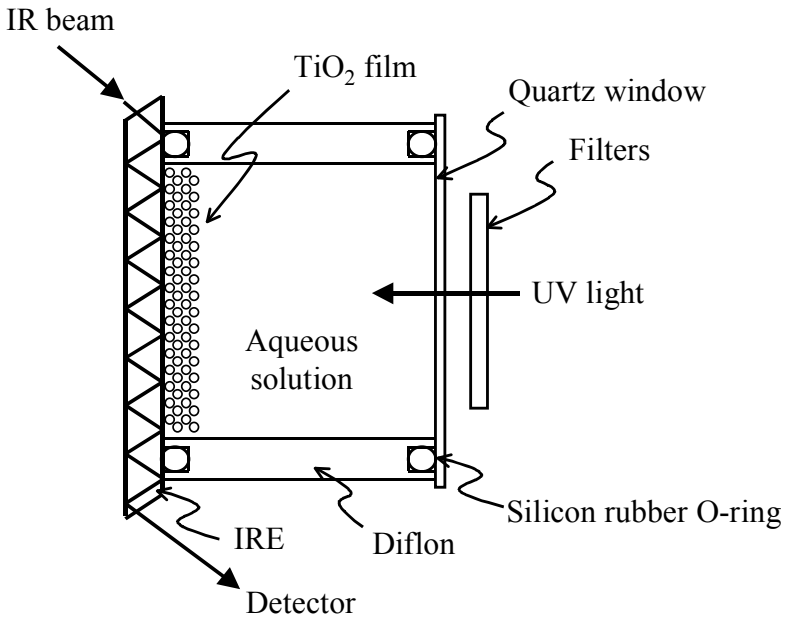

Figure 1 Schematic illustration of a spectral cell used for in-situ MIR-IR measurements.

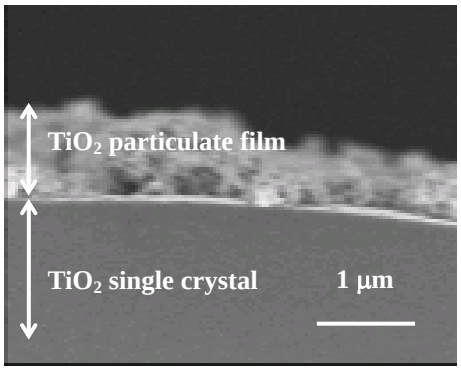

Figure 2 Cross-sectional SEM of a TiO_2 particulate film on a single crystal TiO_2 wafer.

Results

Figure 2 shows a cross-sectional SEM of a TiO_2 (TIO-2, anatase) film, prepared on a TiO_2 single crystal wafer by the dip-coating method. The thickness of the film is about 1 μm, which is of the same order in magnitude as the length of penetration of evanescent IR waves from the ZnSe IRE into an aqueous solution.[41] The UV irradiation for photocatalytic reaction was carried out from the side of the TiO_2/solution interface (Figure 1). The penetration depth (α^{-1}) of the UV light is of the order of several hundred nanometers (α^{-1} = 250 nm at λ = 380 nm),[42,43] which is also of the same order in magnitude as the TiO_2-film thickness.

Figure 3(A) shows an MIRIR spectrum of a particulate TiO_2 film (TIO-5, mainly rutile) in contact with pure water before UV irradiation. A ZnSe prism with no TiO_2 was used as the reference sample. A broad band peaked at 3350 cm^{-1} and a relatively sharp band at 1647 cm^{-1} can be assigned to the OH stretching and the HOH bending modes of water, respectively. Weak bands in a region of 2990 to 2850 cm^{-1} can be assigned to the CH stretching of hydrocarbon contamination at the TiO_2 surface, which could not be removed by a heat-treatment at 500°C in O_2, as discussed later. A weak band at 1475 cm^{-1} may be assigned to carbonate (CO_3^{2-}) ions[44] at the TiO_2 surface. Relatively strong absorption observed below 850 cm^{-1} is due to lattice vibrations of TiO_2.[45] The origin of a weak band at 954 cm^{-1} is not clear; it might be assigned to the antisymmetric Ti-O stretching mode of the Ti-O-Ti [34,46] at the TiO_2 surface. For comparison, Figure 3(B) shows a transmission FTIR spectrum of pure water. The OH stretching and HOH bending modes appear at 3410 and 1644 cm^{-1}, respectively. The shoulder at about 3260 cm^{-1} is assigned to Fermi resonance between the OH stretching and the binary overtone of the HOH bending modes.[47] A slight swelling in 2000 to 2300 cm^{-1} can be ascribed to the second overtone of the librational mode of water[48]. It should be noted that the OH stretching and HOH bending modes in spectrum (A) are slightly different in both spectral position and shape from

those in spectrum (B). Besides, the librational mode of water[48] below 1000 cm^{-1} appearing in spectrum (B) is not observed in spectrum (A). These results suggest that spectrum (A) really detects water within the TiO_2 film, which is in a slightly different situation from bulk water, as reported by McQuillan et al.[34]

Figure 4(A) shows MIRIR spectra of a TiO_2 (TIO-5) film in contact with O_2-saturated pure water as a function of the UV-irradiation time. The spectrum of the TiO_2 film before UV irradiation was taken as the spectral reference. A significant decrease in the band intensity at 3377 cm^{-1} in spectrum (c) suggests that the amount of water within the TiO_2 film decreased by the irradiation. The origin of week bands at 3693 and 3645 cm^{-1} is not clear at present. McQuillan et al. reported similar bands at 3600 and 3480 cm^{-1} and interpreted them as indicating the formation of hydroxyls weakly bound to the surface or interfacial water which is free from hydrogen bond with bulk water. [34] The appearance of broad bands in regions of 1250-1120 and 1100-870 cm^{-1} indicates the formation of some new species, as discussed later. Decreases in the band intensity at 2963 and 2847 cm^{-1} can be attributed to removal of the aforementioned contaminating hydrocarbons at the TiO_2 surface by photoinduced oxidation reactions. A swelling at 1613 cm^{-1} and a depression at 1660 cm^{-1} might tentatively be attributed to a slight lower-energy shift of the bending mode of water at 1647 cm^{-1}. Similar but less marked changes in spectra were observed for TiO_2 films in contact with N_2-bubbled (deoxygenated) pure water, as shown in Figure 4(B), indicating that the spectral changes of Figure 4(A) are caused by photocatalytic reduction of dissolved oxygen.

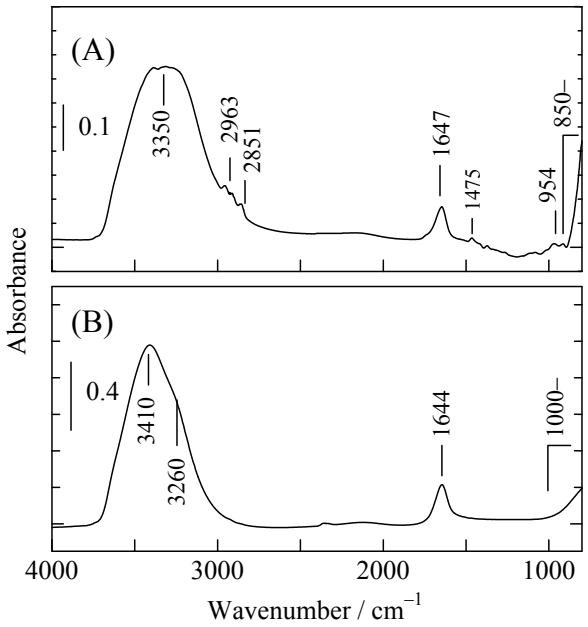

Figure 3 (A) A MIR-IR spectrum of a TiO_2 (TIO-5, mainly rutile) film in contact with pure water, and (B) a transmission FTIR spectrum of bulk water.

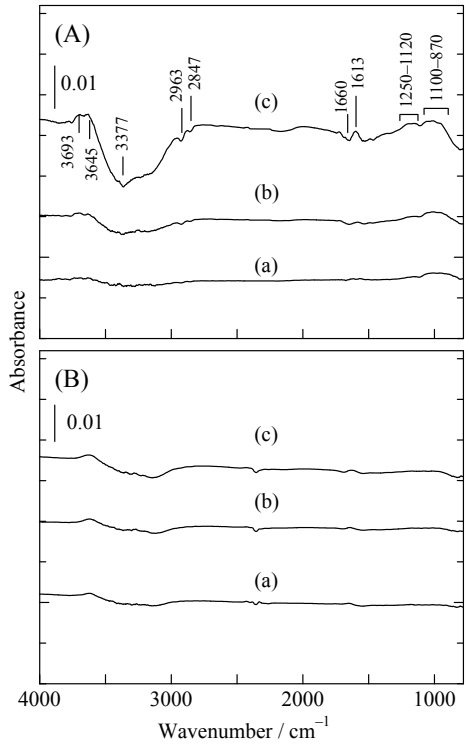

Figure 4 MIR-IR spectra of a TiO_2 (TIO-5) film in (A) O_2- and (B) N_2-saturated pure water as a function of the UV-irradiation time: (a) 8 min, (b) 16 min, and (c) 24 min. The TiO_2 film before the UV irradiation is used as the reference sample.

Figure 5 shows time courses of the MIRIR spectra in the region of 1550 to 750 cm^{-1} in an expanded form. The spectral changes by UV irradiation for TiO_2 (TIO-5) films in contact with O_2-saturated aqueous solutions strongly depended on the solution pH. For a neutral solution of pH 7 (Figure 5B), two bands appeared at 1023 and 943 cm^{-1}, together with a broad band in the 1250-1120 cm^{-1} region. The spectral change in an acidic solution of pH 4.5 (Figure 5A) was rather similar to that in the neutral solution, except that the band at 1023 cm^{-1} became weaker, whereas the 1250-1120 cm^{-1} band became stronger. In addition, new bands appeared at around 887 and 838 cm^{-1}. The spectral change in an alkaline solution of pH 11.8 (Figure 5C) is, on the other hand, considerably different from those for the neutral and acidic solutions, showing the appearance of only the sharp band at 943 cm^{-1}. An extended tail on the higher energy side will most probably be attributed to slight overlapping of other bands, because the tail is essentially removed in isotope-effect experiments, as explained later (Figure 10B). From these results, it is apparent that at least two individual species are photo-produced at the TiO_2 surface; one giving the 943 cm^{-1} band and the other giving the 1250-1120 cm^{-1} band, which will hereafter be referred to species X and Y, respectively.

In order to clarify the chemical origins for species X and Y, We measured time courses of the MIRIR spectra in the dark after stopping the UV irradiation. The 943-cm^{-1} band for the alkaline solution (Figure 5C) became weaker, whereas the 1250-1120 cm^{-1} band became stronger, as shown in Figure 6, suggesting that species X was transformed into species Y. Figure 7 compares the changes of the peak intensities for the 943 and 1250-1120 cm^{-1} bands between pH 4.5 and 11.8 in the dark after stopping the UV irradiation. In both solutions, the amount of X decreases and that of Y increases, but the rate of the change is higher in the acidic solution than in the alkaline solution. This result strongly suggests that the transformation of X to Y is caused by protonation.

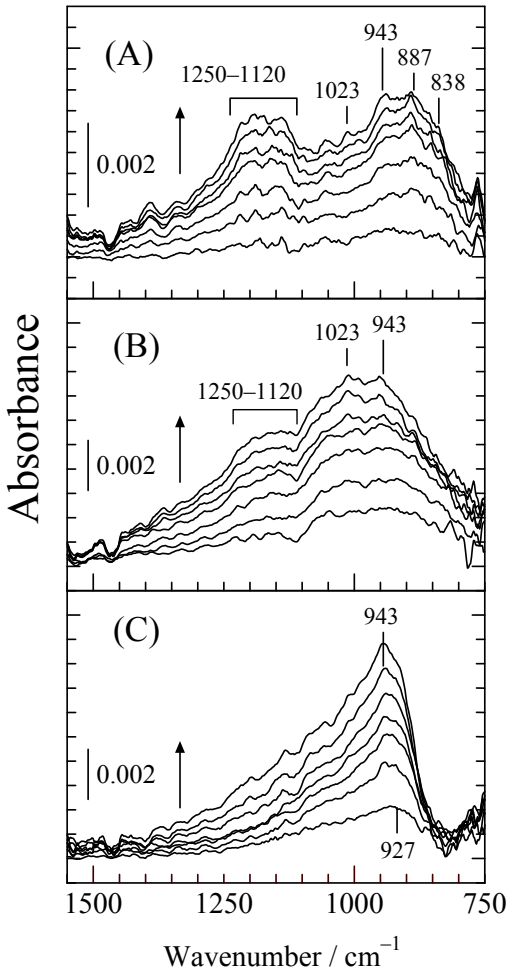

Figure 5 Time courses of MIR-IR spectra for TiO_2 (TIO-5) films in O_2-saturated aqueous solutions of pH (a) 4.5, (b) 7.0, and (c) 11.8. Spectra were recorded in times of 3, 6, 9, 12, 15, 18, and 21 min after the start of UV irradiation. The absorbance was changed nearly parallel to the irradiation time. Arrows in the figure indicate the direction of spectral changes with time.

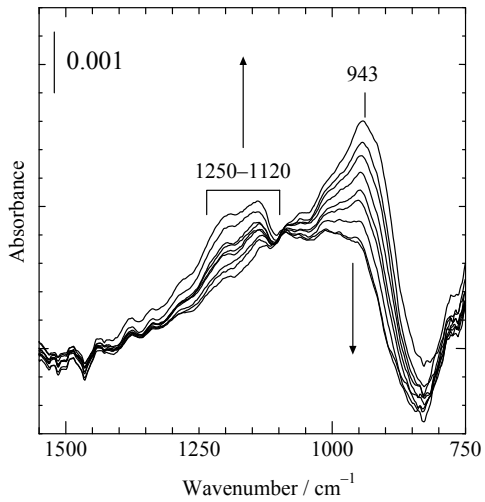

Figure 6 Time course of the MIR-IR spectrum for a TiO_2 film (TIO-5) in an O_2-saturated alkaline solution of pH 11.8 in the dark after the stop of UV irradiation for 21 min. Spectra were recorded in 0, 6, 9, 15, 21, 24 30, 60, and 80 min after the stop of the UV irradiation. Arrows in the figure indicate the direction of spectral changes with time.

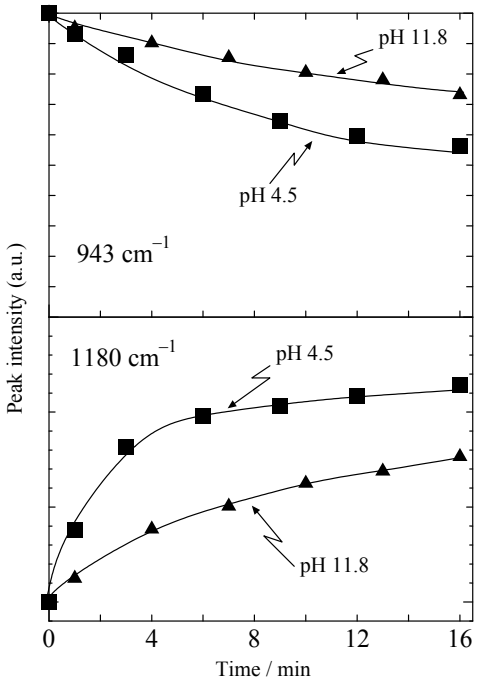

Figure 7 The band intensities at 943 and 1180 cm^{-1} in O_2-saturated aqueous solutions of pH 11.8 and 4.5 as a function of time in the dark after the stop of UV irradiation.

We mentioned earlier that the spectral changes were caused by the photocatalytic reduction of dissolved O_2. In order to confirm the conclusion, We examined the effect of addition of Fe^{3+} and ethanol to the aqueous solution, since Fe^{3+} and ethanol are known to act as efficient electron and hole scavengers, respectively. The UV irradiation in the presence of Fe^{3+} gave no absorption bands at 943 and 1250-1120 cm^{-1}, assigned to species X and Y (Figure 8a), whereas that in the presence of ethanol gave these bands (Figure 8b) though the spectrum was made complex by mixing of absorption bands assigned to ν(C=O), δ(CH_3), δ(CH_2), δ(HOC), and ν(CO) of acetaldehyde formed by photooxidation of ethanol. Figure 9 shows the peak intensity at 943 cm^{-1} vs. time in the presence of Fe^{3+} and ethanol. The addition of ethanol enhanced the appearance of the 943-cm^{-1} band, while that of Fe^{3+} completely suppressed it. These results give strong support to the aforementioned conclusion.

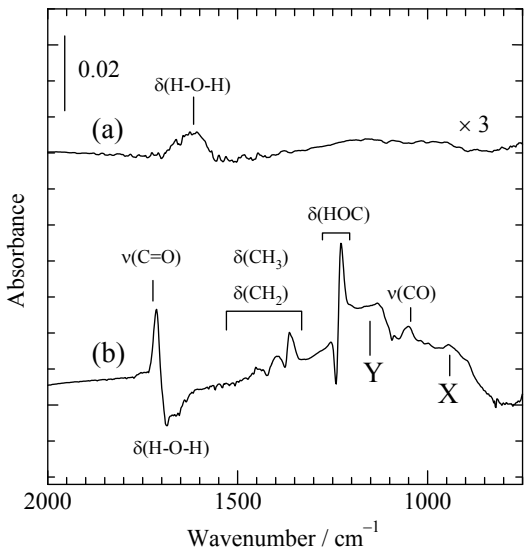

Figure 8 MIR-IR spectra for a TiO_2 (TIO-5) film after 21-min UV irradiation in O_2-saturated aqueous solutions containing (a) 10 mM Fe^{3+} and (b) 25 wt% ethanol.

We also mentioned earlier that the transformation of X to Y was caused by

protonation. In order to confirm this conclusion, we did isotope-effect experiments by using deuterated water (D_2O). Figures 10(A) and 10(B) show the MIRIR spectra for a TiO_2 (TIO-5) film in O_2-saturated D_2O under neutral (pD 6.5) and alkaline (pD 11.2) conditions, respectively. Comparison of these spectra with Figures 5(B) and 5(C) shows that the 943-cm^{-1} (X) band in H_2O shifts only slightly to 926 or 931 cm^{-1} in D_2O. On the other hand, the 1250-1120 cm^{-1} (Y) band in H_2O is missing in D_2O, and instead, a new band appears at about 740-770 cm^{-1} in D_2O. The former result for the 943-cm^{-1} band indicates that this band is inactive for H-D exchange, namely, this band is arising from a specie not containing H. On the other hand, the latter results for the 1250-1120 cm^{-1} band indicates that this band is active for the H-D exchange and arising from a protonated species, which is in harmony with the aforementioned conclusion.

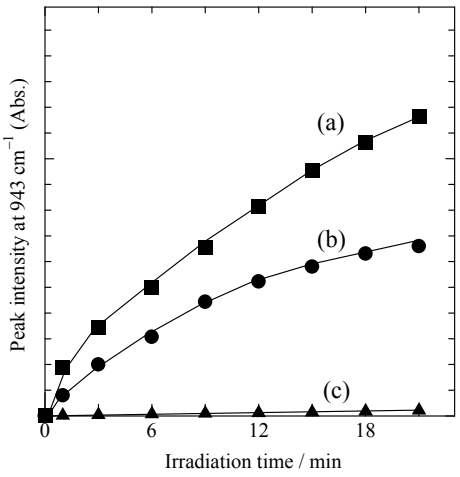

Figure 9 The band intensity at 943 cm^{-1} as a function of the UV-irradiation time in O_2- saturated (a) 25 wt% ethanol aqueous solution, (b) pure water, and (c) 10 mM Fe^{3+} aqueous solution.

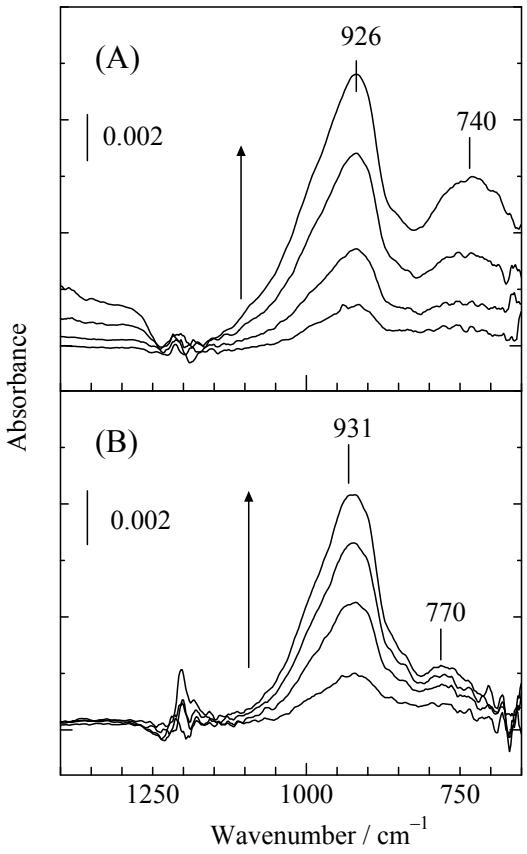

Figure 10 Time courses of MIR-IR spectra for TiO_2 (TIO-5) films in O_2-saturated D_2O of pD (a) 6.5 and (b) 11.2. Spectra were recorded in times of 3, 6, 12, and 24 min after the start of the UV irradiation. Arrows in the figure indicate the direction of spectral changes with time.

We tried to investigate the chemical reactivity of species X and Y. The addition of methanol, ethanol, propanol, and carbon monoxide to the cell solution in the dark after the stop of UV illumination did not seem to change the band intensities for X and Y in a time range of 10 to 30 min, though we could not get a definite conclusion on this point owing to complex and unsteady nature of the observed spectra, probably caused by inhomogeneous slow diffusion of added reagents into the TiO_2 film. In this connection, the fact that the bands for X and Y were observed after the UV irradiation even in the presence of ethanol (Figure 8b) strongly suggests that X and Y have a low reactivity to ethanol.

We also made experiments using TiO_2 (TIO-2, anatase) films, to investigate a difference in the

photoreactivity between rutile and anatase TiO_2. The experiments with TIO-2 (anatase) gave quite similar results to the case of TIO-5 (mainly rutile), including the pH-dependent formation of species X and Y and the transformation of X to Y in the dark, though the rate of formation of X and Y for TIO-2 is much higher than that for TIO-5 probably because of the smaller size and the larger surface area for the former. The similar behavior of rutile and anatase-type TiO_2 film gives further support to the reproducibility of the present results.

Discussion

Photocatalytic reactions on TiO_2 particles in aqueous solutions will in general involve various types of active intermediates, formed by reactions of both photogenerated conduction-band electrons (e^-) and valence-band holes (h^+). In the MIRIR spectra in the present work, however, intermediate species produced by photogenerated electrons (i.e. photocatalytic reduction of dissolved O_2) were observed, as mentioned in the preceding section (Figures 4 and 8). Some of photogenerated holes may be consumed to oxidize contaminating hydrocarbons at the TiO_2 surface, as indicated by the decreases in the CH-stretching band (Figure 4A). However, it is evident that the oxidation of water by photogenerated holes occurs because gas-bubble formation was clearly seen in the TiO_2 film by eyes after the UV irradiation and the amount of the bubbles was increased much by the addition of Fe^{3+} to the solution. Apparently no observation of intermediates of the water oxidation might thus be attributed to either their high reactivity and short lifetime or undesirable spectral positions of their IR bands (e.g. the O-O stretching mode of Ti-O-O-Ti as a possible intermediate[49] is reported [50,51] to be below 750 cm^{-1}).

Let us first consider the assignment of the two bands (X and Y) peaked at 943 cm^{-1} and 1250-1120 cm^{-1}, respectively (Figure 5). Both the bands should arise from the

photocatalytic reduction of O_2, as mentioned earlier. The predominant appearance of the 943 cm^{-1} band in an alkaline solution, together with the faster appearance of the 1250-1120 cm^{-1} band in lower-pH solutions, suggests that species X is transformed to Y by protonation. That Y is a protonated species was clearly confirmed by the isotope experiment using D_2O (Figures 5 and 10). We can thus conclude, as the most plausible assignment, that the 943-cm^{-1} band is due to a surface peroxo species, $Ti(O_2)$, and the 1250-1120 cm^{-1} band is due to a surface hydroperoxo species, TiOOH, respectively. The transformation of X to Y can be expressed as follows.

$$Ti(O_2)\ (X) + H^+ \rightarrow TiOOH\ (Y) \qquad (1)$$

The above assignment for species X is supported by reported IR studies of O_2 complexes of 3d metals. In general, dioxygen adducts of 3d metals show characteristic bands assigned to the O-O stretching mode in the range of 1300-600 cm^{-1}.[50-59] The bands are classified into two groups; superoxo species, MOO, exhibiting the O-O stretching band in a 1300-1100 cm^{-1} region, and peroxo species, $M(O_2)$, exhibiting the O-O stretching band in a 1000-680 cm^{-1} region.[50] For titanium adducts, it is reported that the O-O stretching band for superoxo, TiOO, lies at 1220-1140, while that for peroxo, $Ti(O_2)$, lies at 950-890 cm^{-1}.[51,56-59] Thus, species X having the band at 943 cm^{-1} is reasonably assigned to peroxo species.

The assignment for species Y to surface TiOOH is derived directly from the fact that it is the first product of protonation of surface peroxo species (equation 1). The assignment is also in harmony with reported spectral data[60,61], though there is complexity that further protonation may proceed to some extent and resultant H_2O_2 shows bands similar to those of TiOOH. It is reported, from IR studies[60,61] of Ti-silicalite molecular sieve (TS-1) exposed to H_2O_2, that the O-O stretching band for TiOOH is at 837 cm^{-1} and that for physisorbed H_2O_2 is at 880 cm^{-1}. Based on the results, We can tentatively assign the bands at 838 and 887 cm^{-1} in Figure 5A to

the O-O stretching modes for TiOOH and physisorbed H_2O_2, respectively. Accordingly, the 1250-1120 cm^{-1} band for Y can be assigned to the OOH bending mode for TiOOH (or TiOOH and physisorbed H_2O_2). This assignment is supported by the fact that the 838- and 887-cm^{-1} bands in Figure 5, assigned to the OO stretching for TiOOH and physisorbed H_2O_2, become stronger, with decreasing pH, in parallel with the 1250-1120 cm^{-1} band assigned to the OOH bending for the same TiOOH (and physisorbed H_2O_2). The assignment is also in harmony with an expectation that the OOH bending mode of TiOOH (1250-1120 cm^{-1}) lies at a somewhat lower energy than that of gaseous H_2O_2 (1270-1280 cm^{-1} [62-64]) owing to replacement of H by Ti.

The above assignment is further supported by the isotope experiments. Comparison of Figures 5 and 10, on the basis of the above assignment, suggests that the OO stretching band for TiOOH at 837 cm^{-1} in H_2O (Figure 5A) is shifted to a band at 740-770 cm^{-1} for TiOOD in D_2O (Figure 10A), whereas the OOH bending band for TiOOH at 1250-1120 cm^{-1} in H_2O is shifted to a band at around 900 cm^{-1} for TiOOD in D_2O, though the latter 900-cm^{-1} band is completely overlapping with the 926-931-cm^{-1} band for Ti(O_2) and appearing only as a tail on the higher energy side. The assignment of the 740-770 cm^{-1} band to the OO stretching for TiOOD is supported by the fact that it becomes stronger with decreasing pH (or pD), similarly to the 837 cm^{-1} band for TiOOH. Thus, the isotope shift for the OO stretching for TiOOH is calculated to be 97-67 cm^{-1}, and that for the OOH bending is 350-220 cm^{-1}. These values are quite reasonable, compared with the reported shifts for gaseous H_2O_2 by mono-deuteration from H_2O_2 to HDO_2, about 80 cm^{-1} for the O-O stretching mode and 290 cm^{-1} for the OOH bending mode[63,65].

Based on the above assignment for species X and Y, We can propose a possible reaction scheme for the photocatalytic reduction of O_2 at the TiO_2 surface, as shown in Scheme 1. The reduction of O_2 may be initiated by electron capture at H_2O-adsorbed Ti(4+) sites, immediately followed by an attack of an O_2 molecule, leading to the formation of superoxo

species, TiOO·, as a precursor of surface peroxo species, $Ti(O)_2$, though TiOO· was not detected in the present work probably because of its short life time. It is well established in vacuum or gaseous systems that photogenerated electrons are captured at surface Ti(4+) sites to produce Ti(3+) sites, using low-temperature ESR measurements under controlled atmospheres[13,14,66] as well as surface-analyses with XPS, SHG, and TPD[67-70]. O_2 can readily attack on them, resulting in e.g., superoxo species. Surface peroxo species, $Ti(O_2)$, is formed by further reduction of TiOO· with an electron. $Ti(O_2)$ has a closed-shell electronic structure and is expected to be fairy stable.

It is to be noted that Scheme 1 is in harmony with other features of the observed spectral changes. A significant decrease in the band intensity for the OH stretching mode of water at 3377 cm^{-1} (spectrum (c) of Figure 4A) can be explained by a decrease in the amount of water within the TiO_2 film, caused by accumulation of tiny O_2 (or CO_2) gas bubbles produced by oxidative reactions of photogenerated holes. The explanation is supported by enhancement of the decrease in the intensity of the OH stretching band by addition of Fe^{3+} ions to the solution.

The 1023 cm^{-1} band appearing in a neutral solution (Figure 5B), which is weak in an acidic solution (Figure 5A) and nearly absent in an alkaline solution (Figure 5C), is active for the isotopic H-D exchange (compare Figures 5B and 10), indicating that the corresponding species contains H atoms. A tentative assignment of this band is the O-O stretching mode of hydroperoxo radicals, HO_2·, present in the solution phase (Scheme 1). Recent negative-ion photoelectron spectroscopy showed that hydroperoxo radicals had the O-O stretching mode at 1102 cm^{-1} at 200 K.[71] The p*K*a of HO_2· is 4.88 and thus it is transformed into O_2^-· radicals in alkaline solutions, which can explain the absence of the 1023 cm^{-1} band in an alkaline solution. On the other hand, in acidic solutions, an effective disproportionation reaction may occur with H^+ ions as a catalyst,

$HO_2\cdot + HO_2\cdot \rightarrow H_2O_2 + O_2$ (2)

which leads to a decrease in the $HO_2\cdot$ concentration. The $HO_2\cdot$ radicals in solution can be produced either via desorption of surface superoxo radicals, $TiOO\cdot$, or via direct electron transfer from the TiO_2 conduction band to adsorbed O_2, both followed by protonation. The latter direct electron transfer can be effective in alkaline solutions, as observed at single crystal TiO_2 (rutile) electrodes[72].

It is finally to be noted that the observed spectral changes (Figures 4-10), especially the band intensities, are more or less affected by reactions of the (electron-induced) intermediates in scheme 1 with photogenerated holes or hole-induced intermediates (a kind of reverse reactions). Further detailed studies are necessary to get definite conclusions on these reactions. Such studies are now under way.

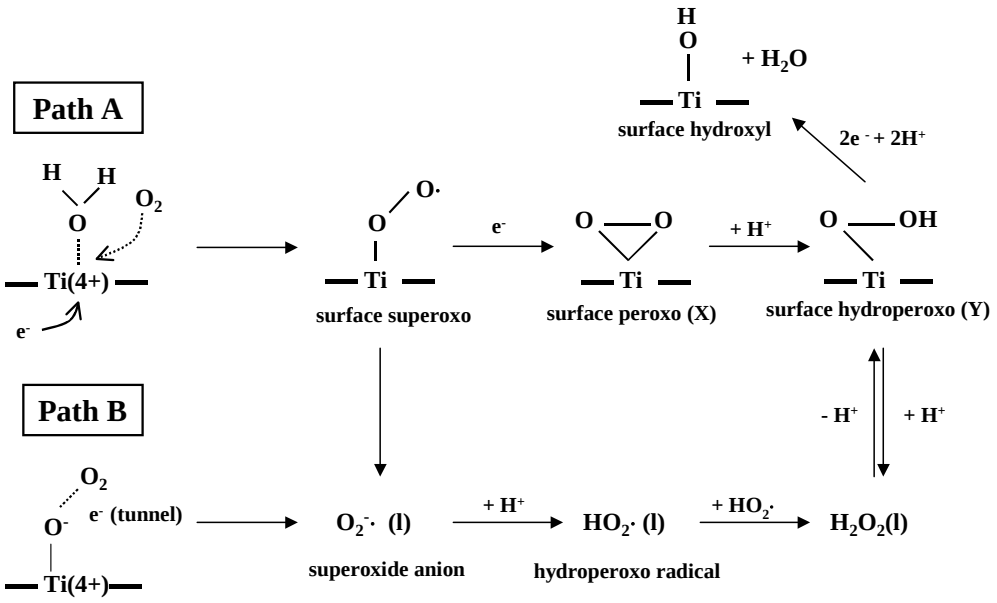

Scheme 1 Reaction schemes for the O_2 reduction, initiated by photoexcited electrons in the conduction band.

Conclusions

The MIRIR technique has allowed the *in-situ* direct detection of surface intermediates of the photocatalytic O_2 reduction at the TiO_2 surface in aqueous solutions, proving that it is really a powerful tool for mechanistic studies. Detailed investigations under various conditions have revealed that surface peroxo species, $Ti(O_2)$, is primarily produced, probably via Ti-OO· as a precursor, which is then transformed to surface hydroperoxo, TiOOH, by protonation in the dark. The work in the present chapter has also revealed that the rates of the primary steps strongly depend on the pH solution, thus opening a new possibility of control of successive reaction processes by a change of the solution pH. Further studies of the primary mechanisms of

photocatalytic reactions will serve for control or improvement of complex photocatalytic reactions in various application fields.

References

(1) Fujishima, A. ; Honda, K., *Nature* **1972**, *238*, 37.

(2) Khan, S. U. M.; Al-Shahry, M.; Ingler, W. B., Jr. *Science* **2002**, *297*, 2243.

(3) Wang, R.; Hashimoto, K.; Chikuni, M.; Kojima, E.; Kitamura, A.; Shimohigashi, M.; Watanabe, T. *Nature* **1997**, *388*, 431.

(4) Asahi, R.; Morikawa, T.; Ohwaki, T.; Aoki, K.; Taga, Y. *Science* **2001**, *293*, 269.

(5) Ollis, D. S.; Al-Ekabi, H.; Eds., *Photocatalytic Purification and Treatment of Water and Air*; Elsevier, Amsterdam, **1993**.

(6) Fujishima, A.; Rao, T. N.; Tryk, D. A. *J. Photochem. Photobiol. C: Photochem. Rev.* **2000**, *1*, 1.

(7) Schiavello, M. *Heterogeneous Photocatalysis*; John Wiley & Sons Ltd, New York, **1997**.

(8) Hoffmann, M. R.; Martin, S. T.; Choi, W.; Bahnemann, D. W. *Chem. Rev.* **1995**, *95*, 69.

(9) Naccache, C.; Mariaudeau, P.; Che, M.; Tench, A. J. *Trans. Faraday. Soc*. **1971**, *67*, 506.

(10) Mariaudeau, P.; Vedrine, J. C.; *J. Chem. Soc. Faraday Trans. 2* **1976**, *72*, 472.

(11) Gonzalez-Elipe, A. R.; Munuera, G.; Soria, J. *J. Chem. Soc. Faraday Trans.* **1979**, *75*, 748.

(12) How, R. F.; Gräetzel, M.; *J. Phys. Chem*. **1987**, *91*, 3906.

(13) Anpo, M.; Aikawa, N.; Kodama, S.; Kubokawa, Y. *J. Phys. Chem.* **1984**, *88*, 3998.

(14) Anpo, M.; Yabuta,.; Kodama, S.; Kubokawa, Y. *Bull. Chem. Soc. Jpn.* **1986**, *59*, 259.

(15) Einaga, H.; Ogata, A.; Futamura, S.; Ibusuki, T. *Chem. Phys. Lett*. **2001**, *338*, 303.

(16) Jaeger, C. D.; Bard, A. J. *J. Phys. Chem*., **1979**, *83*, 3146.

(17) Kaise, M.; Kondoh, H.; Nishihara, C.; Nozoe, H.; Shindo, H.; Nimura, S.; Kikuchi, O. *J. Chem. Soc. Chem. Commun*. **1993**, 395.

(18) Kaise, M.; Nagai, H.; Tokuhashi, K.; Kondo, S.; Nimura, S.; Kikuchi, O. *Langmuir* **1994**, *10*, 1345.

(19) Somorjai, G. A. *Introduction to Surface Chemistry and Catalysis*; John Wiley & Sons, New York, **1994**; pp324-329.

(20) Clark, R. J. H.; Hester R. E. *Spectroscopy for Surface*; John Wiley & Sons, New York, **1998**; pp219-272.

(21) Szczepankiewicz, S. H.; A. Colussi, J.; Hoffmann, M. R. *J. Phys. Chem. B* **2000**, *104*, 9842.

(22) Szczepankiewicz, S. H.; Moss, J. A.; Hoffmann, M. R. *J. Phys. Chem. B* **2002**, *106,* 7654.

(23) Sato, S.; Ueda, K.; Kawasaki, K.; Nakamura, R. *J. Phys. Chem. B* **2002**,*106,* 9054.

(24) Nakamura, R.; Sato. S. *Langmuir* **2002**, *18,* 4433.

(25) Nakamura, R.; Sato. S. *Langmuir* **2001**,*17,* 2298.

(26) Harrick, N. J. *Internal Reflection Spectroscopy*; John Wiley & Sons, New York, **1967.**

(27) Suëtaka. W. *Surface Infrared and Raman Spectroscopy*; Plenum press, New York, **1996**.

(28) Dobson, K. D.; Roddick-Lanzilotta, A. D; McQuillan, A. J. Vibrational Spectroscopy **2000,** *24*, 287.

(29) Dobson, K. D.; McQuillan, A. J. *Spectrochim. Acta A* **2000**, *56*, 557.

(30) Connor, P. A.; McQuillan, A. J. *Langmuir* **1999**, *15,* 2916.

(31) Ronson, T. K.: McQuillan, A. J. *Langmuir* **2002**, *18,* 5019.

(32) McWhirter, M. J.; McQuillan, A. J. Bremer, P. J. Colloids Surfaces B **2002**, *26*, 365.

(33) Nazeeruddin, M. K.; Amirnasr, M.; Comte, P.; Mackay J. R.; McQuillan, A. J.; Houriet, R., Grätzel, M. *Langmuir* **2000**, *16,* 8525.

(34) Connor, P. A.; Dobson, K. D.; and McQuillan, A. J. *Langmuir* **1999**,*15,* 2402.

(35) Osawa, M. *Bull. Chem. Soc. Jpn*. **1997**, *70*, 2861.

(36) Ferri, D.; Buergi, T.; Baiker, A. *J. Phys. Chem. B* **2001**, *105*, 3187.

(37) Buürgi, T.; Baiker, A. *J. Phys. Chem. B* **2002**, *106,* 10649.

(38) Ekström, G. N.; McQuillan, A. J. *J. Phys. Chem. B* **1999**, *103,* 10562.

(39) Gerischer, H., Heller, A. *J. Elecctrochem. Soc*. **1992** *139*, 113.

(40) Nakamura, R.; Sato. S. *J. Phys. Chem. B* **2002**, *106,* 5893.

(41) The intensity of the evanescent wave reaches 1/e at 0.9 μm from the ZnSe surface with a wavenumber of 1650 cm^{-1}.

(42) Eagles, D. M. *J. Phys. Chem. Solids* **1964**, *25*, 1243.

(43) Poznyak. K. S.; Sviridov. V. V.; Kulak. A. I.; and Samtsov. M. P. *J. Electroanal. Chem.*, **1992**, *340*, 73.

(44) Yates, D. J. C. *J. Phys. Chem.* **1961**, *65*, 746.

(45) Farmer, V. C., Ed. *The infrared Spectra of Minerals*; Mineral Society: London, **1974**.

(46) Kushto, G. P.; Zhou, M.; Andrews, L.; Bauschlicher, C. W. J. *J. Phys. Chem. A* **1999**, *103,* 1115.

(47) Ataka, K.; Yotsuyanagi, T.; Osawa, M. *J. Phys. Chem.* **1996**, *100,* 10664.

(48) Devlin, J. P.; Sadlej, J.; Buch, V. *J. Phys. Chem. A.* **2001**, *105*, 974.

(49) Kisumi, T.; Tsujiko, A.; Murakoshi, K.; Nakato, Y. *J. Electroanal. Chem*, **2003**, in press.

(50) Nakamoto, K., *Infrared and Raman Spectra of Inorganic and Coordination Compounds*; John Wiley & Sons, New York, **1986**.

(51) Ohno, T.; Masaki, Y.; Hirayama, S.; Matsumura, M., *J. Catal*. **2001**, *204*, 163.

(52) Gillard, R. D.; McCleverty, J. A, *Comprehensive coordination chemistry*; Pergamon press, Oxford, **1987**.

(53) Andrews, L.; Chertihin, G. V.; Ricca, A.; Bauschlicher, C. W. *J. Am. Chem. Soc.* **1996**, *118,* 467.

(54) Citra, A.; Chertihin, G. V.; Andrews, L.; Neurock, M. *J. Phys. Chem. A* 1997, *101,* 3109.

(55) Zhou, M.; Andrews, L. *J. Phys. Chem. A* **1999**,*103,* 5259.

(56) Gutsev, G. L.; Rao, B. K.; Jena, P. *J. Phys. Chem. A* **2000**, *104,* 11961.

(57) Muller J., K.; Schwarzenbach, G. *Inorg. Chem.* **1970**, *9,* 2381.

(58) Miksztal, R.; Valentine, J. S. *Inorg. Chem.* **1984**, *23*, 3548.

(59) Kristine, F. J.; Shepherd, R. E.; Siddiqui, S. *Inorg. Chem.* **1981**, *20*, 2571.

(60) Tozzola, G.; Mantegazza, M. A.; Ranghino, G.; Petrini, G.; Bordiga, S.; Ricchiardi, G.; Lamberti, C.; Zulian, R.; and Zecchina, A. *J. Catal*. **1998**, *179*, 64.

(61) W. Lin and H. Frei, *J. Am. Chem. Soc*. **2002**, *124*, 9293.

(62) Giguere, P. A.; and Srinivasan, T. K. K. *Chem. Phys. Lett*. **1975**, *33*, 479.

(63) Engdahl, A.; Nelander, B.; and Karlström, G. *J. Phys. Chem. A* **2001**, *105,* 8393.

(64) Goebel, J. R.; Ault, B. S.; Del, B. J. E. *J. Phys. Chem. A* **2001**, *105,* 11365.

(65) Pettersson, M.; Tuominen, S.; and Räsänen, M. *J. Phys. Chem. A* **1997**, *101,* 1166.

(66) Anpo, M.; Kubokawa, Y.; Fujii, T.; Suzuki, S. *J. Phys. Chem.* **1984**, *88,* 2512.

(67) Shultz, A. N.; Jang, W.; Hetherington, W. M.; Baer, D.R.; Wang, L-Q.; Engelhard, M.H. *Surf. Sci.* **1995**, *399*, 114.

(68) Shultz, A. N.; Hetherington, W. M.; Baer D.R.; Engelhard, M.H. Wang, L-Q. *Surf. Sci.* **1997**, *392*, 1.

(69) Henderson, M. A.; Epling, W. S.; Perkins, C. L.; Peden ,C. H. F.; Diebold, U. *J. Phys. Chem. B* **1999**, *103,* 5328.

(70) Linsebigler, A.; Lu, G.; Yates, J. T. Jr. *J. Phys. Chem.* **1996**, *100,* 6631.

(71) Ramond, T. M.; Blanksby, S. J.; Kato, S.; Bierbaum, V. M.; Davico, G. E.; Schwartz R. L.; Lineberger, W. C.; Ellison, G. B. *J. Phys. Chem. A* **2002**, *106,* 9641.

(72) Tsujiko, A.; Itoh, H.; Kisumi, T.; Shiga, A.; Murakoshi, K.; Nakato, Y. *J. Phys. Chem. B* **2002**, *106,* 5878.

Chapter 2

Primary Intermediates of Oxygen Photoevolution Reaction on TiO_2 (Rutile) Particles, Revealed by *In Situ* FTIR Absorption and Photoluminescence Measurements

Introduction

Photo-induced oxidation of water and organic compounds at TiO_2 or related metal-oxide semiconductor surfaces has attracted much attention from the points of view of solar-to-chemical conversion (water splitting)[1-4] and environmental cleaning (photodecomposition of dirt or harmful materials)[5-7]. Recently, this reaction was added a new interest by a finding[8-10] of photoinduced increase in the hydrophilicity of the TiO_2 surface. In addition, this reaction has become more and more attractive recently by another finding[11-19] that doping of metal oxides such as TiO_2 with nitrogen, sulfur, carbon, or other elements leads to an extension of the photoactivity to the visible-light region.

For achieving successful applications of the phenomena to energy and environmental technologies, the improvement of the efficiency and stability through elucidation of reaction mechanisms is of essential importance. A number of studies have been made on the reaction mechanism of oxygen photoevolution on TiO_2 electrodes or particles, using electrochemical[20-32] and spectroscopic[33-47] methods, but reported mechanisms are rather scattered and detailed mechanisms still remain unclear yet.

For example, Wilson et al. first reported[20] the formation of a surface state as a possible intermediate of oxygen photoevolution reaction on n-TiO_2, as detected by a negative potential sweep after UV irradiation under anodic bias. Salvador et al. studied the reaction mechanism in detail[21-24] and reported that the Wilson's surface state could be attributed to adsorbed hydrogen peroxide, $H_2O_{2\,ad}$, produced by coupling of surface ·OH radicals formed through oxidation of surface OH group (Ti-OH_s) with photogenerated holes (h^+)

$$\text{Ti-OH}_s + h^+ \rightarrow [\text{Ti} \cdot \text{OH}]_s^+ \qquad (1)$$

Many other workers have also assumed reaction (1) as the initiation step of the oxygen photoevolution reaction on TiO_2.

On the other hand, the laboratory which the author belonged found[25-27, 48-52] that a photoluminescence (PL) band peaked at 840 nm was emitted from a UV-illuminated n-TiO_2 surface. Our later detailed studies[51,52] using in-situ photocurrent and PL measurements have shown that the PL band is emitted only from the (100) face of TiO_2 (rutile) and is assigned to an electronic transition from the conduction band to a vacant level of a "surface-trapped hole", which acts as a precursor of the oxygen photoevolution reaction. Our studies have also shown that the oxygen photoevolution is not initiated by reaction (1) but a nucleophilic attack of an H_2O molecule to a surface lattice O site accompanied by bond breaking.

$$[\text{Ti-O-Ti}]_s + h^+ + H_2O \rightarrow [\text{Ti-O}\cdot\ \text{HO-Ti}]_s + H^+ \qquad (2)$$

The (100) face of TiO_2 (rutile) has the unique atomic structure and thus the surface-trapped hole at this face is expected[51] to lie at the bottom of atomic grooves present at this face (cf. Figure 9) and be stabilized by steric hindrance enough to emit a recombination luminescence as the PL, contrary to the case of other faces. It is worth noting here that reaction (1) is an electron-transfer type reaction, whereas reaction (2) is a Lewis acid-base type reaction, and therefore their energetics and kinetics are quite different from each other.

There is also confusion in mechanistic studies by spectroscopic methods. Jaeger and Bard[53], and recently Schwarz et al.[54] reported, using a spin-trapping method, that hydroxyl (·OH) radicals were produced on UV irradiated TiO_2 powder in aqueous solutions. However, it was pointed out by Nosaka et al.[55] that the water photooxidation reaction at TiO_2 produced no free ·OH radical and spin-trapping agents reacted with "surface-trapped holes" (assigned to adsorbed ·OH radicals), giving ESR signals similar to those reported. The ESR detection of ·OH radicals on irradiated TiO_2 (anatase) at 77 K was also reported by Anpo et al.,[56] though their ESR signal showed no spectral change by $H_2O \rightarrow D_2O$ exchange. On the other hand, Howe and

Grätzel[57] first reported by ESR measurements that photogenerated holes were trapped at lattice O atoms (or Ti-O-Ti sites) at low temperatures of 4.2 or 77 K, not producing ·OH radicals. Later Micic et al.[58,59] confirmed this conclusion and showed clearly that not ·OH radicals but Ti-O· radicals were produced, in harmony with the mechanism of reaction (2).

The surface intermediates on irradiated TiO_2 were also studied by other spectroscopic methods. Szczepankiewicz et al.[60] reported by diffuse reflectance FTIR spectroscopy that a new band, assignable to surface ·OH radicals, appeared at 3683 cm^{-1} for UV irradiated TiO_2 (P25 and pure anatase) powder in an oxygen atmosphere. Yates et al.[61], on the other hand, reported that ·OH radicals did not play any important role in photoinduced oxidation of trichloroethylene on TiO_2 (P25) in the gas phase. Hashimoto et al.[62] also reported, by measuring the quantum yield of formation of ·OH radicals by means of a fluorescence probe method, that the formation of ·OH radicals was not be the major process on irradiated TiO_2 (anatase) in aqueous solutions. In addition, recent ultraviolet photoelectron spectroscopic (UPS) studies[63-65], combined with scanning tunnel microscopic (STM) inspection[63,66], revealed that the O-2p levels for bridging hydroxyl groups (Ti-OH-Ti) at the (110) face and terminal hydroxyl groups (Ti-OH) at the (100) face are both far below the top of the valence band of TiO_2 (rutile).

It is evident that in-situ direct spectroscopic detection of reaction intermediates is of crucial importance for clarification of molecular mechanisms. In chapter 1, it was described that multiple internal reflection (MIR) infrared (IR) absorption spectroscopy could be successfully applied to in situ observation of primary intermediates of photocatalytic O_2 reduction on TiO_2 in contact with aqueous solutions.[67] The IR spectroscopy has in general a serious difficulty in application to aqueous systems owing to strong IR absorption of water[68]. The difficulty can be overcome to a large extent by using internal reflection techniques[69]. The single internal reflection (SIR) mode was successfully applied to detection of various interfacial species by

McQullan et al.[70-74] The advantage of the MIR mode lies in its high detection sensitivity. This mode can detect a surface species of a submonolayer amount even in contact with an aqueous medium.

In the present chapter, the author applied the MIR-IR technique to detection of surface intermediates of the oxygen photoevolution reaction on particulate TiO_2 (rutile) films. A diamond single crystal prism was used as an internal reflection element (IRE) instead of a ZnSe prism in a previous work[67], to get high spectral sensitivity in a low-frequency region from 1500 to 600 cm^{-1}, in which surface intermediates of the oxygen photoevolution reaction are expected to show vibrational bands. We have succeeded in detecting surface peroxo species as primary intermediates of the oxygen photoevolution reaction, which supports reaction (2) as the initiation reaction.

Experimental

TiO_2 powder, called JRC-TIO-3 by the Catalysis Society of Japan, was used for the multiple internal reflection infrared (MIR-IR) measurements. The powder is well characterized by the Society as one of the reference catalysts and reported to be composed of 100 % rutile particles with the average primary diameter (d_{av}) of 30-50 nm and surface area of 51 m^2/g. The surface of the TiO_2 particles was first cleaned by heating at 600°C in an O_2 atmosphere for 5 h, followed by UV-irradiation in O_2-saturated water for 1 h and ultrasonic agitation for 30 min. The cleaned particles were then dried and kept under vacuum ($< 1\times10^{-3}$ Torr).

Single crystal TiO_2 (rutile) wafers for PL measurements were obtained from Earth Chemical Co., Ltd. They had 99.99% in purity, 10 mm×10 mm in area and 1.0 mm in thickness, and (110)-cut alkali-polished surfaces. The wafers were washed by rinsing with acetone and

ultrasonic agitation in pure water for 5 min, and reduced in a stream of hydrogen at 550 °C for 3 h to get n-type semiconductivity. Specimens of about 0.3 Ω cm were used for experiments.

All other chemicals, $H_2{}^{18}O$ (Aldrich, 99.9 atom%), NaOH (Wako), HCl (Wako), H_2SO_4 (Wako), Na_2SO_4 (Wako), H_2O_2 (Wako), methanol (Wako), and $FeCl_3$ (Aldrich), were of reagent grade and used as received without further purification. Solutions were prepared using pure (Milli-Q) water with a conductivity of 18 $M\Omega^{-1}$ cm^{-1}. Nitrogen or oxygen gas was bubbled through the solution either to remove dissolved air (oxygen) or to dissolve oxygen.

A spectral cell for the MIR-IR experiment is illustrated schematically in Figure 1. A diamond single-crystal disc of 3 mm in diameter and 0.25 mm in thickness, affixed to a ZnSe single crystal having an inlet and an outlet for IR light, was used as the internal reflection element (IRE). An experimental set (for MIR experiments) furnished with this IRE and reflection mirrors was commercially available and we obtained it from S. T. Japan Inc. In most cases, 10 μL of aqueous TiO_2 slurry (10 mg/mL) was spread on the diamond disc with a plastic pipette and dried in air. The inner volume of the cell, including the aqueous solution, was approximately 40 μL. The IR light was reflected about 9 times at the diamond/TiO_2·solution interface, as calculated from the geometry of the IRE.

The spectral cell was placed in the sample chamber of an FTIR spectrometer (Bio-Rad FTS 575C) with a deuterated triglycine sulfate (DTGS) detector. Before measurements, the sample chamber was purged with N_2 and the TiO_2 film was kept in the dark for about 60 min. The IR intensity (I) vs. wavelength (λ) was obtained by averaging 400 scans at a resolution of 4 cm^{-1}, with a processing time of 6 min for one spectrum. All MIRIR absorption spectra were obtained in the form of absorbance, log (I_0/I), using an appropriate reference sample giving I_0.

UV irradiation of the TiO_2 film was carried out by a 365-nm band from a 200-W Hg-Xe lamp (Hypercure 200 UV, Yamashita Denso) with an optical guide, chosen by use of a

band-pass filter (Asahi Techno Glass UV-D36A). A neutral density (metal net) filter and an IR-cut filter were also used to avoid cell heating. The incident UV light intensity at the position of the sample surface was approximately 1 mW cm^{-2}, as measured with a thermopile (Eppley Laboratory). Further details on the MIRIR method were described in a previous paper[67].

Photocurrent density (j) vs. potential (U) curves for single crystal n-TiO_2 electrodes were measured with a commercial potentiostat and a potential programmer, using a Pt plate as the counter electrode and an "Ag/AgCl/sat. KCl" electrode as the reference electrode. The illumination was carried out by the 365-nm band from a 500-W high-pressure mercury lamp, obtained by use of band-pass filters. The PL intensity (I_{PL}) vs. U curves were measured simultaneously with the j-U curve measurements.

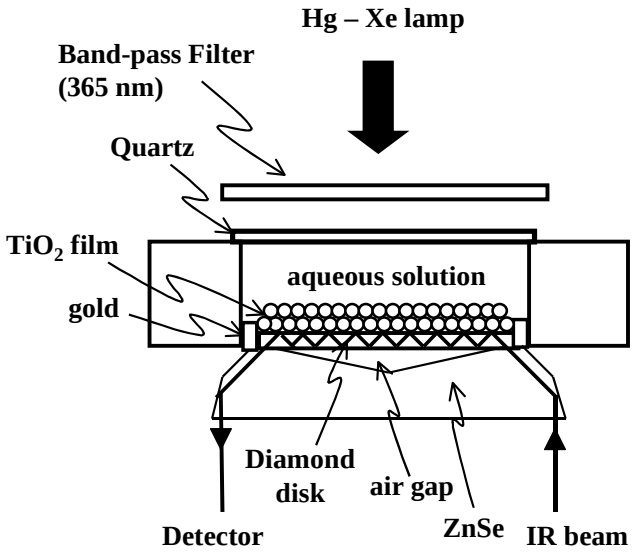

Figure 1 Schematic illustration of a spectral cell used for in-situ MIR-IR absorption measurements.

Results

In situ FTIR measurements: Figure 2 shows MIR-IR absorption spectra for a particulate TiO_2 film in contact with a deoxygenated aqueous solution of 10 mM Fe^{3+} (pH 2.4). The absorption spectra after UV irradiation are plotted as a function of the illumination time, with the TiO_2 film before UV irradiation taken as the spectral reference. In general, both photogenerated conduction-band electrons (e^-) and valence-band holes (h^+) cause photoreactions at the TiO_2 surface for a particulate system, each producing various surface intermediates. The Fe^{3+} ions in Figure 2 were added to the solution as an electron scavenger in order to suppress the formation of surface intermediates caused by the conduction-band electrons[67].

The UV irradiation caused the appearance of a new peak at 838 cm^{-1} and shoulders at 812 and 928 cm^{-1}, as seen in Figure 2. The shoulder at 812 cm^{-1} was relatively prominent in the short irradiation times of 1 and 10 min, contrary to the 928-cm^{-1} band. The noise level in the region from 700 to 1000 cm^{-1} was confirmed to be less than 2×10^{-4} in absorbance after averaging by 400-time accumulation adopted in the present work. The appearance of the new bands at 838 and 812 cm^{-1} was independent of the presence or absence of dissolved oxygen in the solution, strongly suggesting that these bands were arising from intermediates of oxidation reaction of water by photogenerated holes. The independence of the IR bands on the concentration of dissolved O_2 also indicates that the concentration of 10 mM Fe^{3+} is sufficiently high to capture all photogenerated electrons in TiO_2. In accordance with this result, Ohno et al. reported[75] that the quantum efficiency of the oxygen photoevolution for suspended TiO_2 in aqueous Fe^{3+} was independent of the Fe^{3+} concentration in the range of 2 to 8 mM Fe^{3+}.

The diamond prism is completely transparent in a low-frequency region from 1500 to 600 cm^{-1} and thus has a high spectral sensitivity in this region, as mentioned earlier. However,

the prism has strong absorption in a region from 1900 to 2200 cm^{-1}, in which no spectral measurement is possible. Besides, the diamond prism shows a large number of absorption bands in a high-frequency region from 2300 to 4000 cm^{-1} probably owing to impurities in crystal, and therefore the prism is not necessarily suitable for spectral measurements even in this high-frequency region. Nevertheless, in the present work, We could observe small decreases in absorption bands due to contaminating hydrocarbons at around 2900 cm^{-1} by UV irradiation.

Spectra (a) in Figure 3 (solid lines) show FTIR spectra for a TiO_2 film in contact with a deoxygenated alkaline solution of pH 11.9, obtained by similar experiments to Figure 2. In this case, however, no electron scavenger was added to the solution because Fe^{3+} ions were unstable in pH ≥3, causing an oxyhydroxide precipitate. Instead the we used Pt-loaded TiO_2 particles in which Pt could act as a kind of electron scavenger because hydrogen evolution occurred on Pt by the conduction-band electrons. Only the 812-cm^{-1} band appeared by UV irradiation in an alkaline solution [spectra (a) in Figure 3], contrary to the case of an acidic solution in Figure 2. This result was confirmed by the fact that an FTIR spectrum [spectrum (b) in Figure 3] for Pt-loaded TiO_2, prepared in the same way as above, in contact with a deoxygenated acidic solution of pH 2.4 with no Fe^{3+}, showed the main band at 838 cm^{-1} and shoulders at 812 and 900-1000 cm^{-1}, similar to the spectra in Figure 2, though the band width or shape is somewhat different between Figure 2 and spectrum (b) in Figure 3. The reason for such a difference in detailed spectral features is unknown at present. The appearance of the 812-cm^{-1} band by UV irradiation in spectra (a) of Figure 3 is accompanied by a slight decrease in absorbance at about 1010 cm^{-1}, the reason for which is also unknown. Such small spectral deviations might most probably arise from low signal to noise ratios due to weak absorption intensities for the Pt-loaded TiO_2 system, owing to inefficient capture of conduction-band electrons by loaded Pt relative to Fe^{3+} ions.

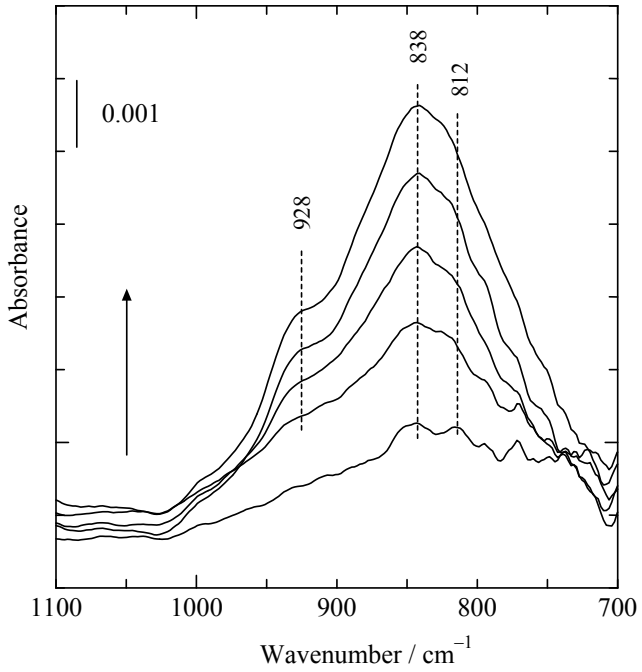

Figure 2 MIR-IR spectra of a TiO_2 film in contact with a deoxygenated aqueous solution of 10 mM Fe^{3+} (pH 2.4), recorded in 1, 10, 20, 30, and 40 min after the start of UV irradiation. A TiO_2 film before irradiation is taken as the reference. The arrow in the figure indicates the direction of the spectral change with the irradiation time.

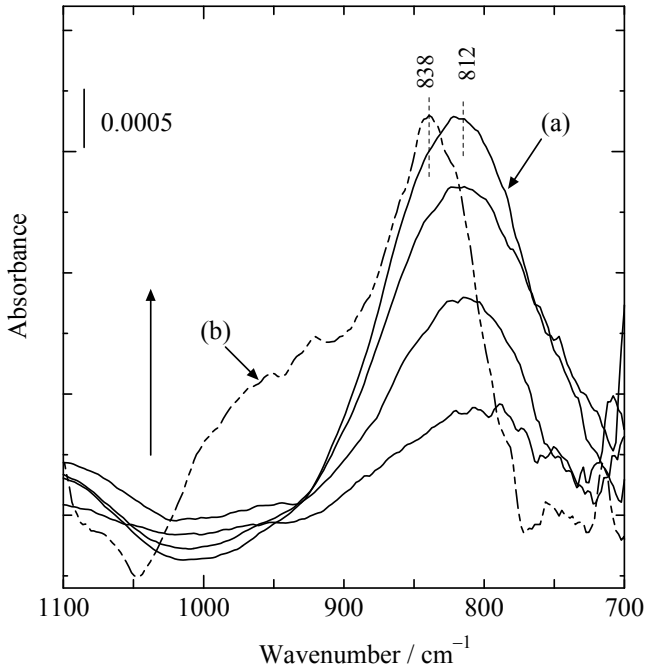

Figure 3 Spectra (a) (solid curves): MIR-IR spectra of a film of Pt-loaded TiO_2 in contact with aqueous 0.01 M NaOH of pH 11.9, recorded in 1, 10, 20, and 30 min after the start of UV irradiation. The arrow in the figure indicates the direction of the spectral change with time. Spectrum (b) (broken curve): MIR-IR spectrum for Pt-loaded TiO_2 in contact with 0.01 M HCl of pH 2.4 after 30-min UV irradiation. Spectrum (b) is expanded by a factor of 1.4 in absorbance.

We suggested above that the new bands at 838 and 812 cm^{-1} were arising from intermediates of the hole-induced oxidation reaction of water. In order to confirm this conclusion, we did several experiments. First, we examined the effect of adding methanol as a hole scavenger to the solution. Figure 4(A) shows an MIRIR spectrum, before UV irradiation, for a TiO_2 film in contact with an aqueous solution of 10 mM Fe^{3+} containing 25wt% methanol, the TiO_2 film in contact with an aqueous solution of 10 mM Fe^{3+} being taken as the spectral reference. The spectrum in Figure 4(A) shows bands at 1110, 1020, 944, and 905 cm^{-1}, of which the 1020- and 1110-cm^{-1} bands can be assigned to the C-O stretching of methanol and methoxy ($Ti\text{-}OCH_3$) species, respectively[43,76]. The origins of the 944- and 905-cm^{-1} bands are at present

unknown, though these bands are only observed for methanol-containing systems and evidently arising from methanol. The UV irradiation caused decreases in the intensities of these bands, as shown in Figure 4(B), indicating the effective occurrence of photo-oxidation of methanol at the TiO_2 surface. (Note that the absorbance scale is different between Figures 4A and 4B.) However, no absorption band appeared at 838 cm^{-1} in Figure 4(B), indicating no occurrence of the photooxidation of water. This result is quite reasonable if we take into account that methanol is more easily oxidized than water and thus the oxidation of methanol suppresses the water oxidation.[29,43,49] In other words, this result indicates that the band at 838 cm^{-1} in Figure 2 is arising from intermediates of the photooxidation reaction of water. Similarly, no appearance of the 812-cm^{-1} band was observed for Pt-loaded TiO_2 particles in an alkaline solution of pH 12.1 when 25wt% methanol was added to the solution.

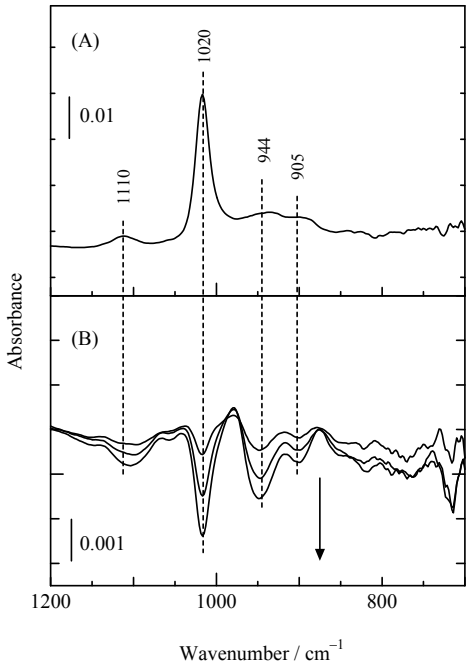

Figure 4 (A) An MIR-IR spectrum before UV irradiation for a TiO_2 film in contact with an aqueous solution containing 10 mM Fe^{3+} and 25wt% methanol. (B) MIR-IR spectra for the TiO_2 film, recorded in 1, 10, and 20 min after the start of UV irradiation. The arrow in the figure indicates the direction of the spectral change with time.

Second, we did isotope-labeling experiments by using $H_2{}^{18}O$ as a solvent. Spectrum (a) of Figure 5(A) shows the MIRIR spectrum for a particulate TiO_2 film in contact with $H_2{}^{18}O$ containing 10 mM Fe^{3+}. Spectrum (b) is measured under the same conditions as (a) except that $H_2{}^{16}O$ is used. Spectrum (b) is thus the same as in Figure 2. Both spectra (a) and (b) are for a relatively short irradiation time of 20 min, because the shoulder bands are more prominently observed in the shorter irradiation time, as mentioned earlier. We can see that spectrum (a) is shifted to the lower frequency side than spectrum (b) and has a larger number of shoulders than spectrum (b). This result is also in harmony with the conclusion that the observed bands are arising from intermediates of the water photooxidation reaction, as discussed in detail in the next section. Figure 5(B) shows some spectra for TiO_2 in contact with $H_2{}^{18}O$ with 10 mM Fe^{3+},

obtained independently by repeated experiments under the same conditions, in order to indicate the extent of experimental reproducibility in the spectra.

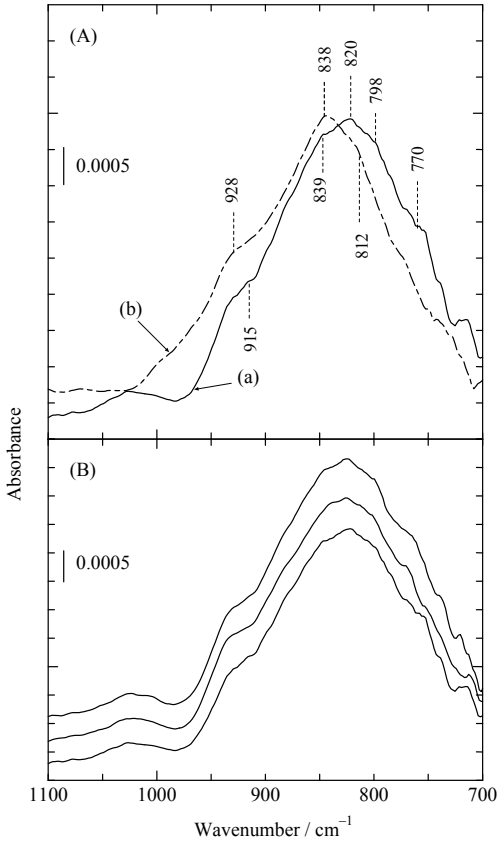

Figure 5 (A) MIR-IR spectra for a TiO_2 film in contact with (a) $H_2{}^{18}O$ and (b) $H_2{}^{16}O$, both containing 10 mM Fe^{3+}, observed after 20-min UV irradiation. (B) Spectra obtained independently by repeated experiments under the same conditions as (a) of Figure 5(A).

Third, we measured an MIR-IR spectrum for a particulate TiO_2 film on which hydrogen peroxide (H_2O_2) was adsorbed. Spectrum (a) in Figure 6 shows an IR spectrum for a particulate TiO_2 film exposed to an aqueous solution (pH 3.3) of 30% H_2O_2, with the TiO_2 film exposed to pure water used as the spectral reference. Spectrum (b) shows, for reference, the same spectrum as that in Figure 2 after the 20-min irradiation. We can see that the exposure of TiO_2 to H_2O_2 gives rise to a band peaked at 839 cm^{-1}, which is nearly identical with the 838-cm^{-1} band in Figure 2, and an additional sharp band at 877 cm^{-1}. The latter 877-cm^{-1} band

was observed when a diamond prism (IRE) with no TiO_2 film was exposed to the H_2O_2 solution, indicating that it can be assigned to free (or physically adsorbed) H_2O_2.[77, 78] On the other hand, the former 839-cm^{-1} band was observed only for a diamond prism with a TiO_2 film.

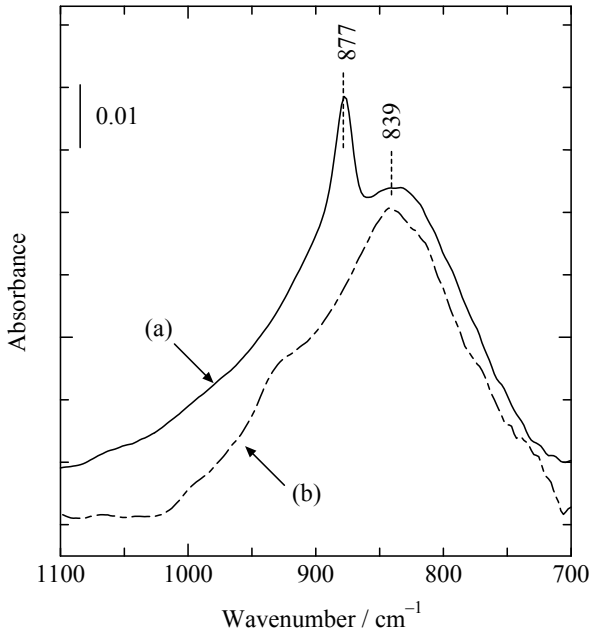

Figure 6 Spectrum (a): An MIR-IR spectrum of a TiO_2 film in contact with an aqueous solution of 30% H_2O_2. Spectrum (b): The same spectrum as that after the 20-min irradiation in Figure 2, for reference, with 13 times expansion in absorbance.

In situ PL measurements: The laboratory which the author belonged reported in previous papers[25-27,48-52] that photoelectrochemical etching of single crystal n-TiO_2 (rutile) electrodes in aqueous H_2SO_4 produced rectangular nano-holes or grooves in the <001> direction, with the (100) face selectively exposed at the walls of the holes and grooves. We also reported that the PL band peaked at 840 nm was observed only for the photoetched and thus the (100)-face exposed electrodes[51,52]. Figure 7 shows the photocurrent (*j*) vs. potential (*U*) and the PL

intensity (I_{PL}) vs. U for such a photoetched n-TiO_2 (rutile) electrode in an acidic (pH 1.2) and an alkaline (pH 11.9) solution. The UV irradiation was performed at 0.2 mW cm^{-2}. Both the I_{PL} vs. U and the j vs. U curves were measured in a positive potential scan simultaneously. The reported flat-band potential (U_{fb}) for rutile n-TiO_2[79,80] is indicated with a pH-correction of 0.059 V/pH. The PL intensity takes the maximum near the onset potential of the photocurrent, indicating that this is a surface carrier recombination luminescence. The weakening of the PL in potentials more negative than the U_{fb} can be explained to be due to chemical reduction of the TiO_2 surface (or formation of some reduced surface species such as Ti^{3+} acting as non-radiative recombination centers).

Figure 8 shows PL spectra for a photoetched n-TiO_2 (rutile) electrode. Spectrum (a) was observed in an acidic (pH 1.2) solution at 0 V vs. Ag/AgCl, whereas spectrum (b) was observed in an alkaline (pH 12.8) solution at –0.8 V, both with the irradiation intensity of 0.2 mW cm^{-2}. The spectral distributions of stray light, observed at 1.0 and 0.4 V, were taken as the background for spectrum (a) and (b), respectively. The spectral shape of both spectra (a) and (b) was not corrected for the spectral sensitivity of a photomultiplier used (Hamamatsu Photonics PMA100), but we can see that the PL spectra in acidic and alkaline solutions had the same position and shape with each other, indicating that the PL-emitting species is free from an acid-base equilibrium (or protonation and deprotonation).

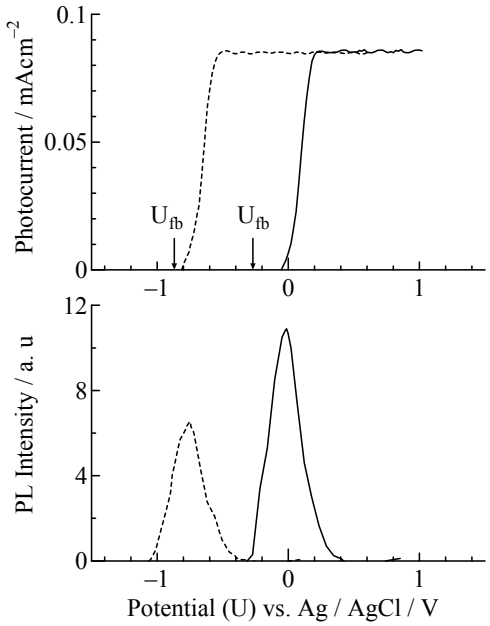

Figure 7 *j-U* and I_{PL}-*U* curves in an acidic (pH 1.2, solid curves) and an alkaline (pH 11.9, broken curves) solution for a photoetched n-TiO_2 electrode, observed by UV illumination at an intensity of 0.2 mWcm^{-2}. The I_{PL} is measured at 840 nm. The scan rate is 50 mV s^{-1}.

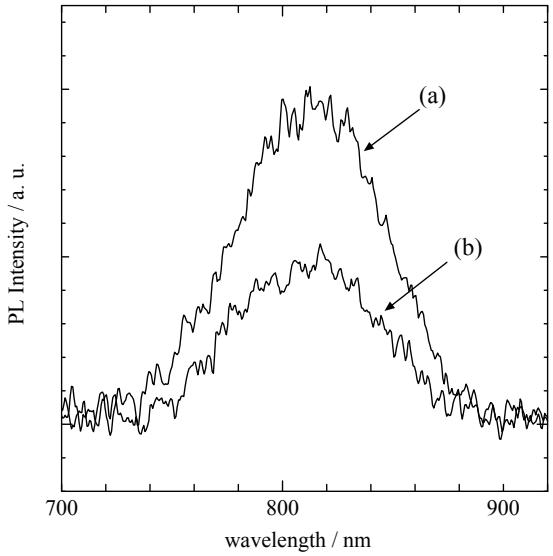

Figure 8 The PL spectrum for a photoetched n-TiO_2 electrode, observed in (a) acidic (pH 1.2) and (b) alkaline (pH 12.8) solutions.

Discussion

We mentioned in the preceding section that the UV irradiation of a particulate TiO_2 film in contact with an acidic solution with 10 mM Fe^{3+} caused the appearance of new bands at 838, 812, and 928 cm^{-1} (Figure 2). We also mentioned there that the new IR bands could be explained to be arising from surface intermediates of the oxygen photoevolution reaction on TiO_2 particles.

To what surface species are these bands assigned? The 838-cm^{-1} band for UV-irradiated TiO_2 in Figure 2 can be assigned to the O-O stretching mode of surface TiOOH species, for the following reasons. We have to note first in Figure 6 that this band is nearly identical with the 839-cm^{-1} band for H_2O_2-adsorbed TiO_2 in their spectral position and shape. Recent IR studies reported[77] that the exposure of Ti-silicalite molecular sieves (TS-1) to 30% H_2O_2 gave two IR bands at 837 and 877 cm^{-1} and that the former 837-cm^{-1} band could be assigned to the O-O stretching mode of a surface hydroperoxo species (TiOOH) whereas the latter 877-cm^{-1} band assigned to free H_2O_2. The IR bands at 839 and 877 cm^{-1} in spectrum (a) of Figure 6 are quite the same as the reported bands at 837 and 877 cm^{-1} [77] and thus can be assigned in the same way as the literature[77]. This implies that the 838-cm^{-1} band is assigned to TiOOH.

The shoulder at 812 cm^{-1} in Figure 2, on the other hand, appears as the main peak in an alkaline solution [spectrum (a) of Figure 3]. This result can be understood reasonably if we assume that the 812-cm^{-1} band is assigned to a surface peroxo species of a bridge type, Ti-O-O-Ti. It is very likely that the oxygen photoevolution reaction first produces Ti-O-O-Ti as a surface intermediate, but in an acidic solution, it changes into a hydroperoxo species, Ti-OOH, by protonation (or acid-catalyzed hydrolysis).

$$\text{Ti-O-O-Ti} + H_2O \rightarrow \text{Ti-OOH HO-Ti} \qquad (3)$$

The assignment of the 812-cm^{-1} band to Ti-O-O-Ti is also supported by IR studies of metal-dioxygen complexes[81-85], which report that the O-O stretching mode of a bridged peroxo species (μ-peroxo) is observed in a region of 790 to 840 cm^{-1}. A shoulder at 928 cm^{-1} in Figure 2 may tentatively be assigned to the O-O stretching of surface peroxo species, $Ti(O_2)$,[67,86-89] produced by photocatalytic reduction of O_2 molecules evolved by the oxygen photoevolution reaction.

The above assignments for the 838- and 812-cm^{-1} bands are in harmony with isotope labeling experiments. Spectrum (a) in Figure 5(A), observed for UV-irradiated TiO_2 in contact with $H_2{}^{18}O$, shows a number of IR bands at 915, 839, 820, 798, and 770 cm^{-1}, which can be understood reasonably on the basis of the above assignments. It is reported[77], by experiments of exposure of TS-1 to $H^{18}O^{18}OH$, that the O-O stretching band for TiOOH shifts from 837 cm^{-1} for Ti-^{16}O-^{16}OH to 793 cm^{-1} for Ti-^{18}O-^{18}OH, with an isotopic shift of 44 cm^{-1}. Accordingly we can assign the shoulder at 839 cm^{-1} in spectrum (a) to the O-O stretching mode for Ti-^{16}O-^{16}OH, the peak at 820 cm^{-1} to that for Ti-^{16}O-^{18}OH and Ti-^{18}O-^{16}OH, and the shoulder at 798 cm^{-1} to that for Ti-^{18}O-^{18}OH. It is quite reasonable that an observed isotopic shift of 19 cm^{-1} between Ti-^{16}O-^{18}OH or Ti-^{18}O-^{16}OH (820 cm^{-1}) and Ti-^{16}O-^{16}OH (838 cm^{-1}) is half the shift between Ti-^{16}O-^{16}OH (839 cm^{-1}) and Ti-^{18}O-^{18}OH (798 cm^{-1}).[81-85] On the other hand, the shoulder at 770 cm^{-1} can be assigned to the O-O stretching of Ti-^{18}O-^{18}O-Ti. The assignment also gives a reasonable isotope shift of 42 cm^{-1} for Ti-^{16}O-^{16}O-Ti (812 cm^{-1}) and Ti-^{18}O-^{18}O-Ti (770 cm^{-1}).[85-89]

Based on the above assignments, let us now consider the mechanism of the oxygen photoevolution reaction on TiO_2 (rutile). As mentioned in the Introduction section, we can say that two essentially different mechanisms have been proposed thus far. One mechanism assumes that the oxygen photoevolution is initiated by reaction (1), i.e., the oxidation of a surface OH

group by a photogenerated hole, which can be called “surface-OH oxidation mechanism”. The other mechanism assumes that the water photooxidation is initiated by reaction (2), a nucleophilic attack of a H_2O molecule on a surface-trapped hole at a lattice O site, which can be called “nucleophilic attack mechanism”. In the former “surface-OH oxidation mechanism”, resultant surface ·OH radicals, formed by reaction (1), couple with each other and produce H_2O_2.

$$2\,[\mathrm{Ti}\cdot\mathrm{OH}]_s^+ + 2H_2O \rightarrow H_2O_2 + 2\,\mathrm{Ti\text{-}OH} + 2H^+ \quad (4)$$

Resulting H_2O_2 is an easily oxidized compound and it will be oxidized further by photogenerated holes, finally resulting in molecular oxygen.

$$H_2O_2 + 2\,h^+ \rightarrow O_2 + 2H^+ \quad (5)$$

Accordingly, in the “surface-OH oxidation mechanism”, we can expect $\cdot OH_s$, $H_2O_{2\,ad}$, and Ti-OOH formed from $H_2O_{2\,ad}$, as surface reaction intermediates.

On the other hand, in the “nucleophilic attack mechanism”, reaction (2) produces surface $[\mathrm{Ti\text{-}O}\cdot\ \mathrm{HO\text{-}Ti}]_s$ radicals accompanied by bond breaking. When two radicals $[\mathrm{Ti\text{-}O}\cdot\ \mathrm{HO\text{-}Ti}]_s$ are produced accidentally in adjacent positions, they couple with each other, forming surface peroxo species, TiOOTi.

$$2\,[\mathrm{Ti\text{-}O}\cdot\ \mathrm{HO\text{-}Ti}]_s \rightarrow [\mathrm{Ti\text{-}O\text{-}O\text{-}Ti}]_s + [\mathrm{Ti\text{-}O\text{-}Ti}]_s + H_2O \quad (6)$$

Resultant $[\mathrm{Ti\text{-}O\text{-}O\text{-}Ti}]_s$ is expected to have a considerable steric distortion and thus be more reactive than the original $[\mathrm{Ti\text{-}O\text{-}Ti}]_s$ and therefore it will easily cause a reaction similar to reaction (2), finally leading to oxygen evolution together with restoration of the original $[\mathrm{Ti\text{-}O\text{-}Ti}]_s$.

$$[\mathrm{Ti\text{-}O\text{-}O\text{-}Ti}]_s + h^+ + H_2O \rightarrow [\mathrm{Ti\text{-}O\text{-}O}\cdot\ \mathrm{HO\text{-}Ti}]_s + H^+ \quad (7)$$

$$[\mathrm{Ti\text{-}O\text{-}O}\cdot\ \mathrm{HO\text{-}Ti}]_s + h^+ \rightarrow [\mathrm{Ti\text{-}O\text{-}Ti}]_s + O_2 + H^+ \quad (8)$$

Thus, in this mechanism, we can expect $[\mathrm{Ti\text{-}O\text{-}O\text{-}Ti}]_s$ and Ti-OOH as surface intermediates.

The in-situ FTIR studies in the present work give confirmative support to the latter "nucleophilic attack mechanism", as discussed below. First, the formation of surface peroxo species, TiOOH and TiOOTi, as reaction intermediates (Figures 2 and 3), strongly supports the "nucleophilic attack mechanism", as understood from the above arguments.

Second, the experiment of Figure 6 shows that the exposure of TiO_2 to H_2O_2 leads to a clear appearance of the 877-cm^{-1} band assigned to free (physically adsorbed) H_2O_2, indicating that this band should be observed if H_2O_2 was produced at the TiO_2 surface. Thus, no appearance of this band in Figure 2 indicates that H_2O_2 (or ·OH radicals as a precursor of it) was not produced as an intermediate of the oxygen photoevolution reaction. One might point out a possibility that H_2O_2, even if it was produced, would react with Fe^{2+}, formed by the reduction of Fe^{3+}, and disappear (Fenton reaction). We cannot exclude this possibility, but no appearance of the 877-cm^{-1} band in the spectrum for Pt-loaded TiO_2 in an acidic solution with no Fe^{3+} [spectrum (b) in Figure 3] indicates that this possibility is not important. Furthermore, under the assumptions that the "surface-OH oxidation mechanism" is the correct mechanism and that all produced H_2O_2 molecules react with Fe^{2+} and disappear, we can explain no appearance of the 877-cm^{-1} band but we cannot explain the production of surface peroxo species (TiOOH and TiOOTi) themselves. (The direct formation of TiOOTi via coupling of two adjacent $[Ti \cdot OH]_s^+$ radicals is impossible because of a long distance between the two radicals or the two Ti atoms.) In harmony with the above argument, Fujishima et al.[90] reported very recently that H_2O_2 formation was not detected on UV irradiated TiO_2 powder (P25) in the presence of Ag^+ as an electron acceptor.

Third, the "nucleophilic attack mechanism" is strongly supported by the isotope labeling experiments (Figure 5). We have to note first that the formation of ^{18}O-containing surface species, such as Ti-^{16}O-^{18}OH, Ti-^{18}O-^{16}OH, Ti-^{18}O-^{18}OH, and Ti-^{18}O-^{18}O-Ti, clearly

shows that surface TiOOH and TiOOTi, detected spectroscopically, are really formed by the water photooxidation reaction. The more important point is the formation of surface species containing both ^{16}O and ^{18}O such as Ti-^{16}O-^{18}OH and Ti-^{18}O-^{16}OH, which can be explained only by the "nucleophilic attack mechanism" for the following reasons. It is reported[91] by using $H_2{}^{18}O$ that oxygen exchange between surface hydroxyl groups of TiO_2 and water in contact with it occurs quantitatively and rapidly in the dark at room temperature, whereas that between lattice oxygen and contacting water hardly occurs under the same conditions. This implies that, for TiO_2 in contact with $H_2{}^{18}O$, all surface hydroxyl groups are substituted by ^{18}OH. Thus, the incorporation of ^{16}O into TiOOH unambiguously demonstrates that the water photooxidation is initiated by a nucleophilic attack of $H_2{}^{18}O$ to lattice oxygen (Ti-^{16}O-Ti). If the water photooxidation proceeded via the "surface-OH oxidation mechanism", only Ti-^{18}O-^{18}OH could be formed.

The "nucleophilic attack mechanism" is further supported by PL measurements. We mentioned in the preceding section that the PL spectra in acidic and alkaline solutions are the same in spectral position and shape with each other (Figure 8), indicating that the PL-emitting species is free from an acid-base equilibrium (i.e. it causes neither protonation nor deprotonation) in the pH range from 1 to 12. This result is in harmony with "nucleophilic attack mechanism" because, in this mechanism, the PL band is arising from the surface-trapped holes at the bottom of atomic grooves at the (100) face[51] (Figure 9). On the other hand, this result cannot be explained by the "surface-OH oxidation mechanism", for, in this mechanism, surface ·OH radicals or related species have to be a possible PL-emitting species. Actually, Salvador et al.[92] claimed long ago that the PL band was arising from adsorbed H_2O_2 or ·OH radicals. However, such species as H_2O_2 and ·OH cause deprotonation reaction in the pH range from 1 to 12, since pK_a of ·OH is reported to be 11.5[93] and that of H_2O_2 11.8[94]. The deprotonation reaction

should largely change the electronic energy level for a luminescent species (·OH or H_2O_2), thus causing a large spectral shift in the PL band, contrary to the experimental result.

Finally, it is interesting to note that UPS studies have shown[64] that the top of the O-2p levels for surface hydroxyl groups (Ti-OH) at the rutile TiO_2 (100) face is about 1.8 eV below the top of the valence band, E_v^s, at the surface. This implies that surface hydroxyl groups cannot be oxidized by photogenerated holes in the valence band. Although the above energy is obtained under vacuum (i.e. at the TiO_2/vacuum interface), the same conclusion holds even for the TiO_2/water interface. A difference is that a cation formed by photoelectron ejection at the TiO_2 surface is stabilized at the TiO_2/water interface additionally by electronic polarization of water. A simple calculation of the electronic polarization energy ΔG_{el} of water for surface Ti-OH by use of the Born equation, $\Delta G_{el} = (e^2/8\pi\varepsilon_0 r)(1-1/n^2)$, where r is the van der Waals radius for OH group of Ti-OH and n the refractive index of water, leads to a value of ΔG_{el} = 2.1 eV for r = 0.15 nm. For a surface species such as Ti-OH, only one half of this ΔG_{el} (namely 1.1 eV) contributes because water occupies only a half space at the TiO_2/water interface. We can thus conclude that the top of the O-2p levels for Ti-OH at the TiO_2/water interface is about (1.8 – 1.1 =) 0.7 eV below the E_v^s and thus Ti-OH cannot be oxidized by valence-band holes.

In conclusion, we can propose a reaction scheme of Scheme 1 as the most plausible molecular mechanism for the oxygen photoevolution reaction at the TiO_2 (rutile) surface in contact with aqueous solutions of pH less than about 12. Of various intermediates, surface peroxo species, TiOOTi and TiOOH, are directly detected by in situ FTIR experiments. Scheme 1 is supported by isotope labeling experiments and PL measurements. It is to be noted also that the surface species TiOOTi and TiOOH can really be regarded as intermediates of the oxygen photoevolution reaction on TiO_2, because it is reported[95] that stoichiometric oxygen evolution and Fe^{3+} reduction proceed with a high quantum efficiency of 17% under UV irradiation of a

TiO_2 (rutile)-8 mM Fe^{3+} system.

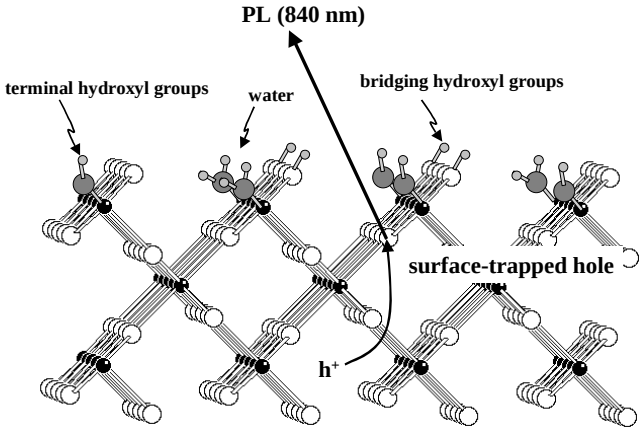

Figure 9 A schematic surface-lattice model for the (100) face of TiO_2 (rutile) in contact with an aqueous electrolyte, together with a photoluminescent process arising from a recombination of a surface-trapped hole at an atomic groove and an electron in the conduction band.

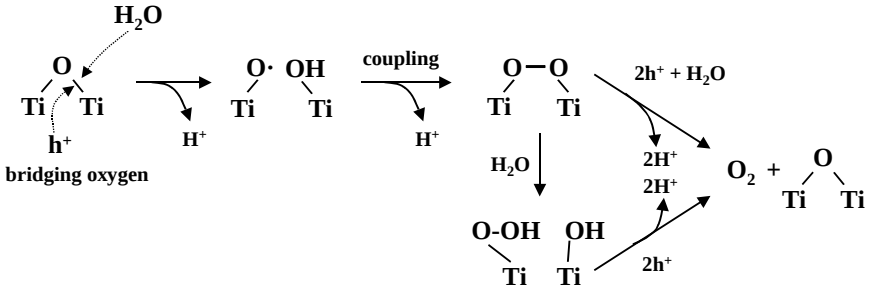

Scheme 1 A reaction scheme for the oxygen photoevolution reaction on TiO_2 (rutile) in contact with an aqueous solution of pH of 1 to about 12.

References

(1) Fujishima, A. ; Honda, K., *Nature* **1972**, *238*, 37.

(2) Sato, S, and White, M. *J., Chem. Phys. Lett.,* **1980**, *72,* 83.

(3) Khan, S. U. M.; Al-Shahry, M.; Ingler, W. B., Jr. *Science* **2002**, *297*, 2243.

(4) Kato, H.; Asakura, K.; and Kudo, A. *J. Am. Chem. Soc*. **2003**, *125*, 3082.

(5) Ollis, D. S.; Al-Ekabi, H.; Eds., *Photocatalytic Purification and Treatment of Water and Air*; Elsevier, Amsterdam, **1993**.

(6) Fujishima, A.; Rao, T. N.; Tryk, D. A. *J. Photochem. Photobiol. C: Photochem. Rev.* **2000**, *1*, 1.

(7) Hoffmann, M. R.; Martin, S. T.; Choi, W.; Bahnemann, D. W. *Chem. Rev.* **1995**, *95*, 69.

(8) Wang, R.; Hashimoto, K.; Chikuni, M.; Kojima, E.; Kitamura, A.; Shimohigashi, M.; Watanabe, T. *Nature* **1997**, *388*, 431.

(9) Sakai, N.; Fujishima, A.; Watanabe, T.; and Hashimoto, K. *J. Phys. Chem.* B. **2003**, *107,* 1028.

(10) White, J. M.; Szanyi, J.; and Henderson, M. A. *J. Phys. Chem.* B. **2003**, *107,* 1028. *107,* 9029.

(11) Kudo, A. Catalysis Surveys from Asia. **2003**, *7*, 31.

(12) Sato, S., *Chem. Phys. Lett.* **1986**, 123, 126.

(13) Asahi, R.; Morikawa, T.; Ohwaki, T.; Aoki, K.; Taga, Y. *Science* **2001**, *293*, 269.

(14) Hitoki, G.; Takata, T.; Kondo, J. N.; Hara, M.; Kobayashi, H.; and Domen, K.; *Chem. Commun.* **2002**, 1698.

(15) Ishikawa, A.; Takata, T.; Kondo, J. N. Hara, M. Kobayashi, H.; and Domen, K. *J. Am. Chem. Soc*. **2002**, *124*, 13547.

(16) Kato, H.; and Kudo, A.; *J. Phys. Chem. B* **2002**, *106,* 5029.

(17) Zou, A.; Ye, J.; Sayama, K.; and Arakawa, H. *nature* **2001**, *414*, 625.

(18) Ohno, T.; Mitsui, T.; and Matsumura, M.; *Chem. Lett.* **2003**, *32*, 364.

(19) Irie, H.; Watanabe, Y.; and Hashimoto, K.; *Chem. Lett.* **2003**, *32*, 772.

(20) Wilson, R. H. *J. Electrochem. Soc*. **1980**, *127*, 228.

(21) Salvador, P.; Gutiérrez, C. *Chem. Phys. Lett.* **1982**, *86*, 131.

(22) Salvador, P.; Gutiérrez, C. *J. Phys. Chem.* **1984**, *88,* 3696.

(23) Salvador, P.; Gutiérrez, C. *J. Electroanal. Chem.*, **1984**, *160*, 117.

(24) Salvador, P.; Gutiérrez, C. *Surf. Sci.,* **1983**, *124,* 398.

(25) Nakato, Y.; Tsumura, A.; Tsubomura, H. *Chem. Phys. Lett*. **1982**, *85,* 387.

(26) Nakato, Y.; Tsumura, A.; Tsubomura, H. *J. Phys. Chem.* **1983**, *87,* 2402.

(27) Nakato, Y.; Ogawa, H.; Moria, K.; Tsubomura, H. *J. Phys. Chem.* **1986**, *86,* 6210.

(28) Ulmann, M.; Tacconi, N.R.; and Augustynski, J. *J. Phys. Chem.* **1986**, *90,* 6523.

(29) Ulmann, M.; and Augustynski, *Chem. Phys. Lett.* **1987**, *141*, 154.

(30) Gerischer, H. *Electrochim. Acta* **1990**, *35*, 1677.

(31) Smandex, B.; and Gerisher, H. *Electrochim. Acta* **1989**, *34*, 1411.

(32) Poznyak. K. S.; Sviridov. V. V.; Kulak. A. I.; and Samtsov. M. P. *J. Electroanal. Chem.*, **1992**, *340*, 73.

(33) Lawless, D.; Serpone, N.; and Meisel, D. *J. Phys. Chem.* **1990**, *94*, 331.

(34) Rajh, T.; Sapomjic, Z. V.; Micic, O. I. *Langmuir* **1992**, *8*, 1265.

(35) Nakaoka, Y.; Nosaka, Y.; J. *Photochem. Photobio. A.* **1997**, *110*, 299.

(36) Liao, L.-F., Lien, C.-F., Shieh, D.-L., Chen, M.-T., and Lin J.-L. *J. Phys. Chem. B* **2002**, *106,* 11240.

(37) Szczepankiewicz, S. H.; Moss, J. A.; Hoffmann, M. R. *J. Phys. Chem. B* **2002**, *106,* 7654.

(38) Christensen, P.A; Eameaim, J.; Hamnett, A.; and Lin, W. F. *Chem. Phys. Lett.* **2001**, *344*,

488.

(39) Fujihara, K.; Izumi, S.; Ohno, T.; Matsumura, M. *J. Photochem. Photobio. A.* **2000**, *132*, 99.

(40) Ikeda, S.; Sugiyama, N.; Pal, B.; Marcïç, G.; Palmisano, L.; Noguchi, H.; Uosaki, K.; and Ohtani, B. *Phys. Chem. Chem. Phys*., **2001**, *3*, 267.

(41) Shaw. K.; Christensen, P.; and Hamnett, A.; *Electrochim. Acta* **1996**, *41*, 710.

(42) Yamakata, A.; Ishibashi, T.; and Onishi. H.; *J. Mol. Cata. A.* **2003**, *199*, 85.

(43) Yamakata, A.; Ishibashi, T.; and Onishi. H.; *J. Phys. Chem. B* **2003**, *107,* 9820.

(44) Wang, C-y.; Groenzin, H.; and Sultz, M. J. *Langmuir* **2003**, *19*, 7330.

(45) Nakamura, R.; Sato. S. *Langmuir* **2002**, *18,* 4433.

(46) Nakamura, R.; Sato. S. *J. Phys. Chem. B* **2002**, *106,* 5893.

(47) Diebold, U. *Surf. Sci. Rep*. **2003**, *48*, 53.

(48) Nakato, Y., Akanuma, H.; Shimizu, J.-I.; Magari, Y. J. *Electroanal. Chem*. **1995**, *396*, 35.

(49) Magari, Y.; Ochi, H.; Yae, S.; and Nakato, Y. *ACS Symposium Series No. 656, Solid/Liquid Electrochemical Interfaces*, The American Chemical Society, Washington, DC, **1996**, p. 297.

(50) Nakato, Y.; Akanuma, H.; Magari, Y.; Yae, S.; Shimizu, J.-I.; Mori, H. *J. Phys. Chem. B* **1997**, *101,* 4934.

(51) Kisumi, T.; Tsujiko, A.; Murakoshi, K., and Nakato, Y. J. *Electroanal. Chem*. **2003**, *545*, 99.

(52) Tsujiko, A.; Kisumi, T.; Magari, Y.; Murakoshi, K.; and Nakato, Y. *J. Phys. Chem. B* **2000**, *104,* 4873.

(53) Jaeger, C. D.; Bard, A. J. *J. Phys. Chem*., **1979**, *83*, 3146.

(54) Schwarz. P. F.; Turro, N. J.; Bossmann. S. H.; Braun, A. M.; Wahab. A.-M. A.; Dürr, H. *J. Phys. Chem*. B **1997**, *101*, 7127.

(55) Nosaka, Y.; Komori, S.; Yawata, K.; Hirakawa, T.; and Nosaka, Y. A. *Phys. Chem. Chem. Phys*., **2003**, *5*, 4731.

(56) Anpo, M.; Shima, T.; Kubokawa, Y. *Chem. Lett*. **1985**, 1799.

(57) Howe, R. F.; Gräetzel, M.; *J. Phys. Chem*. **1987**, *91*, 3906.

(58) Micic, O. I.; Zhang, Y.; Cromack, K. R.; Trifunac, A. D.; and Thurnauer, M. C. *J. Phys. Chem*. **1993**, *97*, 7277.

(59) Micic, O. I.; Zhang, Y.; Cromack, K. R.; Trifunac, A. D.; and Thurnauer, M. C. *J. Phys. Chem*. **1993**, *97*, 13284.

(60) Szczepankiewicz, S. H.; A. Colussi, J.; Hoffmann, M. R. *J. Phys. Chem. B* **2000**, *104*, 9842.

(61) Fan, J.; Yates, J. T., Jr. *J. Am. Chem. Soc*. **1996**, *118*, 4686.

(62) Ishibashi, K.; Fujishima, A.; Watanabe, T.; and Hashimoto, K. *J. Photochem. Photobiol. A* **2000**, *134*, 139.

(63) Brookes, I. M.; Muryn, C. A.; and Thornton. G. *Phys. Rev. Lett.* **2001**, *87*, 266103.

(64) Muryn, C. A.; Hardman, P. J.; Crouch, J. J.; Raiker, G. N.; Thornton. G. D.S.L. law, Surf. Sci. **1991**, *215-242*, 747.

(65) Henderson, M. A. *Surf. Sci. Rep*. **2002**, *46*, 1.

(66) Schaub, R.; Thostrup, P.; Lopez, N., Lægsgaard, E.; Stensgaard, I.; Nørskov, J. K.; and Besenbacher, F. *Phys. Rev. Lett.* **2001**, *87*, 266104.

(67) Nakamura, R.; Imanishi, A.; Murakoshi, K.; and Nakato, Y., *J. Am. Chem. Soc*. **2003**, *125*, 7443.

(68) Clark, R. J. H.; Hester R. E. *Spectroscopy for Surface*; John Wiley & Sons, New York, **1998**; p.219-272.

(69) Suëtaka. W. *Surface Infrared and Raman Spectroscopy*; Plenum press, New York, **1996**.

(70) Connor, P. A.; McQuillan, A. J. *Langmuir* **1999**, *15,* 2916.

(71) Ronson, T. K.: McQuillan, A. J. *Langmuir* **2002**, *18,* 5019.

(72) Nazeeruddin, M. K.; Amirnasr, M.; Comte, P.; Mackay J. R.; McQuillan, A. J.; Houriet, R., Grätzel, M. *Langmuir* **2000**, *16,* 8525.

(73) Connor, P. A.; Dobson, K. D.; and McQuillan, A. J. *Langmuir* **1999**,*15,* 2402.

(74) Ekström, G. N.; McQuillan, A. J. *J. Phys. Chem. B* **1999**, *103,* 10562.

(75) Ohno, T.; Haga, D.; Fujihara, K.; Kaizaki, K.; and Matsumura, M. *J. Phys. Chem. B* **1997**, *101,* 6415.

(76) Yamakata, A.; Ishibashi, T.; and Onishi. H.; *J. Phys. Chem. B* **2002**, *106,* 9122.

(77) W. Lin and H. Frei, *J. Am. Chem. Soc*. **2002**, *124*, 9293.

(78) Tozzola, G.; Mantegazza, M. A.; Ranghino, G.; Petrini, G.; Bordiga, S.; Ricchiardi, G.; Lamberti, C.; Zulian, R.; and Zecchina, A. *J. Catal*. **1998**, *179*, 64.

(79) Butler, M.; Ginley, D. D. *J. Electrochem. Soc*. **1979**, *125*, 228

(80) Tomkiewicz, M. *J. Electrochem. Soc*. **1979**, *126*, 1505.

(81) Yamada, H.; and Hurst, J. K. *J. Am. Chem. Soc*. **2000**, *122*, 5303.

(82) Root, D. E.; Mahroof-Tahir, M.; Karlin, K. D.; and Solomon, E. I. *Inorg. Chem*. **1998**, *37*, 4838

(83) Jones, R.; Summerville, D. A.; and Basols, F. *Chem. Rev*. **1979**. *79*, 2.

(84) Nakamoto, K.; Nonaka, Y.; Ishiguro, T.; Urban, M. W.; Suzuki, M.; Kozuka, M.; Nishida, Y.; and Kida, S. *J. Am. Chem. Soc*. **1982**, *104*, 3386.

(85) Nakamoto, K., *Infrared and Raman Spectra of Inorganic and Coordination Compounds*; John Wiley & Sons, New York, **1986**.

(86) Gutsev, G. L.; Rao, B. K.; Jena, P. *J. Phys. Chem. A* **2000**, *104,* 11961.

(87) Muller J., K.; Schwarzenbach, G. *Inorg. Chem.* **1970**, *9,* 2381.

(88) Miksztal, R.; Valentine, J. S. *Inorg. Chem.* **1984**, *23*, 3548.

(89) Kristine, F. J.; Shepherd, R. E.; Siddiqui, S. *Inorg. Chem.* **1981**, *20*, 2571.

(90) Cai, R.; Kubota, Y.; and Fujishima, A. *J. Catal.* **2003**, *219*, 214.

(91) Sato, S. *J. Phys. Chem.* **1987**, *91,* 2895.

(92) Salvador, P.; and Gutiérrez, C. *J. Phys. Chem.* **1984**, *16,* 3698.

(93) Poskrebyshev, G. A.; Neta, P.; and Huie, R. E. *J. Phys. Chem. A* **2002**, *106,* 11488.

(94) Weast. R. C. *Handbook of chemistry and physics*, **1993**, CRC Press, Boca Raton.

(95) Fujihara, K.; Ohno, T.; Matsumura, M. *J. Chem. Soc., Faraday Trans.* **1998**, 94, 3705.

Chapter 3

Crystal-Face Dependences of Surface Band Edges and Hole Reactivity, Revealed by Preparation of Essentially Atomically-Smooth and Stable (110) and (100) n-TiO_2 (Rutile) Surfaces

Introduction

Titanium dioxide (TiO_2) and related metal oxides have attracted keen attention recently in view of solar-to-chemical conversion (water splitting)[1] and photocatalytic environmental cleaning[2]. Strong merits of these materials lie in the high photoxidation ability and the chemical stability. A serious shortcoming of large band-gaps for these materials is now about to be overcome by findings[3] that doping with N, S, C or other elements leads to extension of the photoactive region to the visible light. For realizing practicable efficient systems, the understanding of photoreaction mechanisms at atomically well-defined surfaces is of crucial importance.

To date, the atomically well-defined TiO_2 surfaces have been prepared by a method of Ar^+-ion sputtering and thermal annealing under ultrahigh vacuum (UHV) conditions[4a]. Very recently, some studies were reported by using this method on the influence of atomic arrangements of the (110), (100), and (001) TiO_2 (rutile) surfaces on catalytic[4a,d] and photocatalytic[4b,c,e-g] reactions of adsorbed molecules. However, we have to note that the TiO_2 surfaces prepared under UHV are quite different in structures and properties from those in actual photocatalyst systems, in which the TiO_2 surfaces are in contact with aqueous solutions or air. For the TiO_2 surfaces in contact with aqueous solutions, significant reconstruction, including hydrolysis and ion-adsorption, should occur. The same holds for the surfaces placed in air because it is reported[5] that more than several monolayers of water are adsorbed on them at room temperature.

There is another problem in the atomically flat surfaces prepared by the Ar^+-ion sputtering and thermal annealing under UHV. Onishi et al. reported[6] that the atomically flat TiO_2 (rutile) (110) surfaces prepared by this method became morphologically rough after

exposition to neutral or alkaline aqueous solutions. This implies that the surfaces of this type are unstable in aqueous solutions.

In the present chapter, the author reports that essentially atomically-smooth TiO_2 (rutile) (110) and (100) surfaces are prepared by an alternative method of chemical etching and thermal annealing under the atmosphere[7]. Interestingly, the TiO_2 surfaces prepared by this method were stable in aqueous solutions of pH 1 to 13, suggesting that they were free from damage and defects that may induce etching reactions. The investigations of crystal-face dependences of surface band edges and hole reactivity became possible by this success in preparation of such atomically smooth and stable TiO_2 surfaces.

Experimental

Single crystal rutile n-TiO_2 (99.99% in purity) wafers, doped with 0.05 wt% Nb oxide, were obtained from Earth Chemical Co., Ltd. The wafers were of an n-type as they were, since a very small amount of doped Nb^{4+} acted as an electron donor. The surfaces of the wafers were cut in parallel to the (100) and (110) faces, and polished mechanochemically with an alkaline solution of colloidal silica particles. The atomically smooth surfaces were obtained by a procedure of washing with acetone, immersing in 20% HF for 10 min, washing with water, drying in a nitrogen stream, and annealing at 600°C for 1 h in air. X-ray photoelectron spectroscopic (XPS) analysis showed that no fluorine atom was left at the surface.

Surface morphology was inspected with an atomic force microscope (AFM, Digital Instruments NanoScope IIIa) at room temperature, the samples being placed in air. All AFM images were obtained in a tapping mode with a silicon tip (Digital Instruments) at a driving frequency of about 280 kHz and a scan rate of 1.5 Hz. Low energy electron diffraction (LEED)

measurements were carried out with the electron energy of 103 eV under a vacuum of 1×10^{-10} Torr at room temperature. In both the AFM and LEED experiments, the as-prepared surfaces were used as samples with no additional pre-treatment.

Photocurrent density (j) vs. potential (U) curves for single crystal n-TiO_2 electrodes were measured with a commercial potentiostat and a potential programmer, using a Pt plate as the counter electrode and an Ag/AgCl/sat.KCl electrode as the reference electrode. The illumination was carried out by the 365-nm band from a 500-W high-pressure mercury lamp, obtained by use of band-pass filters. The PL intensity (I_{PL}) vs. U curves were measured simultaneously with the j-U curve measurements. Electrolyte solutions were prepared by use of regent-grade chemicals and pure water, the latter of which was obtained from deionized water by purification with a Milli-Q Water Purification System. The electrolyte solutions under experiments were bubbled with a nitrogen gas to remove dissolved O_2.

Results and Discussion

The surfaces of the commercially obtained n-TiO_2 wafers were not smooth on an atomic scale, with a number of depressions and grooves of 0.2 to 0.8 nm in depth, as reported previously[8], suggesting that a variety of crystal faces were exposed. Actually, the wafers showed no distinct difference in the surface band edges and the photoelectrochemical behavior between the (110)- and (100)-cut surfaces. However, the aforementioned procedure of immersion in 20% HF and annealing at 600°C largely changed the surface morphology. Figures 1(a) and (b) show AFM images for the (100)- and (110)-cut surfaces after the above procedure. Both the surfaces showed clear step and terrace structures, with the step height of 0.27 nm for the (100) surface and 0.35 nm for the (110) surface, which are in good agreement with the

corresponding step heights in a crystal model of rutile TiO_2 [0.25 nm for (100) and 0.36 nm for (110)]. One may note that some protrusions with the height lower than the single-step height exist in the terrace part of the AFM topography in Figures 1(a) and (b). This will probably be due to experimental noises, though we cannot exclude completely a possibility that small atomic clusters exist here and there at the terrace. We can thus conclude that essentially atomically-smooth surfaces are prepared by the present method.

Figures 1(c) and (d) show LEED patterns for the same (100) and (110) surfaces as above. Both the surfaces gave sharp intense (1×1) LEED spots, indicating the formation of essentially atomically-smooth (100) and (110) surfaces, in agreement with the AFM experiments. We have to note here that no change in the surface morphology occurred by exposition to aqueous solutions of pH 1 to 13, i.e., 0.1 M $HClO_4$, 0.05 M Na_2SO_4 (pH 6.5), pure water, and 0.1 M NaOH, for 90 min, indicating that the atomically smooth (100) and (110) surfaces prepared by the present method were stable enough in aqueous solutions, contrary to the surfaces prepared by the ion sputtering and annealing under UHV[6].

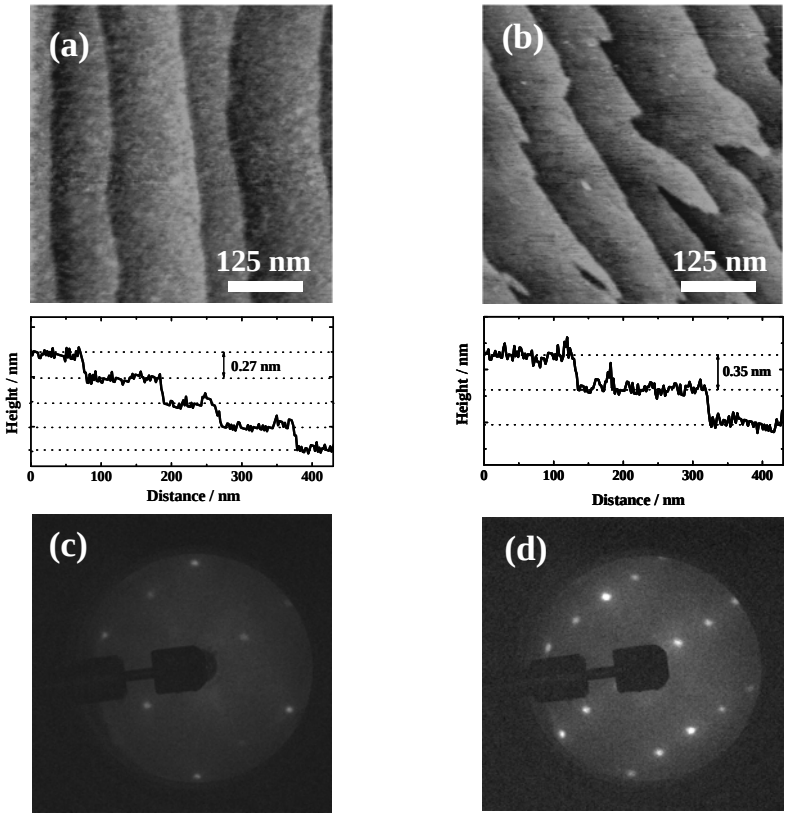

Figure 1 (a) and (b): AFM images, and (c) and (d): LEED patterns, for the (100)- and (110)-cut surfaces, respectively, of 0.05 wt% Nb-doped TiO_2 (rutile) single crystal wafers after surface-smoothing treatments of immersion in 20% HF for 10 min and annealing at 600°C for 1 h in air.

We next investigated the crystal-face dependences of the surface band edges and water photoxidation reaction by using the TiO_2 wafers with the atomically smooth and stable

(100) and (110) surfaces. The n-TiO_2 electrodes were prepared by obtaining ohmic contact with indium-gallium alloy. The surface band edge, or the bottom of the conduction band at the surface of n-TiO_2 (E_c^s) was estimated from the flat-band potential (U_{fb}) by the following equation, which holds if the E_c^s and U_{fb} are measured with respect to the same reference level,

$$E_c^s = -qU_{fb} + \Delta \quad (1)$$

where q is the elementary charge and Δ is a small energy difference between the bottom of the conduction band (E_c) and the Fermi level (E_F) in the interior of a semiconductor. The U_{fb} was determined from Mott-Schottky plots, i.e., plots of the inverse square of the differential capacitance (C) of the n-TiO_2 electrode against the applied electrode potential (U). The C was measured with a Solartron 1260 impedance analyzer combined with a Solartron 1287 potentiostat at the modulation frequency (f) of 10 to 1000 Hz and the amplitude of 5 mV.

Figures 2(a) and (b) show the Mott-Schottky plots for n-TiO_2 electrodes with the atomically smooth (100) and (110) surfaces, respectively. Good straight lines were obtained with no deviation by change in the modulation frequency, indicating that the electrode surfaces were really free from damage and defects. In fact, such frequency-independent good straight lines for n-TiO_2 were first obtained in the present work. The flat-band potential (U_{fb}) was determined from intersection of extrapolation of the straight line with the U axis. Interestingly, the U_{fb} for the (100) surface in 0.1 M $HClO_4$ (pH 1.0), determined to be –0.34 ± 0.01 V, was about 0.10 V more negative than that for the (110) surface, –0.25 ± 0.01 V. A similar difference in the U_{fb} was obtained in 0.1 M NaOH (pH 12.7), namely, the U_{fb} for the (100) surface in 0.1 M NaOH was determined to be –1.06± 0.01 V, whereas that for the (110) was –0.98 ± 0.01 V. The U_{fb} for both surfaces shifted with pH at a rate of –59 mV/pH. The crystal-face dependence of the U_{fb} was reported for anatase-type TiO_2 in an acidic solution though the surface structure in this case was not regulated on an atomic scale[9].

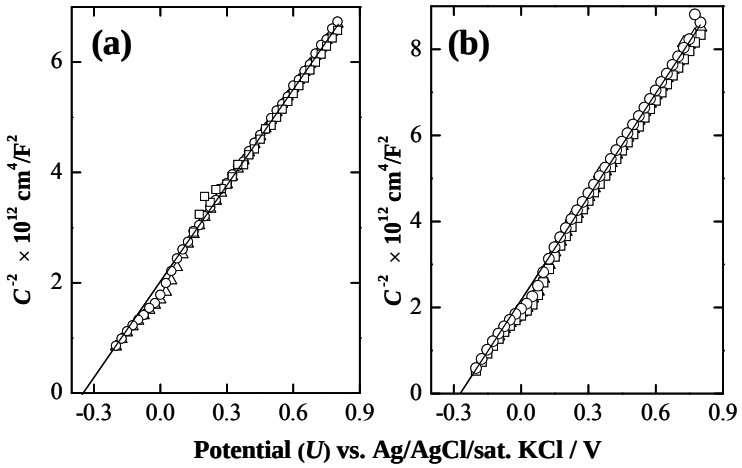

Figure 2 (a) and (b): Mott-Schottky plots for the atomically flat (100) and (110) TiO_2 (rutile) surfaces, respectively. ○ 10 Hz, Δ 100 Hz, and □ 1000 Hz. Electrolyte: 0.1 M $HClO_4$.

The water photoxidation reaction on n-TiO_2 was investigated by measurements of the photocurrent density (j) vs. U and the photoluminescence (PL) intensity (I_{PL}) vs. U. Figure 3(A) compares the j vs. U for the atomically smooth (110) and (100) n-TiO_2 electrodes, where the anodic photocurrent is due to oxygen photoevolution (or water photoxidation). The onset potential of the photocurrent for the (100) surface was about 0.1 V more negative than that for the (110) surface, in agreement with the negative shift in the U_{fb} mentioned above. As the onset potential of the photocurrent is deviated from the U_{fb} to the positive for both the (110) and (100) surfaces, the result may indicate that surface carrier recombination is similar between these surfaces. The j vs. U for the commercially obtained (110)- and (100)-cut n-TiO_2 electrodes with

no surface-smoothing treatment were rather similar to that for the atomically smooth (110) electrode.

Figure 3(B) shows the I_{PL} vs. U for the atomically smooth (110) and (100) n-TiO_2 electrodes, together with the commercially obtained (110)-cut n-TiO_2 with no surface-smoothing treatment for reference. A clear crystal-face dependence of the PL emission was observed, i.e., the PL band, peaked at 840 nm[10], from the atomically smooth (100) surface was much higher in intensity than that from the atomically smooth (110) surface, and no PL was observed from the commercially obtained (110)-cut [and (100)-cut] surfaces with no surface-smoothing treatment. A similar conclusion was reported in a previous paper[8,11], namely, we reported[8,11] that the photoetching of n-TiO_2 (rutile) in aqueous H_2SO_4 led to selective exposition of the (100) face and that the PL was observed only for the photoetched [thus the (100)-face exposed] n-TiO_2 electrode. Such sharp crystal-face dependences clearly indicate that the PL band is due to surface carrier recombination, not due to bulk carrier recombination. This assignment is in agreement with the fact that the PL is observed only in a potential region near the onset potential of photocurrent. The disappearance of the PL at potentials much more negative than the onset potential can be attributed[10a,e] to the formation of reduced surface species such as Ti^{3+} at these negative potentials, with which photogenerated holes recombine non-radiatively.

Now, let us consider what is the PL emitting species and why the (100) face shows strong PL emission. We reported in a previous paper[10a,e] that the PL arose from an intermediate (or a precursor) of oxygen photoevolution reaction on n-TiO_2 (rutile). This conclusion was derived from the findings that both the PL and the oxygen photoevolution were suppressed by addition of a suitable reductant to the electrolyte and that a reductant, which suppressed the PL strongly, suppressed the oxygen photoevolution strongly. There was a good correlation between

the extent of suppression of the PL and that of the oxygen photoevolution among various reductants. If we consider that the PL and the oxygen photoevolution are suppressed by reaction of photogenerated holes with the added reductant, the above result indicates that the luminescent species acts as an intermediate of the oxygen photoevolution reaction.

We further reported later[8] from studies on the photoetching behavior of n-TiO_2 in aqueous H_2SO_4 that a photogenerated hole coming to the surface was trapped there, resulting in a surface trapped hole (STH), and the oxygen photoevolution (water photoxidation) was initiated by a nucleophilic attack of a water molecule (as a Lewis base) to the STH (as a Lewis acid),

$$[Ti–O–Ti]_s + h^+_{VB} \rightarrow [Ti–O\cdots Ti]^+_s \quad (STH) \qquad (2)$$

$$[Ti–O\cdots Ti]^+_s + H_2O \rightarrow [Ti–O\bullet \quad HO–Ti]_s + H^+ \qquad (3)$$

where h^+_{VB} refers to a (photogenerated) valence-band hole. This mechanism was recently confirmed by in situ detection of primary surface intermediates of the oxygen photoevolution reaction by multiple internal reflection FTIR spectroscopy[12] (Chapter 2) and also by studies on the oxygen photoevolution mechanism on visible-light responsive N-doped TiO_2[13] (Chapter 4). In these studies, the PL band was assigned[8,12,13], as a most plausible assignment, to radiative recombination between a conduction-band electron (e^-_{CB}) and a surface-trapped hole, $[Ti–O\cdots Ti]^+_s$.

$$[Ti–O\cdots Ti]^+_s + e^-_{CB} \rightarrow h\nu \,(PL) \qquad (4)$$

The strong PL emission from the (100) face can be explained by the above model. The surface-trapped hole (STH) at the (100) face exists at the bottom of atomic grooves, as schematically shown in Figure 4 by a crystal model, or in other words, the STH exists a little inside the surface, covered with Ti–OH groups. Thus, the STH at this face is hardly attacked by an H_2O molecule and kept stable. Accordingly, the STH at this face can accumulate and cause

strong PL emission. On the other hand, the STH at the (110) face is directly exposed to the aqueous electrolyte and thus may be relatively easily attacked by an H_2O molecule. This implies that the PL from the (110) face may become weak. For the commercially obtained (110)- and (100)-cut surfaces with no surface-smoothing treatment, a variety of crystal faces (with high index numbers and thus with high-density step and kink sites) are exposed, as mentioned before, and the STH at such surfaces will easily undergo the nucleophilic attack of H_2O through the step and kink sites, resulting in no PL emission. We can thus conclude that the sharp crystal-face dependence of the PL emission reflects that of the reactivity of valence-band holes with aqueous electrolytes.

The above model for the PL is supported by the difference in the PL energy between the (100) and (110) faces. Figure 5 compares the PL spectra for the atomically smooth (100) and (110) n-TiO_2 electrodes. Both spectra were observed at 0 V vs. Ag/AgCl, with the spectral distribution of stray light, observed at 1.5 V, being taken as the background. We can see that the PL spectrum for the (100) face is peaked at a longer wavelength (or a lower energy) than that for the (110) face, indicating that the energy level of the STH for the (100) faces, $E(STH_{100})$, is located above that for the (110) faces, $E(STH_{110})$. By taking into account that the PL is assigned to an electronic transition from the conduction band to the STH and that the U_{fb} at the (100) face is about 0.1 V more negative than that at the (110) face (Figure 2), the $E(STH_{100})$ is estimated about 0.14 eV above the $E(STH_{110})$. This difference in the E(STH) between the (100) and (110) faces can be explained on the basis of the aforementioned model of Figure 4 as follows.

It is expected that the formation of STH (eq. 2) is accompanied by distortion in the surface lattice. The energy level for the STH will thus move more upward as the surface lattice is more easily distorted. Comparing the (110) and (100) faces, the Ti-O=Ti_2 network (triply coordinated O atom) at the surface, at which the STH is located (Figure 4), for the (100) face

can be more easily distorted than that for the (110) face, because the Ti-O=Ti_2 network for the (110) face is fixed rigidly from all sides at the surface, whereas that for the (100) face is fixed only from the bulk side of TiO_2 crystal. Accordingly, the $E(STH_{100})$ become to lie above the $E(STH_{110})$, in harmony with the experiment (Figure 5).

We can finally say that the aforementioned models for the mechanism for the water photoxidation reaction and the PL are further supported by the following experiments. We examined the effect of the water photoxidation reaction on the surface morphology of the (100) and (110) surfaces. Figures 6(a) and (b) show AFM images for the atomically smooth (100) and (110) surfaces, respectively, after the water-oxidation photocurrent of 40 mA cm^{-2} flowed for 13 seconds by UV irradiation at 2.0 V vs. Ag/AgCl in 0.1 M $HClO_4$. The intensity of the incident UV light was 80 mW cm^{-2}, and the electricity passing across the unit area of the TiO_2 surface (Q_p) was 0.5 C/cm^2. Both the surfaces became morphologically rough, indicating that the water photoxidation reaction at a high current density (or a high illumination intensity) causes a structural change in the atomically smooth (100) and (110) surfaces. It is reasonable to assume that successive high-frequency occurrence of the water photoxidation reaction such as reaction (2) and (3) will lead to such a structural change. In other words, such a structural change would not occur if the water photoxidation reaction proceeded by a mechanism of the hole oxidation of surface hydroxyl group Ti-OH into Ti •OH radical. It should be mentioned also that the morphological rough surfaces such as shown in Figure 6 show no PL emission nor distinct crystal face dependence of the U_{fb}, thus behave in a similar way to the commercial cut surfaces with no surface-smoothing treatment.

In conclusion, the author has succeeded in preparing the essentially atomically-smooth and stable n-TiO_2 (rutile) (100) and (110) surfaces by the method of HF etching and thermal annealing. The success has enabled us to reveal the clear crystal-face

dependences of the surface band edges and hole reactivity. TiO_2 and related metal oxides are key materials for solar energy conversion and photocatalytic environmental cleaning. The present work has thus opened a new way to investigate the photocatalytic reactivity and stability of these materials on an atomic level, which is important to search for new active materials.

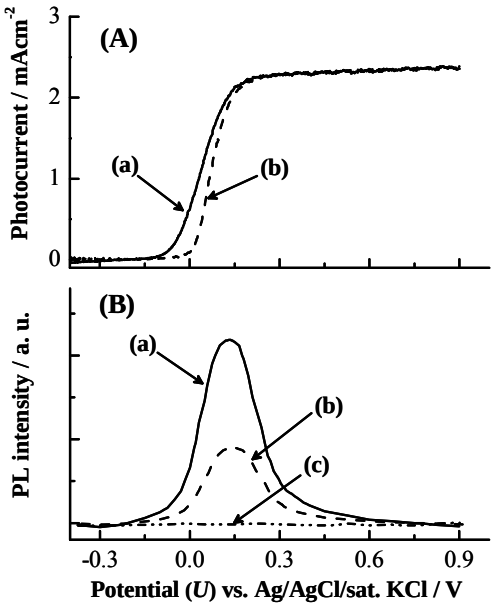

Figure 3 (A) The photocurrent density vs. potential (*U*), and (B) the PL intensity vs. *U* for the TiO_2 (rutile) surfaces. (a): The atomically flat (100) surface, (b) the atomically flat (110) surface, and (c) the commercially obtained (110)-cut surface with no surface-smoothing treatment. Electrolyte: 0.1 M $HClO_4$.

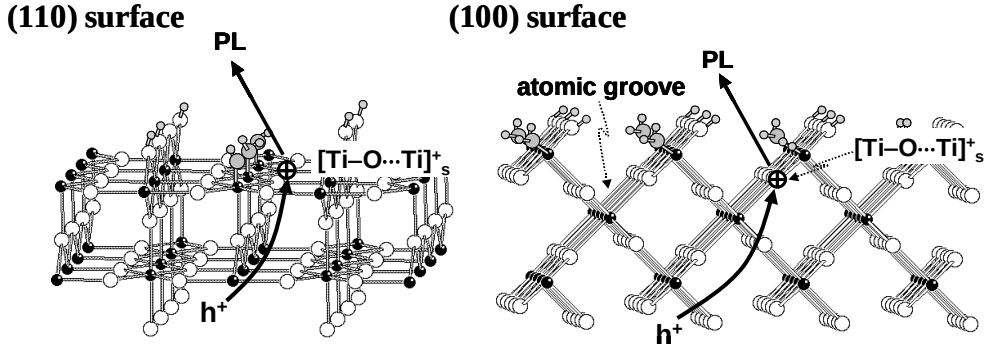

Figure 4 Schematic crystal models for the (110) and (100) TiO_2 (rutile) surfaces in an aqueous electrolyte after consideration of surface reconstruction.

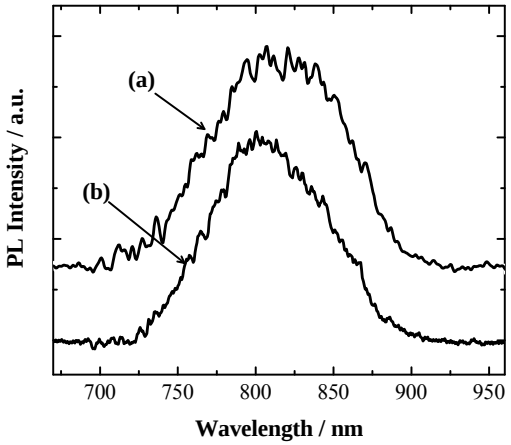

Figure 5 The normalize PL spectrum from the TiO_2 (rutile) surfaces. (a): The PL from the atomically smooth (100) surface, and (b) that from the atomically smooth (110) surface. Electrolyte: 0.1 M $HClO_4$.

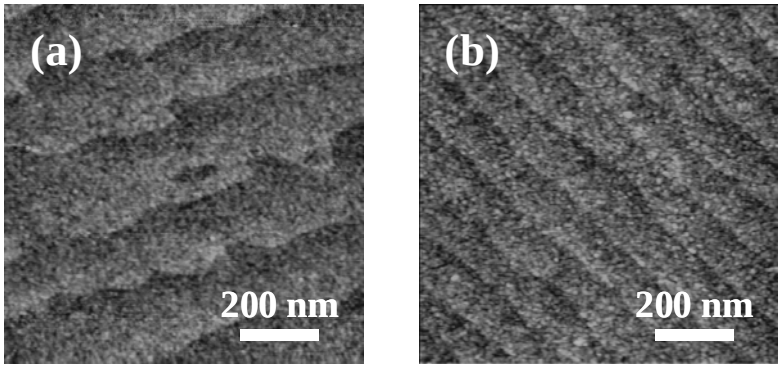

Figure 6 AFM images for the atomically smooth (a) (100)- and (b) (110)-cut surfaces after the water-photoxidation photocurrent of 40 mA cm^{-2} flowed for 13 seconds in 0.1 M $HClO_4$.

References

(1) (a) Fujishima, A.; Honda, K. *Nature* **1972**, *238*, 37. (b) Sato, S.; White, J. M. *Chem. Phys. Lett.* **1980**, *72*, 83. (c) Zou, A.; Ye, J.; Sayama, K.; Arakawa, H. *Nature* **2001**, *414*, 625.

(2) (a) Linsebigler, A.; Lu, G.; Yates, J. T., Jr. *Chem. Rev.* **1995**, *95*, 735. (b) Hoffmann, M. R.; Martin, S. T.; Choi, W.; Bahnemann, D. W. *Chem. Rev.* **1995**, *95*, 69.

(3) (a) Sato, S., *Chem. Phys. Lett.* **1986**, *123*, 126. (b) Asahi, R.; Morikawa, T.; Ohwaki, T.; Aoki, K.; Taga, Y. *Science* **2001**, *293*, 269. (c) Ohno, T.; Mitsui, T.; Matsumura, M. *Chem. Lett.* **2003**, *32*, 364. (d) Ishikawa, A.; Takata, T.; Kondo, J. N.; Hara, M.; Kobayashi, H.; Domen, K. *J. Am. Chem. Soc.* **2002**, *124*, 13547. (e) Irie, H.; Watanabe, Y.; Hashimoto, K. *Chem. Lett*. **2003**, *32*, 772.

(4) (a) Diebold, U. *Surf. Sci. Rep*. **2003**, *48*, 53. (b) Henderson, M. A.; White, J. M.; Uetsuka, H.; Onishi, H. *J. Am. Chem. Soc.* **2003**, *125*, 14974. (c) Mezhenny, S.; Maksymovych, P.; Thompson, T. L.; Diwald, O.; Stahl, D.; Walck, S. D.; Yates, J. T., Jr. *Chem. Phys. Lett.* **2003**, *369*, 152. (d) Henderson, M. A. *Surf. Sci. Rep*. **2002**, *46*, 1. (e)Wilson, J. N.; Idriss, H. *J. Am. Chem. Soc.* **2002**, *124*, 11284. (f) Brinkley, D.; Engel, T. *J. Phys. Chem. B.* **2000**, *104*, 9836. (g) Linsebrigler, A.; Lu, G.; Yates, J. T., Jr. *J. Phys. Chem. B.* **1996**, *100*, 6631.

(5) (a) Nosaka, A. Y.; Fujiwara, T.; Yagi, H.; Akutsu, H.; Nosaka, Y. *J. Phys. Chem. B.* **2004**, *108*, 9121. (b) Suda, Y.; Morimoto, T. *Langmuir* **1987**, *3*, 786.

(6) Uetsuka, H.; Sasahara, A.; Onishi, H. *Langmuir* **2004**, *20*, 4782.

(7) (a) Kawasaki, M.; Takahashi, K.; Maeda, T.; Tsuchiya, R.; Shinohara, M.; Ishiyama, O.; Yonezawa, T.; Yoshimoto, M.; Koinuma, H. *Science* **1994**, *266*, 1540. (b) Yamamoto, Y.; Matsumoto, Y.; Koinuma, H. *Appl. Surf. Sci.* **2004**, *238*, 189.

(8) Kisumi, T.; Tsujiko, A.; Murakoshi, K.; Nakato, Y. *J. Electroanal. Chem.* **2003**, *545*, 99.

(9) Hengerer, R.; Kavan, L.; Krtil, P.; Grätzel, M. *J. Electrochem. Soc.* **2000**, *147*, 1467.

(10) (a) Nakato, Y.; Tsumura, A.; Tsubomura, H. *J. Phys. Chem.* **1983,** *87,* 2402. (b) Nakato, Y.; Ogawa, H.; Moria, K.; Tsubomura, H. *J. Phys. Chem.* **1986,** *86,* 6210. (c) Poznyak. S. K.; Sviridov. V. V.; Kulak. A. I.; Samtsov. M. P. *J. Electroanal. Chem.*, **1992**, *340*, 73. (d) Nakato, Y., Akanuma, H.; Shimizu, J.-I.; Magari, Y. J. *Electroanal. Chem*. **1995**, *396*, 35. (e) Nakato, Y.; Akanuma, H.; Magari, Y.; Yae, S.; Shimizu, J.-I.; Mori, H. *J. Phys. Chem. B* **1997**, *101,* 4934.

(11) Tsujiko, A.; Kisumi, T.; Magari, Y.; Murakoshi, K.; Nakato, Y. *J. Phys. Chem. B* **2000**, *104,* 4873.

(12) Nakamura, R.; Nakato, Y. *J. Am. Chem. Soc.* **2004**, *126*, 1290.

(13) Nakamura, R.; Tanaka, T.; Nakato, Y. *J. Phys. Chem. B* **2004**, *108*, 10617.

Chapter 4

Mechanism for Visible Light Responses in Anodic Photocurrents at N-doped TiO_2 Film Electrodes

Introduction

Photo-induced oxidation and reduction reactions at the surface of TiO_2 particles or thin films have been attracting much attention in view of their possible application to solar energy conversion (water splitting)[1,2] as well as environmental cleaning (photodecomposition of waste materials and harmful compounds)[3,4]. TiO_2 has a high oxidation power under illumination. Also, it is chemically stable, non-toxic, and relatively inexpensive, but it has a serious disadvantage in that it can absorb only UV light.

Recent studies have revealed that the shortcoming of TiO_2 can be overcome by doping with other elements such as nitrogen [5,6], sulfur[7,8], carbon[9-11], etc. For example, Asahi et al.[5] reported that nitrogen-doped TiO_2 showed the photocatalytic activity for decomposition of acetone and methylene blue in wavelengths up to 550 nm. Khan et al.[9] also reported that carbon doping of TiO_2 extended the photoactive region for water oxidation from 400 to 535 nm, thus leading to a large increase in the water-splitting efficiency under white-light illumination.

The method of doping is thus indeed effective but we have to note that some problems may arise from this method. It is widely recognized[12] that doping of metal oxides with other elements produces electronic mid-gap states associated with dopants. The trapping of photogenerated holes at such mid-gap states will cause a decrease in their oxidation power. In addition, the doping may have a possibility to induce instability of TiO_2 owing to introduction of lattice distortion and bond weakening. It is thus important to investigate the mechanism of photooxidation reactions and stability for doped TiO_2, compared with those[3,4,13-15] for non-doped TiO_2. To date, a number of studies have been made[16-23] on the origin of the visible-light responses for doped TiO_2, but no clear experimental evidence has been given, and thus definite mechanism still seems to remain in dispute. In the present chapter, the author reports a definite mechanism for visible-light responses in water photooxidation (oxygen photoevolution) on

N-doped TiO_2, as revealed by photocurrent measurements with film electrodes.

Experimental

Nitrogen-doped TiO_2 powder was prepared by dry[5] and wet[6] methods. In the dry method, anatase TiO_2 powder (ST01, Ishihara Sangyo Co.) was heated at 550°C in an alumina tube reactor under dry NH_3 gas flow for 3 h. This sample will hereafter be called Sample A. In the wet method, 100 mL of aqueous solution of 28 % ammonia was added drop-wise to 25 mL of 95.0 % titanium tetraisopropoxide (TTIP) at 0°C with stirring, and a resulting precipitate was washed well with pure water. After evaporation of water, the white precipitate was gradually heated in air to raise the temperature slowly at a rate of 1°C/min up to 400°C, followed by maintaining at 400°C for 6 h[6]. The slow temperature raise was important to get high photoactivity. This sample will be called Sample B.

Film electrodes of N-doped TiO_2 for photocurrent measurements were prepared as follows: N-doped TiO_2 powder (0.25 g) was ground in a mortar for 1 h with 0.5 mL water and 0.1 mL acetylacetone added, and then transferred to 5 mL of 1.5 % HNO_3 under stirring, followed by addition of Triton X-100 at a ratio of 0.5 g per 20 mL solution. A resultant colloidal TiO_2 solution was applied on transparent conductive oxide (F-doped SnO_2) films on glass plates (Nippon Sheet Glass Co. Ltd., resistance ca. 20 Ω/square) using a spin coater at 2000 rpm, and heated at 150°C with an electric furnace. This procedure was repeated 6 times, and the TiO_2 films thus obtained were finally heated at 400°C for 3 h in air. A copper wire was attached on an edge of the F-SnO_2 film with silver paste, and the whole part, except a 1.0 × 1.0 cm^2 TiO_2-film area, was covered with epoxy resin for insulating.

Photocurrents for non-doped and N-doped TiO_2 film electrodes were measured as a

function of wavelength (λ), using a 350-W xenon lamp (Ushio) as the light source and a monochromator (Bunkoh-Keiki Co., M10-T) with a band width of 10 nm. The incident photon to current efficiency (IPCE) was calculated from the photocurrent by an equation

$$\text{IPCE}\ (\lambda) = 1240 \times j(\lambda) / \lambda\, I_0(\lambda) \times 100 \qquad (1)$$

where λ is the wavelength of light in a unit of nm, $j(\lambda)$ is the photocurrent density in mA cm^{-2} under illumination at λ, and $I_0(\lambda)$ the incident light intensity in mW cm^{-2} at λ. A Pt plate was used as the counter electrode, and an Ag/AgCl/sat. KCl was used as the reference electrode.

Results and Discussion

X-ray diffraction (XRD) analysis demonstrated that both sample A and B had an anatase form. SEM inspection showed that the film of sample A was about 3 μm thick and composed of TiO_2 particles of 0.2 to 1.0 μm in diameter, while that of sample B was about 5 μm thick and composed of particles of 0.5 to 1.5 μm in diameter. Both Sample A and B exhibited pale yellow color. In fact, the UV-visible absorption spectra for both samples showed a shoulder band at around 440 nm, indicating that nitrogen is really doped. However, XPS analysis showed no clear N 1s peak at 396 eV, assignable to N of Ti-N bonds[19,21], probably owing to a too small amount of N atoms in the N-doped TiO_2 film, though an N 1s peak at 400 eV probably assignable to adsorbed nitrogen compounds such as NO_x[24] or NH_x[22] was observed.

Figure 1 shows the IPCE vs. λ for an N-doped TiO_2 (sample A) film electrode in 0.1 M $HClO_4$, compared with that for a non-doped TiO_2 (ST01) film. The N doping caused an extension of photoresponse up to about 550 nm, as reported[5,6]. Since the electrolyte contains only indifferent (stable) ions, the observed photocurrents for both electrodes can be attributed to photooxidation of water (photoevolution of oxygen), though it was difficult to detect evolved

oxygen experimentally owing to a low current density.

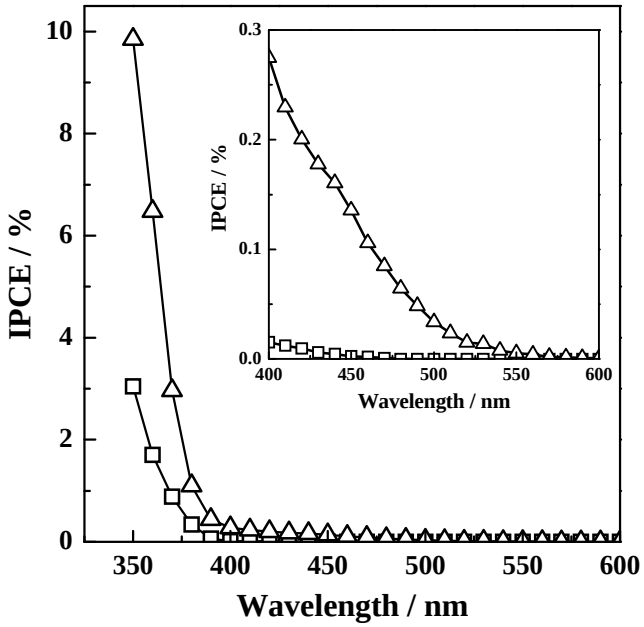

Figure 1 IPCE vs. λ for (Δ) N-doped TiO_2 (sample A) and (□) non-doped TiO_2 (ST01) in 0.1 M $HClO_4$ at 0.5 V vs. Ag/AgCl. The insert shows an expanded IPCE vs. λ in the visible-light region.

Figure 2 shows the effect of addition of 6 M methanol to the electrolyte (0.1 M $HClO_4$). The IPCE for N-doped TiO_2 (sample A) under UV illumination exhibited a large increase by a factor of 6 to 7 by the addition of methanol (Figure 2(a)), whereas that under visible-light illumination exhibited only a little increase by a factor of 1.1 to 1.4 (Figure 2(b)). Similarly, Figure 3 shows the effect of addition of other reductants such as 0.5 mM I^-, hydroquinone (H_2Q), SCN^-, and Br^-. The IPCE under UV illumination was increased by addition of all reductants (Figure 3(a)), whereas that under visible-light illumination was

increased only by addition of I^- and H_2Q (Figure 3(b)).

We made similar experiments for sample B and obtained quite the same results as the case of sample A. This indicates that the difference in the enhancement of the IPCE by addition of reductants between the visible- and UV-light irradiation is not due to a particular method of sample preparation but arising from the N doping itself.

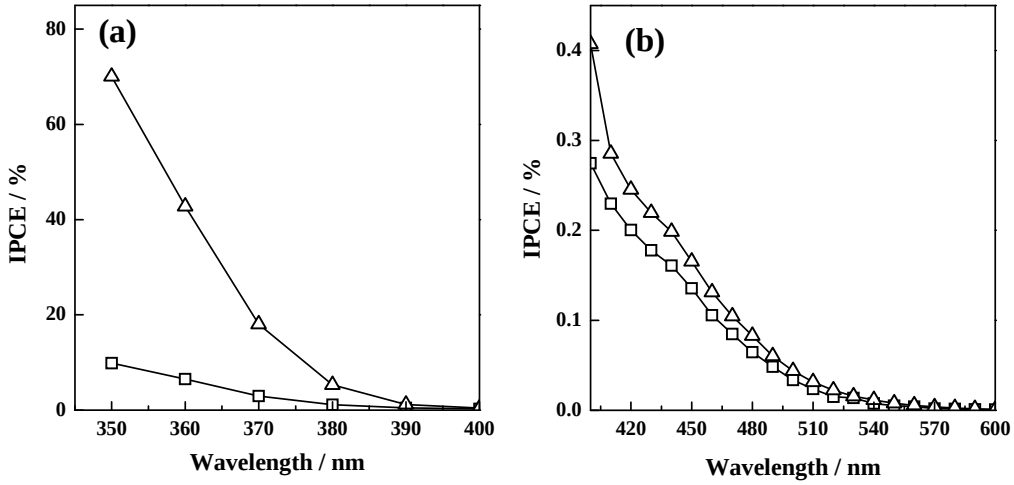

Figure 2 IPCE vs. λ for N-doped TiO_2 (sample A) in 0.1 M $HClO_4$ with (triangle) and without (square) 6 M methanol in the (a) UV and (b) visible-light regions. The electrode potential was 0.5 V vs. Ag/AgCl.

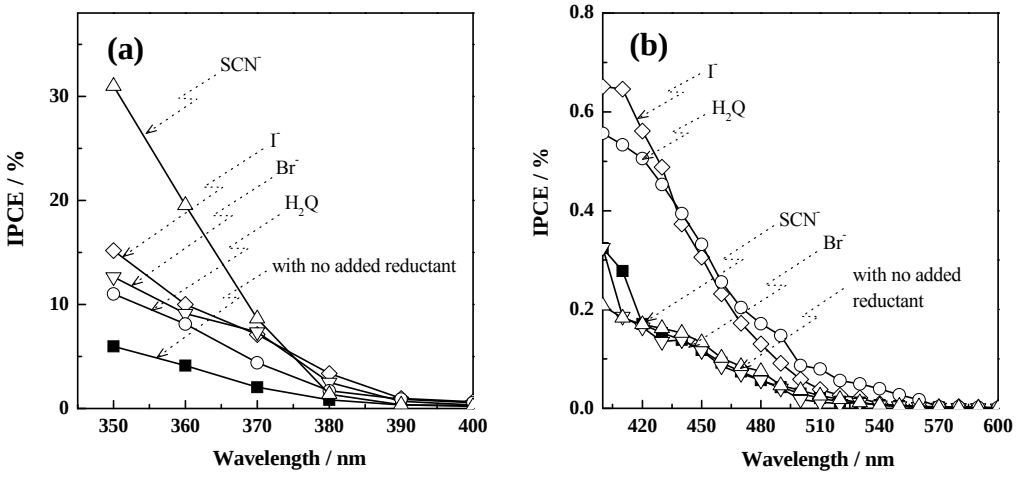

Figure 3 Effect of addition of 0.5 mM I^-, H_2Q, SCN^- and Br^- as a reductant on the IPCE vs. λ in the (a) UV- and (b) visible-light regions for N-doped TiO_2 (sample A) in 0.1 M $HClO_4$. The electrode potential was 0.5 V vs. Ag/AgCl.

As to the origin of visible light responses for N-doped TiO_2, different groups have proposed different mechanisms to date, and no definite conclusion has been obtained yet, as mentioned in the Introduction section. For example, Asahi et al.[5] reported, on the basis of calculations of band structures, that visible light responses for $TiO_{2-x}N_x$ (x = 0.25 and 0.12) arose from band narrowing by mixing of N 2p and O 2p orbitals. Ihara et al.[18] reported that N-doped TiO_2 powder contained not only N but also O vacancies and electronic levels due to the O-vacancies, lying slightly below the conduction band edge, were responsible for visible-light responses. Irie et al. reported[19] that $TiO_{2-x}N_x$ with $0.005 \leq x < 0.02$ showed low activity for photooxidation of 2-propanol under visible-light irradiation, compared with UV irradiation, similarly to the present work, and explained the result as being due to formation of an N-induced narrow band slightly above the top of the valence band. The conclusion of Irie et al. was, however, not decisive because their used method of product analysis included serious problems, as explained later. On the other hand, Sakatani et al. reported[20], using ESR measurements, that the visible responses arose from paramagnetic N species (such as NO, NO_2, etc.) that were existing initially in the dark and produced by UV and visible irradiation, though without showing any electronic band structure. However, Diwald et al. reported very recently[22], using XPS analysis, that doped nitrogen was existing in a form of NH_x in single crystal TiO_2 (rutile). In addition, Ihara et al. reported[18], using diffuse reflection IR spectroscopy, that NO_2, NO, and NH_3 were produced at the surface of N-doped TiO_2 in the course of its preparation.

In the present chapter, we have measured anodic photocurrents that arise only from the photooxidation reactions, in contrast to the case of photoreaction products, and succeeded in obtaining a definite conclusion on the mechanism. First, let us consider why the IPCE is enhanced by addition of a reductant to the electrolyte. Oxygen photoevolution reaction on TiO_2 in the absence of reductants produces a number of surface reaction intermediates[25,26], leading to

efficient carrier recombination especially in powdered systems without any band bending. On the other hand, photooxidation reactions of reductants such as methanol, I^-, H_2Q, SCN^-, and Br^- by photogenerated holes in general proceed effectively with much less surface intermediates, which leads to much less carrier recombination and hence high IPCE's. In addition, for methanol, current doubling mechanism[27] may contribute to the increase in the IPCE[28].

We mentioned earlier that all reductants added [such as methanol, I^-, hydroquinone (H_2Q), SCN^-, and Br^-] increased the IPCE under UV illumination, whereas only I^- and H_2Q increased the IPCE under visible-light illumination (Figures 2 and 3). This result implies, based on the above argument, that all the reductants are oxidized under the UV illumination, whereas only I^- and H_2Q are oxidized under the visible-light illumination. The reduced oxidation power under the visible illumination relative to the UV illumination can never be explained by reported concepts of band narrowing[5] or formation of the O-vacancy levels slightly below the conduction band edge[18]. The reduced oxidation power can only be explained by a mechanism that the doped N-species (such as NH_x[22]) gives rise to an (occupied) mid-gap (N2p) level slightly above the top of the (O2p) valence band, and the visible-light illumination produces "holes" in the mid-gap level, whereas the UV illumination produces holes in the (O2p) valence band, as shown in Figure 4. The differences in the IPCE enhancement between the UV and visible illumination can be attributed to differences in the reactivity of these holes.

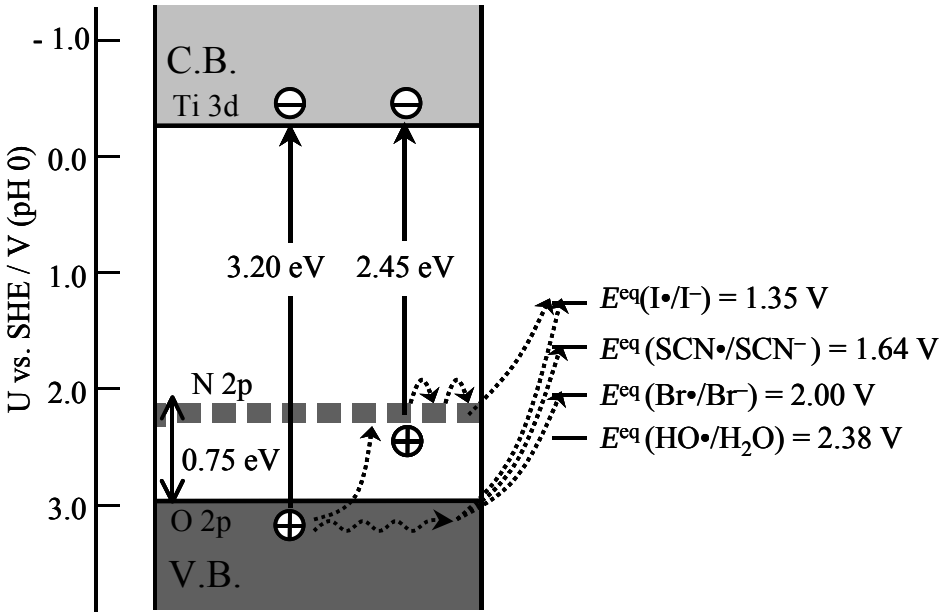

Figure 4 Schematic illustration of expected energy bands for N-doped TiO_2 (anatase) together with some photo-induced electronic processes. C.B.: conduction band, V.B.: valence band, – with a circle: electron, and + with a circle: hole, E^{eq}: reported equilibrium redox potentials[25] for one-electron transfer redox couples indicated in parentheses in the figure.

It is worthwhile to note here that the photocurrent measurement is crucially important to get definite conclusions on reaction mechanism. The product analysis, often used in the literature for photocatalytic reactions in powdered systems, cannot distinguish whether a reaction product comes from a photo-oxidation process or a photo-reduction process. Moreover, the product analysis cannot say anything on whether a certain product of oxidation of an organic compound comes from a direct reaction with photogenerated holes or via reactions with surface intermediates (such as Ti-O· radical) of water photooxidation reaction. It is thus quite difficult to get definite conclusions on the reaction mechanism from the product analysis. On the other

hand, the photocurrent measurement can in general distinguish the above two oxidation processes because the photocurrent largely increases if a direct reaction with photogenerated holes occurs, whereas it hardly increases if an indirect reaction via intermediates of water photooxidation occurs (Figures 2 and 3). It has been reported from the product analysis that a variety of organic compounds such as methylene blue[5], isopropanol[19], and acetone[5,20] are oxidized into CO_2 on N-doped TiO_2 by visible light illumination, whereas the photocurrent measurements in the present work show that even readily-oxidized methanol is hardly oxidized by the visible-light illumination (Figure 2). Such a discrepancy strongly suggests that most of photocatalytic oxidation reactions of organic compounds in powdered N-doped TiO_2 systems proceed via surface intermediates of oxygen reduction or water oxidation, not via direct reactions with holes trapped at the N-induced mid-gap level. The discrepancy thus indicates clearly the limitation of the method of product analysis.

Finally, let us consider why "holes" trapped in the N-induced mid-gap level can only oxidize I^- and H_2Q, though holes in the (O2p) valence band can oxidize all the reductants (Figures 3). In relation to this fact, we have also to note that the "holes" at the N-induced level, which cannot oxidize Br^- and SCN^- (Figure 3), can oxidize water (Figure 1). The former result may be explained by comparing the reported one-electron transfer equilibrium redox potentials[29] for reductants with the energies for the mid-gap N level and the valence band for N-doped TiO_2, which could be estimated from the reported flat-band potential[16] and the conduction band edge[17] (Figure 4). We can expect that the more negative the redox potential of a reductant, the more easily oxidized the reductant is. In fact, the $I\cdot/I^-$ redox level is considerably above the N-induced mid-gap level, suggesting that I^- can be easily oxidized, in agreement with the experiment. We have no reported datum for the one-electron transfer redox level for H_2Q. Little reactivity for SCN^- and Br^-, whose redox level lies above the mid-gap N level (Figure 4), can probably be

attributed to the presence of large reorganization energies[30] in electron transfer reaction for such small ions in aqueous media.

Now, why is water oxidized by the "holes" trapped at the N-induced mid-gap level, in spite that the redox potential for water oxidation ($HO\cdot/H_2O$) is far below this level (Figure 4)? The keen contradiction can be solved if we take into account that the water oxidation is not caused by electron-transfer type reaction. Very recently, the laboratory which the author belonged have reported,[31,32] by using in-situ FTIR and PL measurements, that the water photooxidation on n-TiO_2 (rutile) is not initiated by oxidation of surface OH group ($Ti\text{-}OH_s$) with photogenerated holes (h^+)

$$Ti\text{-}OH_s + h^+ \rightarrow [Ti \cdot OH]_s^+ \qquad (2)$$

but initiated by a nucleophilic attack of an H_2O molecule (Lewis base) to a surface hole (Lewis acid), accompanied by bond breaking.

$$[Ti\text{-}O\text{-}Ti]_s + h^+ + H_2O \rightarrow [Ti\text{-}O\cdot\ HO\text{-}Ti]_s + H^+ \qquad (3)$$

The easiness of occurrence of reaction (3) will not have any direct relation with the redox potential such as $E_{eq}(HO\cdot/H_2O)$ in Figure 4, but have a strong relation with the basicity of H_2O or the energy of an intermediate radical $[Ti\text{-}O\cdot\ HO\text{-}Ti]_s$ that is roughly giving the activation energy for the reaction. In other words, the above-mentioned contradiction can be regarded as giving strong support to the validity of our previously reported[31,32] mechanism for the water photooxidation on TiO_2.

The above arguments indicate that the oxidation power of surface holes strongly depends on the reaction mechanism and we cannot discuss it without knowledge on the mechanism. In relation to this statement, it is interesting to note that the large IPCE enhancements by reductants under the UV illumination relative to the visible illumination (Figures 2 and 3) show that most of holes generated in the (O2p) valence band for N-doped

TiO_2 can escape from trapping at the N-induced mid-gap level, and reach the surface and directly react with the solution (Figure 4). The result is quite strange in view of a conventional concept that valence-band holes are in general effectively trapped by an impurity mid-gap state. Detailed investigations of the mechanism will give new insights into understanding of the valence-band holes and impurity-level holes and their mutual interactions.

In conclusion, the work in the present chapter has given definite evidence to the mechanism that visible-light responses for N-doped TiO_2 arise from formation of an N-induced (occupied) mid-gap level slightly above the valence band edge. Investigations of the effect of addition of various reductants to the electrolyte have revealed that the oxidation power of surface holes strongly depends on the reaction mechanism and we cannot discuss it without knowledge on the mechanism. The investigations have also clarified the limitation of the method of product analysis that has often been used in the literature to elucidate reaction mechanisms.

References

(1) Fujishima, A. ; Honda, K. *Nature* **1972**, 238, 37.

(2) Sato, S. and White, M. *Chem. Phys. Lett*. **1980**, 72, 83.

(3) Hoffmann, M. R.; Martin, S. T.; Choi, W.; Bahnemann, D. W. *Chem. Rev*. **1995**, 95, 69.

(4) Ollis, D. F.; Al-Ekabi, H.; Eds., *Photocatalytic Purification and Treatment of Water and Air*; Elsevier, Amsterdam, 1993.

(5) Asahi, R.; Morikawa, T.; Ohwaki, T.; Aoki, K.; Taga, Y. *Science* **2001**, 293, 269.

(6) Sato, S. *Chem. Phys. Lett*. **1986**, 123, 126.

(7) Umebayashi, T.; Yamaki, T.; Itoh, H.; Asai, K. *Appl. Phys. Lett*. **2002**, 81, 454.

(8) Ohno, T.; Mitsui, T.; and Matsumura, M. *Chem. Lett*. **2003**, 32, 364.

(9) Khan, S. U. M.; Al-Shahry, M.; Ingler, W. B. Jr. *Science* **2002**, 297, 2243.

(10) Sakthivel, S.; Kisch, H. *Angew. Chem. Int. Ed*. **2003**, 42, 4908.

(11) Irie, H.; Watanabe, Y.; and Hashimoto, K. *Chem. Lett*. **2003**, 32, 772.

(12) Diebold, U. *Surf. Sci. Rep*. **2003**, 48, 53.

(13) Nakamura, R.; Imanishi, A.; Murakoshi, K.; and Nakato, Y. *J. Am. Chem. Soc*. **2003**, 125, 7443.

(14) Tsujiko, A.; Kisumi, T.; Magari, Y.; Murakoshi, K.; and Nakato, Y. *J. Phys. Chem. B* **2000**, 104, 4873.

(15) Nakato, Y.; Akanuma, H.; Magari, Y.; Yae, S.; Shimizu, J.-I.; Mori, H. *J. Phys. Chem. B* **1997**, 101, 4934.

(16) Sakthivel, S.; Kisch, H. *Chemphyschem*. **2003**, 4, 487.

(17) Lindgren, T.; Mwabora, J. M.; Avendanño, E.; Jonsson, J.; Hoel, A.; Granqvist, C-G.; Lindquist, S-E. *J. Phys. Chem. B* **2003**, 107, 5709.

(18) Ihara, T.; Miyoshi, M.; Iriyama, Y.; Matsumoto, O.; Sugihara, S. *Appl. Catal. B: Env*. **2003**,

42, 403.

(19) Irie, H.; Watanabe, Y.; Hashimoto, K. *J. Phys. Chem. B* **2003**, 107, 5483.

(20) Sakatani, Y.; Nunoshige, J.; Ando, H.; Okusako, K.; Koike, H.; Takata, T.; Kondo, J. N.; Hara, M.; Domen. K. *Chem. Lett*. 2003, *32*, 1156.

(21) Diwald, O.; Thompson, T. L.; Goralski, E. G.; Walck, S. D.; Yates, Jr., J. T. *J. Phys. Chem. B* **2004**, 108, 52.

(22) Diwald, O.; Thompson, T. L.; Zubkov, T.; Goralski, E.G.; Walck, S. D.; Yates, J. T., Jr. *J. Phys. Chem. B* **2004**, *108,* 6004.

(23) Torres, R. G.; Lindgren, T.; Lu, J.; Granqvist, C-G.; and Lindquist, S-E. *J. Phys. Chem. B* **2004**, 108, 5995.

(24) Rodriguez, J. A.; Jirsak, T.; Dvorak, J.; Sambasivan, S.; Fischer, D. *J. Phys. Chem. B* **2000**, 104, 319

(25) Wilson, R. H. *J. Electrochem. Soc*. **1980**, 127, 228.

(26) Ulmann, M.; Tacconi, N. R.; and Augustynski, J. *J. Phys. Chem*. **1986**, 90, 6523.

(27) Morrison, S. R.; Freund, T. *J. Chem. Phys*. **1967**, 47, 1543.

(28) Shiga, A.; Tsujiko, A.; Yae, S.; and Nakato, Y. *Bull. Chem. Soc. Jpn*. **1998**, 71, 2119.

(29) Wardman, P. *J. Phys. Chem. Ref. Data* **1989**, 18, 1637.

(30) Burg, V. K.; and Delahay, P. *Chem. Phys. Lett*. **1981**, 78, 287.

(31) Kisumi, T.; Tsujiko, A.; Murakoshi, K., and Nakato, Y. *J. Electroanal. Chem*. **2003**, 545, 99.

(32) Nakamura, R.; Nakato, Y. *J. Am. Chem. Soc*. **2004**, 126, 1290.

Chapter 5

Oxygen Photoevolution on Tantalum Oxynitride Photocatalysts under Visible-light Irradiation: How Does Water Photoxidation Proceed on an Oxynitride Surface?

Introduction

Photoinduced oxidation reactions of water and organic compounds at the surface of nanocrystalline metal-oxide photocatalysts such as TiO_2 have been attracting keen attention from the points of view of solar energy conversion (water splitting)[1,2] as well as environmental cleaning (photocatalytic decomposition of waste materials and harmful compounds)[3]. Such metal oxides have high oxidation power under illumination, and are chemically stable, non-toxic, and relatively inexpensive. Unfortunately, however, most of the metal oxides have too large band gaps to efficiently absorb the solar light. This is because the valence band of the metal oxides mainly consists of O2p orbitals with deep energies of ca. 3 eV vs. NHE.

Recent studies have shown that the shortcoming of the metal oxides can be overcome by introducing mid-gap levels above the top of the O2p valence band through doping with other elements such as nitrogen[4-7], sulfur[8,9], carbon[10-12], etc. For example, the nitrogen doping of TiO_2 (anatase) produced an N-induced mid-gap level ca. 0.75 eV above the top of the O2p valence band[7], resulting in the extension of the photoactive region up to 550 nm. The carbon doping of TiO_2 is also reported to extend the photoactive region for the water photoxidation up to 535 nm, thus resulting in a large increase in the water splitting efficiency under white-light illumination[10].

Another promising candidate of visible-light responsive photocatalysts is metal oxynitrides, such as TaON, which have the valence bands composed of hybridized N2p and O2p orbitals. Domen et al. reported[13-16] that TaON absorbed the visible light up to ca. 530 nm, with the valence band at 2.2 V vs. NHE, and exhibited a high quantum efficiency of 34 % for the water photoxidation (oxygen photoevolution) in the presence of a sacrificial oxidizing reagent such as Ag^+. They also reported[15-18] that tantalum nitride (Ta_3N_5) exhibited the high photocatalytic activity for the water photoxidation as well, though its valence band was mainly

composed of N2p orbitals and located at 1.6 V vs. NHE.

The reported studies clearly show that the introduction of an (N-induced) mid-gap level or a new valance band (composed of hybridized N2p and O2p orbitals) above the O2p valence band is effective to extend the photoactive region to the visible light. However, problems will arise on the stability and efficiency for such photocatalysts, because it is expected that metal-N bonds in N-doped metal oxides or metal oxynitrides are weak compared with metal-O bonds in metal oxides and that photogenerated holes are trapped at higher N2p-induced levels at the surface, resulting in a large decrease in the oxidation power compared with the O2p valence-band holes. In addition, the N-doping will introduce more or less distortion in metal-oxide crystals, leading to their destabilization. It is thus quite important to clarify how the water photoxidation proceeds at the metal-oxynitride surface, why photogenerated holes with a character of N2p holes can oxidize water, and why the metal oxynitride is stable under the water photoxidation reaction.

In the present work, we have studied the mechanism of the water photoxidation (oxygen photoevolution) at the surface of TaON on the basis of our previous studies on the mechanisms of this reaction at the surface of TiO_2[19-21] and N-doped TiO_2[7]. The present results have strongly demonstrated that the water photoxidation on TaON is initiated by our recently proposed new mechanism of a nucleophilic attack of a water molecule on a surface hole (a Lewis acid-base mechanism), not by the conventional mechanism of oxidation of surface OH group by the hole (an electron-transfer type mechanism). The nucleophilic-attack mechanism has explained why the photogenerated holes with a character of N2p holes can oxidize water.

Experimental Section

TaON powder was prepared by nitridation of commercial Ta_2O_5 powder (Wako,

purity: 99.8 %) according to the literature[15]: Namely, Ta_2O_5 powder was initially heated in an alumina tube reactor under a flow of N_2 gas. After the temperature rose to 800°C, the N_2 gas was replaced by an NH_3 gas (purity: 99.999 %) and the powder was kept at 800°C under the NH_3 flow of a flow rate of 10mL/min for 10 h. Then, the NH_3 gas was replaced by an N_2 gas again and the powder was cooled down to room temperature over a period of time of 2-3h. As a reference sample, Ta_3N_5 powder was also prepared by similar thermal nitridation of Ta_2O_5 powder under a flow of NH_3 gas at 800°C for 10 h, though in this case the flow rate was increased to 1000 mL/min.

Experiments of photocatalytic reactions were carried out in a Pyrex reaction vessel attached to a closed gas circulation system, with which a gas chromatograph (Shimadzu, GC14-B) was directly connected. An evacuation pump was also connected with this line via a cold trap. The photocatalytic oxidation of water into O_2 was performed in 200 mL of a 2 mM $FeCl_3$ aqueous solution with 200 mg of TaON powder. The air in the reaction vessel and the gas-circulation system was removed by repeated cycles of evacuation and introduction of Ar gas, until the air (N_2 and O_2) became undetectable by the gas chromatograph. After 150 Torr of Ar gas was introduced in the reaction system, the sample solution was irradiated from the horizontal side of the vessel with a 300-W Xe lamp (Ushio) as the light source through a UV cut-off filter (Irie Seisakusho, L-42, transparent in $\lambda \geq 420$ nm), together with a water filter (5 cm long) and an IR-cut filter (Irie Seisakusho, IRA-25S) to avoid solution heating. The evolved gas (O_2 and N_2) was detected by the gas chromatograph with a TCD detector.

Particulate TaON film electrodes for photocurrent measurements were prepared by adopting the low-temperature annealing method reported for TiO_2 films[22], in order to avoid oxidation at the TaON surface at elevated temperatures. Namely, TaON powder (1g) was suspended into pure water (5 mL) by stirring. The resultant colloidal solution of TaON was then

spin-coated at 2000 rpm onto transparent conductive oxide (F-doped SnO_2 or FTO, 20 Ω/square) films, on which an ethanol solution of 50 mM KOH had, in advance, been applied with a spin coater at 1000 rpm to get strong adhesion between TaON and FTO under low-temperature annealing. The TaON-coated glass was then dried in air, and heated at 150°C for 15 min with an electric furnace. The above TaON coating was repeated twice, and finally the TaON film was heated at 150°C for 30 min. A copper wire was attached on an edge of the F-SnO_2 film with silver paste, and the whole part, except a 1.0 × 1.0 cm^2 TaON-film area, was covered with epoxy resin for insulating.

Photocurrents for TaON film electrodes were measured as a function of wavelength (λ), using a 350-W xenon lamp (Ushio) as the light source together with a monochromator (Bunkoh-Keiki Co., M10-T) with a band width of 10 nm. The incident photon to current efficiency at λ, IPCE (λ), was calculated from the photocurrent by an equation

$$\text{IPCE}(\lambda) = 1240 \times j(\lambda) / \lambda I_0(\lambda) \times 100 \qquad (1)$$

where λ is the wavelength of incident light in a unit of nm, $j(\lambda)$ is the photocurrent density in mA cm^{-2} under illumination at λ, and $I_0(\lambda)$ the incident light intensity in mW cm^{-2} at λ. A Pt plate was used as the counter electrode, and an Ag/AgCl/sat. KCl was used as the reference electrode. The electrolyte solutions under experiments were bubbled with a nitrogen gas to remove dissolved O_2.

In situ multiple internal reflection FTIR (MIR-IR) absorption spectra were measured by the same experimental setup as used in a previous paper[20]. 10 μL of aqueous TaON slurry (10 mg/mL) was spread with a plastic pipet on a multiple internal reflection element (prism) made of a diamond single crystal and dried in air. Spectra were recorded at the resolution of 4 cm^{-1} and the accumulation of 400 scans, using an FTIR spectrometer (Bio-Rad FTS 575C) with a deuterated triglycine sulfate (DTGS) detector. The IR light was reflected about 9 times at the

diamond/TaON solution interface. The light source for photocatalytic reactions was a 200-W Hg-Xe lamp (Hypercure 200 UV, Yamashita Denso). A UV cut filter ($\lambda \geq 420$ nm) and an IR-cut filter were used.

Results

1. Photocatalytic experiments.

Figure 1 shows XRD patterns for TaON and Ta_3N_5 powder prepared in the present work, together with that for Ta_2O_5 for reference. The XRD pattern for TaON contained no peak assigned to Ta_2O_5 and Ta_3N_5, implying that the prepared TaON sample contained no Ta_2O_5 nor Ta_3N_5. XPS analysis of the N1s region of TaON showed the strong peak at 397 eV, which was reported[14] to be assigned to the Ta-N bond. The surface atomic ratio of nitrogen to oxygen ($R_{N/O}$) for TaON was estimated from the relative peak areas of N1s (397 eV, Ta-N bond) and O1s (531 eV, Ta-O bond) corrected for the sensitivity factor. The $R_{N/O}$ for the TaON powder was 0.7 and a little smaller than unity. After annealing at a high temperature of 400 °C in air for 2h, the amount of nitrogen further decreased and $R_{N/O}$ reached 0.4.

Figure 2 shows the time course of photocatalytic O_2 evolution from TaON (200 mg) suspended in 200 mL of a 2 mM Fe^{3+} aqueous solution (pH 2.3) under visible-light ($\lambda \geq 420$ nm) irradiation. O_2 gas was evolved, together with a trace amount of N_2, under visible-light irradiation, confirming that TaON powder could oxidize water into oxygen, as reported by Domen et al[13,15]. The rate of O_2 evolution decreased with the reaction time owing to a decrease in the Fe^{3+} concentration, as is understood from Figure 2 that the amount of evolved O_2 approaches the total amount of O_2 (100 μmol) evolved by stoichiometric reduction of Fe^{3+}. Interestingly, the O_2 evolution was completely suppressed when methanol (0.5w%) was added

to the aqueous TaON suspension (Figure 2), demonstrating that the photoxidation of methanol proceeded predominantly over the water photoxidation, or in other words, that the evolved O_2 came from the water photoxidation.

Figure 3 shows the action spectrum of the anodic photocurrent (or the IPCE vs. wavelength) for a freshly prepared particulate TaON film electrode in 0.1 M $HClO_4$ (pH 1.1) at a potential of 0.7 V vs. Ag/AgCl. The IPCE for a Ta_2O_5 film electrode is also included for reference. The action spectrum of the anodic photocurrent for TaON agreed well with its absorption spectrum (broken line in Figure 3), extending up to ca. 530 nm. Since the O_2 evolution was confirmed by the photocatalytic experiment with a TaON suspension, as shown in Figure 2, the anodic photocurrents can be attributed to the photoxidation of H_2O to O_2. It was reported[15] that the efficiency of the O_2 photoevolution from a TaON suspension in the presence of Ag^+ ions as an electron acceptor strongly depended on the pH of the suspension, the O_2 evolution largely deceasing with the decrease in pH. However, in the present work, the IPCE for the TaON film in an alkaline solution of pH 12.7 was nearly the same as that in an acidic solution of pH 1.1, both being measured at a potential of 0.7 V vs. Ag/AgCl.

Figure 4 shows the effect of addition of a reductant such as I^-, SCN^-, Br^- and methanol to the electrolyte on the IPCE vs. λ for a freshly prepared TaON film electrode. The IPCE was increased largely by addition of I^-, whereas no increase in the IPCE was observed for the addition of SCN^-, Br^-, and methanol. We also observed no increase in the IPCE by the addition of ethanol, 1-propanol, and acetic acid (though not shown in the figure). In general, when photogenerated holes react with such reactants, they produce much less surface reaction intermediates than when the holes react with water[7,23]. The surface reaction intermediates act as effective surface carrier recombination centers especially for nano-sized particulate TaON electrodes with no band bending. Therefore, when photogenerated holes react with a reactant, a

large increase in the IPCE should be observed compared with the case of the water photoxidation owing to much less surface carrier recombination. The difference in the enhancement of the IPCE in Figure 4 can thus be regarded as reflecting the difference in the reactivity of reductants with photogenerated holes. We can then conclude that photogenerated holes in the valence band at the TaON surface can efficiently oxidize I^-, but cannot oxidize SCN^-, Br^-, methanol, ethanol, 1-propanol, and acetic acid.

As to the stability of the particulate TaON film electrode, we confirmed that the spectral shape in the action spectrum of the anodic photocurrent (the IPCE vs. λ for the O_2 photoevolution, Figure 3) and the effect of addition of reductants on the IPCE (Figure 4) were not altered after prolonged visible-light irradiation in 0.1 M $HClO_4$ for 20 h, though the amount of the anodic photocurrent for TaON slightly decreased. Since it was reported[15] that the oxygen photoevolution from the TaON photocatalyst proceeded without any noticeable decrease in the activity, this decrease in the photocurrent is probably due to slight peeling off of TaON particles from the FTO glass substrate under solution stirring.

2. In Situ MIR-IR Investigations of Surface Reaction Intermediates

We reported in previous papers[20,24] that the multiple internal reflection FTIR (MIR-IR) spectroscopy was sensitive enough to detect surface reaction intermediates of submonolayer amounts and could be applied to in-situ monitoring of photocatalytic reactions on particulate TiO_2 films in contact with aqueous solutions. By using a diamond single crystal as an multiple internal reflection element (IRE), we can measure IR absorptions in a low-frequency region from 1500 to 650 cm^{-1} with a high spectral sensitivity, in which surface reaction intermediates of the water photoxidation exhibit absorption bands due to the O-O stretching vibration mode[20,24]. In this work, we have applied this method to the photocatalytic reaction at TaON particulate films under visible-light irradiation.

Figure 5 shows MIR-IR spectra for particulate Ta_2O_5 and TaON films before irradiation for reference in later discussion. Spectrum (a) is for a particulate Ta_2O_5 film under dry air. It exhibits weak peaks at 839 and 942 cm^{-1} and a strong broad shoulder below 780 cm^{-1}. The latter broad shoulder can be assigned[25-28] to phonon modes for crystalline Ta_2O_5 such as Ta-O and Ta-O-Ta stretching vibrations, while the former two peaks can be assigned[25-28] to phonon modes for oxygen-deficient crystalline phases such as TaO and TaO_2 included as impurities in the Ta_2O_5 film. Spectrum (b) is for a TaON film, measured after nitridation of Ta_2O_5 powder at 800°C under an NH_3 atmosphere. It exhibits new peaks at 782 and 827 cm^{-1} together with a strong broad shoulder below 780 cm^{-1}. Although no information is at present available about vibrational spectra for TaON itself, by referring to vibrational spectra reported for well studied oxynitrides such as AlON[29], GaON[29], and SiON[30-33], the former two peaks may be assigned to N-Ta-O phonon modes of non-stoichiometric TaON phases present as impurities, while the latter shoulder may be assigned to phonon modes for crystalline TaON. The presence of the non-stoichiometric TaON phases may be supported by a result of XPS analysis that the $R_{N/O}$ for TaON powder prepared in this work is 0.7, a little smaller than unity, as mentioned before.

Figure 6 shows in situ MIR-IR absorption spectra for photoinduced species at a particulate TaON film in contact with pure water of pH 7 under visible-light ($\lambda \geq 420$ nm) irradiation. The spectrum for the TaON film before irradiation was taken as the spectral reference. The 782- and 827-cm^{-1} bands, assigned above to the N-Ta-O phonon modes, appeared as depressions (or negative peaks), and the (negative) peak height increased with the irradiation time up to 30 min. On the other hand, a new broad band appeared in the region of 1350 to 900 cm^{-1}. The negative 782- and 827-cm^{-1} bands and the broad band in 1350 to 900 cm^{-1} both became much weaker when the TaON surface was in advance oxidized by heating at 400°C

until the surface atomic N/O ratio decreased from 0.7 to 0.4. Thus, the photoinduced (negative and positive) bands in Figure 6 can be regarded to be due to the photoinduced surface oxidation in the TaON powder.

In order to confirm the above conclusion, we did isotopic labeling experiments by using $H_2{}^{18}O$ as a solvent, instead of $H_2{}^{16}O$. Spectrum (a) in Figure 7 shows an MIR-IR spectrum for a particulate TaON film in contact with pure $H_2{}^{18}O$, whereas spectrum (b) is that for TaON in contact with pure $H_2{}^{16}O$. Both spectra (a) and (b) show essentially the same spectral changes, i.e., the appearances of the negative bands at 782 and 827 cm^{-1} and the broad band in the range of 1350-900 cm^{-1}, but the latter broad band in $H_2{}^{18}O$ is considerably distorted compared with that in $H_2{}^{16}O$, namely, the broad band in $H_2{}^{18}O$ (spectrum a) is largely depressed in intensity on the high-frequency side compared with that for $H_2{}^{16}O$ (spectrum b). This result clearly indicates that the broad band in the range of 1350-900 cm^{-1} is due to certain oxidized surface species formed by reaction of photogenerated holes with H_2O at the TaON surface under visible-light irradiation, in harmony with the aforementioned conclusion.

We mentioned earlier that O_2 gas was evolved from an aqueous suspension of TaON powder under visible-light irradiation when 2 mM Fe^{3+} was added to the suspension as a sacrificial electron acceptor (Figure 2). Figure 8 shows the effect of addition of 10 mM Fe^{3+} on the photoinduced MIR-IR spectra for a particulate TaON film. An MIR-IR spectrum of free HOOH ($H^{16}O^{16}OH$) in an aqueous HOOH solution is also included for reference. It is to be noted that the photoinduced MIR-IR spectrum in $H_2{}^{16}O$ with 10 mM Fe^{3+}, spectrum (a) in Figure 8, shows a new weak absorption band at 872 cm^{-1}, in addition to the negative bands at 782 and 827 cm^{-1} and the broad band in the range of 1350-900 cm^{-1} that were observed without Fe^{3+} (Figure 7 b). Since Fe^{3+} acts as an efficient electron acceptor, it is likely that the 872-cm^{-1} bands is due to a surface intermediate of the water photoxidation reaction. We can mention that

the 872-cm^{-1} band in $H_2{}^{16}O$ is located at nearly the same wavenumber as that for the O-O stretching band, ν(O-O), of free HOOH ($H^{16}O^{16}OH$) peaked at 877 cm^{-1} [34,35] in spectrum (c) of Figure 8. However, almost no peak assigned to the bending band, δ(O-O-H), of free HOOH, peaked at 1380 cm^{-1} [34,35], was observed in spectrum (a) of Figure 8. This implies that the 872 cm^{-1}-band can be assigned to the ν(O-O) band of a certain peroxo species at the TaON surface, which may tentatively assigned to adsorbed H_2O_2, since it is expected that the δ(O-O-H) mode of adsorbed HOOH decreases in intensity by interaction with surface Ta atoms.

The above assignment of the 872-cm^{-1} band has been supported by ^{18}O-isotopic labeling experiments. Spectrum (b) in Figure 8 clearly shows that the photoinduced MIR-IR spectrum in $H_2{}^{18}O$ with 10 mM Fe^{3+} also shows a new weak absorption band at 851 cm^{-1}, at a position slightly deviated from 872 cm^{-1} in $H_2{}^{16}O$, together with a shoulder at 872 cm^{-1}. It is reported[20,36] experimentally that the ^{18}O isotopic shift of the ν(O-O) mode for surface peroxo species between ^{16}O-^{16}O and ^{18}O-^{16}O is 19 cm^{-1}, while that between ^{16}O-^{16}O and ^{18}O-^{18}O is 42 cm^{-1}. Thus, the observed shift of 21 cm^{-1} (872 → 851 cm^{-1}) in the present work can be reasonably assigned to the oxygen isotopic shift of the ν(O-O) mode of surface peroxo species between ^{16}O-^{16}O and ^{18}O-^{16}O.

Discussion

Domen et al. recently reported[13,15] that tantalum oxynitride (TaON) functioned as a visible-light (λ < 520 nm) driven photocatalyst for the oxidation of H_2O into O_2 in the presence of an appropriate electron acceptor. The prominent feature of TaON is that the photocatalytic water oxidation occurs, though its valence band should be composed of hybridized N2p and O2p orbitals. In the present work, we have confirmed that the photocatalytic O_2 evolution

occurs from a TaON suspension in the presence of Fe^{3+} (Figure 2). However, we have found that the TaON surface is slightly oxidized under visible-light irradiation (Figures 6 and 7), indicating that the oxygen photoevolution on TaON actually occurs on a thin Ta-oxide overlayer. We have also found that (1) a certain surface peroxo species is formed in the course of the O_2 photoevolution reaction (Figure 8) and (2) TaON cannot oxidize reductants such as SCN^-, Br^-, methanol, ethanol, iso-propanol, and acetic acid (Figure 4) in spite that it can oxidize H_2O into O_2.

Now, let us consider how the water photoxidation proceeds at the surface of TaON under visible-light irradiation, based on our recently reported mechanism for this reaction on the TiO_2 (rutile) surface under UV irradiation[19-21]. The key of the mechanism is that the water photoxidation reaction is not initiated by the oxidation of surface OH group ($Ti–OH_s$) with photogenerated holes (h^+),

$$Ti–OH_s + h^+ \rightarrow [Ti\ \bullet OH]_s^+ \qquad (2)$$

but by a nucleophilic attack of an H_2O molecule (Lewis base) to a surface-trapped hole (Lewis acid) at surface lattice oxygen ($Ti\text{-}O\text{-}Ti_s$), accompanied by bond breaking.

$$[Ti–O–Ti]_s + h^+ + H_2O \rightarrow [Ti–O\bullet \quad HO–Ti]_s + H^+ \qquad (3)$$

The O_2 evolution occurs via formation of a surface peroxo species, as shown in Scheme 1. This conclusion was obtained by in situ spectroscopic studies such as MIR-IR absorption[20] and photoluminescence (PL) measurements[19,20] and supported by mechanistic studies using atomically-flat single crystal TiO_2 (rutile) electrodes[21]. This conclusion is also supported by the following reported results: (1) ESR measurements at low temperature[37-39] showed that photogenerated holes on TiO_2 produced no •OH radical but Ti–O• radicals. (2) Recent ultraviolet photoelectron spectroscopic (UPS) studies indicated[40-42] that the O2p level for terminal hydroxyl group ($Ti–OH_s$) on TiO_2 (rutile) was far below the top of the O2p valence

band of TiO_2 (rutile). The latter fact indicates that reaction (2) is energetically impossible. It is important to note here that reaction (2) is an electron-transfer-type reaction, whereas reaction (3) is a Lewis acid-base-type reaction, and therefore their energetics and kinetics are quite different from each other.

Now, it will be reasonable to assume that the water photoxidation at the surface of TaON under visible-light irradiation proceeds by a similar mechanism to that on TiO_2 (rutile). As mentioned earlier, the oxygen photoevolution on TaON actually occurs at the surface of a thin Ta-oxide overlayer (Figures 8). The initial formation of such a surface thin Ta-oxide layer is expected to proceed as follows. The valence band of TaON is constituted by hybridized N2p and O2p orbitals, in which the contribution of the N2p orbitals is much larger than the O2p orbitals at the top of the valence band[43]. Thus, photogenerated holes will initially be trapped at surface lattice N atoms, resulting in a surface trapped hole which may be represented as $[Ta–N\cdots Ta]^+_s$ (reaction (4)).

$$[Ta–N–Ta]_s + h^+ \rightarrow [Ta–N\cdots Ta]^+_s \quad (4)$$

In this surface trapped hole, the Ta–N bond becomes weaker by trapping a hole (i.e. one electron is missing in the bonding orbital). Once this happens, the hole-trapped site acts, due to its positive charge, as an active site for a nucleophilic reagent (Lewis acid). In an aqueous solution, an H_2O molecule acts as a nucleophilic reagent (Lewis base) and hence attacks to the surface trapped hole, accompanied by the bond breaking and attachment of OH group, similarly to reaction (3).

$$[Ta–N\cdots Ta]^+_s + H_2O \rightarrow [Ta–N\bullet \quad HO–Ta]_s + H^+ \quad (5)$$

Further reactions of $[Ta–N\bullet \quad HO–Ta]_s$ with holes and water finally result in the formation of surface Ta–O–Ta bonds, or in other words, the oxidation of the TaON surface, with a release of N_2 gas.

$$2[\text{Ta–N•}\quad\text{HO–Ta}]_s + 2h^+ \rightarrow 2[\text{Ta–O–Ta}]_s + 2H^+ + N_2 \qquad (6)$$

Following reactions of photogenerated holes with water on a thin Ta-oxide layer will proceed by a similar mechanism to that on TiO_2. Namely, the O_2 photoevolution is initiated by the nucleophilic attack of H_2O molecules to surface trapped holes at surface lattice O atoms ($Ta–O–Ta_s$).

$$[\text{Ta–O–Ta}]_s + h^+ + H_2O \rightarrow [\text{Ta–O•}\quad\text{HO–Ta}]_s + H^+ \qquad (7)$$

$$[\text{Ta–O•}\quad\text{HO–Ta}]_s + h^+ \rightarrow [\text{Ta–O–O–Ta}]_s + H^+ \qquad (8)$$

$$[\text{Ta–O–O–Ta}]_s + H_2O + 2h^+ \rightarrow [\text{Ta–O–Ta}]_s + O_2 + 2H^+ \qquad (9)$$

We have to note that this mechanism is in agreement with the in-situ MIR-IR measurements for surface intermediates on TaON powder. We mentioned in the preceding section that the weak absorption band peaked at 872 cm^{-1}, assigned to the ν(O-O) band of the surface peroxo species (weakly adsorbed HOOH), appeared in the course of the O_2 photoevolution reaction (Figure 8 a). The ^{18}O isotopic labeling experiments (Figure 8 b) revealed that the surface peroxo species, though it was produced in $H_2{}^{18}O$, contained both O^{18} and ^{16}O (Figure 8 b). This result clearly shows that the surface peroxo species is formed by the above-mentioned reaction scheme (reactions 7 and 8), as is seen from the following consideration. Once TaON is immersed with $H_2{}^{18}O$, it is expected that surface $Ta–{}^{16}OH$ group on TaON is readily converted into $Ta–{}^{18}OH$, whereas the surface lattice oxygen still remains in the form of $[Ta–{}^{16}O–Ta]$ even in contact with $H_2{}^{18}O$, since it is reported[44] that oxygen exchange between water and surface lattice oxygen in metal oxides in general hardly occurs at room temperature in the dark. The incorporation of ^{16}O into the surface peroxo species is therefore possible only when water molecules ($H_2{}^{18}O$) attack the surface lattice oxygen existing in the form of the surface trapped holes $[Ta–{}^{16}O\cdots Ta]^+_s$, such as reaction (7).

The aforementioned mechanism (reactions 7, 8 and 9) is further supported by the

observed effect of the addition of reductants to the electrolyte on the IPCE. Figure 3 shows that TaON can oxidize H_2O into O_2 by visible-light irradiation of up to ca. 530 nm, at which the light absorption starts, whereas Figure 4 shows that photogenerated holes on TaON cannot oxidize reductants such as SCN^-, Br^-, and alcohols like methanol and ethanol, which have the redox potentials for the oxidation much more negative than water.

This discrepancy can be understood if we take into account that the photoxidation of reductants such as SCN^- and Br^- may indeed occur by an electron-transfer mechanism, but the water photoxidation proceeds not by the electron-transfer mechanism but by the Lewis acid-base mechanism (reactions 7, 8 and 9). Figure 9 shows the energy band diagram for TaON[16], together with the equilibrium redox potentials (E^{eq}_{redox}) for the reductants as one-electron transfer redox couples. The E^{eq}_{redox} for $I^-/I\bullet$ (1.35 V[45]) is much more negative than the top of the valence band of TaON, E_V^s, lying at 2.2 V, and thus we can expect that I^- is efficiently oxidized by holes, in harmony with the experimental result (Figure 4). Note here that the E^{eq}_{redox} for $SCN^-/SCN\bullet$ (1.64 V[45]) and $Br^-/Br\bullet$ (2.00 V[45]) are more negative than E_V^s, though both SCN^- and Br^- are not oxidized by photogenerated holes (Figure 4). This may be explained by taking into account the presence of the large reorganization energies (λ) for small ions in an aqueous solution. In fact, the state density distributions for the occupied levels, estimated from reported λ values[46] for SCN^- and Br^-, have little overlap with the top of the valence band of TaON at which photogenerated holes lie, as shown in Figure 9.

As to the case of the water oxidation, the E^{eq}_{redox} for ($H_2O/\bullet OH$), lying at 2.38 V[45], is more positive than E_V^s (2.2 V) and much more positive than those for SCN^- and Br^-. This result clearly indicates that the electron-transfer type oxidation of H_2O by photogenerated holes is energetically impossible, or in other words, the water photoxidation on TaON cannot be explained by this mechanism. On the other hand, in the mechanism of the nucleophilic attack of

H_2O molecules (Lewis base) to surface trapped holes at surface lattice O atoms (Lewis acid), the reaction rate is not directly governed by the redox potential E^{eq}_{redox} for H_2O/•OH. The reaction rate will rather be governed by the Gibbs energy of formation of intermediate radicals such as [Ta-O• HO-Ta]$_s$ which includes the distortion energy of the surface TaON (or Ta-oxide) lattice. Thus, the above-mentioned contradiction can be regarded as giving strong support to the validity of our previously reported mechanism of the Lewis acid-base mechanism for the water photoxidation on metal oxides or oxynitrides.

Finally, it will be important to consider how methanol or other alcohols are photoxidized on TaON under visible-light irradiation. We mentioned earlier that the addition of methanol to the electrolyte caused no increase in the IPCE (Figure 4), indicating that photogenerated holes at the TaON surface cannot oxidize methanol. On the other hand, the photocatalytic O_2 evolution was completely suppressed by the addition of methanol to an aqueous TaON suspension (Figure 2), indicating that the photoxidation of methanol proceeds predominantly over the water photoxidation at the TaON surface. The discrepancy can be explained to be due to the fact that methanol does not react directly with photogenerated holes but reacts with some surface intermediates of the water photoxidation reaction, such as [Ta–O• HO–Ta]$_s$. This argument also gives strong support to the validity of the above-mentioned Lewis acid-base mechanism for the water photoxidation, because, if the water photoxidation was initiated by a mechanism of direct oxidation of surface Ta-OH by photogenerated holes, more easily oxidized methanol (or adsorbed methanol such as Ta-OCH_3) would certainly be oxidized by the holes.

Conclusions

The present work has confirmed that the photocatalytic O_2 evolution occurs from a TaON suspension in the presence of Fe^{3+}. The in situ MIR-IR experiments have indicated that the TaON surface is oxidized under visible-light irradiation, indicating that the oxygen photoevolution on TaON actually occurs on a thin Ta-oxide overlayer. The in situ MIR-IR experiments have also shown that a certain surface peroxo species, which may be tentatively assigned to adsorbed HOOH, is formed as an intermediate of the O_2 photoevolution reaction. The experiments on the effect of addition of reductants to the electrolyte on the IPCE have shown that photogenerated holes at the TaON surface cannot oxidize reductants such as SCN^-, Br^-, methanol, ethanol, iso-propanol, and acetic acid, though it can oxidize H_2O into O_2. All these results give strong support to the validity of our recently proposed mechanism for the water photoxidation that it is initiated by a nucleophilic attack of a water molecule (Lewis base) on the surface trapped hole (Lewis acid).

References

(1) Fujishima, A. ; Honda, K. *Nature* **1972**, *238*, 37.

(2) Sato, S. White, M. *Chem. Phys. Lett*. **1980**, *72*, 83.

(3) Hoffmann, M. R.; Martin, S. T.; Choi, W.; Bahnemann, D. W. *Chem. Rev*. **1995**, *95*, 69.

(4) Sato, S. *Chem. Phys. Lett*. **1986**, *123*, 126.

(5) Asahi, R.; Morikawa, T.; Ohwaki, T.; Aoki, K.; Taga, Y. *Science* **2001**, *293*, 269.

(6) Lindgren, T.; Mwabora, J. M.; Avendanño, E.; Jonsson, J.; Hoel, A.; Granqvist, C-G.; Lindquist, S-E. *J. Phys. Chem. B* **2003**, *107*, 5709.

(7) Nakamura, R.; Tanaka, T.; Nakato, Y. *J. Phys. Chem*. *B* **2004**, *108*, 10617.

(8) Umebayashi, T.; Yamaki, T.; Itoh, H.; Asai, K. *Appl. Phys. Lett*. **2002**, *81*, 454.

(9) Ohno, T.; Mitsui, T.; Matsumura, M. *Chem. Lett*. **2003**, *32*, 364.

(10) Khan, S. U. M.; Al-Shahry, M.; Ingler, W. B. Jr. *Science* **2002**, *297*, 2243.

(11) Sakthivel, S.; Kisch, H. *Angew. Chem. Int. Ed*. **2003**, *42*, 4908.

(12) Irie, H.; Watanabe, Y.; Hashimoto, K. *Chem. Lett*. **2003**, *32*, 772.

(13) Hitoki, G.; Takata, T.; Kondo, J. N.; Hara, M.; Kobayashi, H.; Domen, K. *Chem. Commun.* **2002**, 1698.

(14) Hara, M.; Chiba, E.; Ishikawa, A.; Takata, T.; Kondo, J. N.; Domen, K. *J. Phys. Chem. B* **2003**, *107*, 13441.

(15) Hara, M.; Hitoki, G.; Takata, T.; Kondo, J. N.; Kobayashi, H.; Domen, K. *Catal. Today* **2003**, *78*, 555.

(16) Chun, W.-J.; Ishikawa, A.; Fujisawa, H.; Takata, T.; Kondo, J. N.; Hara, M.; Kawai, M.; Matsumoto, Y.; Domen, K. *J. Phys. Chem. B* **2003**, *107*, 1798.

(17) Hitoki, G.; Ishikawa, A.; Takata, T.; Kondo, J. N.; Hara, M.; Domen, K. *Chem. Lett.* **2002**, 736.

(18) Ishikawa, A.; Takata, T.; Kondo, J. N.; Hara, M.; Domen, K. *J. Phys. Chem. B* **2004**, *108*, 11049.

(19) Kisumi, T.; Tsujiko, A.; Murakoshi, K., Nakato, Y. *J. Electroanal. Chem*. **2003**, *545*, 99.

(20) Nakamura, R.; Nakato, Y. *J. Am. Chem. Soc*. **2004**, *126*, 1290.

(21) Nakamura, R.; Ohashi, N.; Imanishi, A.; Osawa, T.; Matsumoto, Y.; Koinuma, H.; Nakato, Y. *J. Phys. Chem. B* **2005**, *109*, 1648.

(22) Ito, S.; Takeuchi, T.; Katayama, T.; Sugiyama, M.; Matsuda, M.; Kitamura, T.; Wada, Y.; Yanagida, S. *Chem. Mater*. **2003**, *15*, 2824.

(23) Shiga, A.; Tsujiko, A.; Yae, S.; Nakato, Y. *Bull. Chem. Soc. Jpn*. **1998**, *71*, 2119.

(24) Nakamura, R.; Imanishi, A.; Murakoshi, K.; Nakato, Y. *J. Am. Chem. Soc*. **2003**, *125*,

7443.

(25) Zhang, J.-Y.; Boyd, I. W. *Appl. Surf. Sci*. **2002**, *186,* 40.

(26) Fang, Q.; Zhang, J.-Y.; Wang, Z. M.; Wu, J. X.; O'Sullivan, B. J.; Hurley, P. K.; Leedham, T. L.; Davies, H.; Audier, M. A.; Jimenez, C.; Senateur, J.-P.; Boyd, I. W. *Thin Solid Films* **2003**, *428,* 248.

(27) Boyd, I. W.; Zhang, J.-Y. *Microelectronics Reliability* **2000**, *40*, 649.

(28) Ono, H.; Hosokawa, Y.; Shinoda, K.; Koyanagi, K.; Yamaguchi, H. *Thin Solid Films* **2001**, *381*, 57.

(29) Franchy, R. *Surf. Sci. Rep*. **2000**, *38*, 195.

(30) Bermudez, V. M. *Thin Solid Films* **1999**, *347*, 195.

(31) Ay, F.; Aydinli, A. *Optical Materials* **2004,** *26*, 33.

(32) Scarlete, M.; McCourt, N.; Butler, I. S.; Harrod, J. F.; *Chem. Mater*. **2001**, *13*, 655.

(33) Pandey, R. K.; Patil, L. S.; Bange, J. P.; Patil, D. R.; Mahajan, A. M.; Patil, D. S.; Gautam, D. K. *Optical Materials* **2004,** *25*, 1.

(34) Engdahl, A.; Nelander, B.; Karlström, G. *J. Phys. Chem. A* **2001**, *105,* 8393.

(35) Pettersson, M.; Tuominen, S.; and Räsänen, M. *J. Phys. Chem. A* **1997**, *101,* 1166.

(36) Lin, W.; Frei, H. *J. Am. Chem. Soc*. **2002**, *124*, 9293.

(37) Howe, R. F.; Gräetzel, M.; *J. Phys. Chem*. **1987**, *91*, 3906.

(38) Micic, O. I.; Zhang, Y.; Cromack, K. R.; Trifunac, A. D.; and Thurnauer, M. C. *J. Phys. Chem*. **1993**, *97*, 7277.

(39) Micic, O. I.; Zhang, Y.; Cromack, K. R.; Trifunac, A. D.; Thurnauer, M. C. *J. Phys. Chem*. **1993**, *97*, 13284.

(40) Brookes, I. M.; Muryn, C. A.; and Thornton. G. *Phys. Rev. Lett.* **2001**, *87*, 266103.

(41) Muryn, C. A.; Hardman, P. J.; Crouch, J. J.; Raiker, G. N.; Thornton. G. D.S.L. law, *Surf.*

Sci. **1991**, *215-242*, 747.

(42) Henderson, M. A. *Surf. Sci. Rep*. **2002**, *46*, 1.

(43) Fang, C. M.; Orhan, E.; de Wijs, G. A.; Hintzen, H. T.; de Groot, R. A.; Marchand, R.; Saillard, J.-Y.; de With, G. *J. Mater. Chem.* **2001**, *11*, 1248.

(44) Sato, S. *J. Phys. Chem.* **1987**, *91*, 2895.

(45) Wardman, P. *J. Phys. Chem. Ref. Data* **1989**, *18*, 1637.

(46) Burg, K. V.; Delahay, P. *Chem. Phys. Lett*. **1981**, *78*, 287.

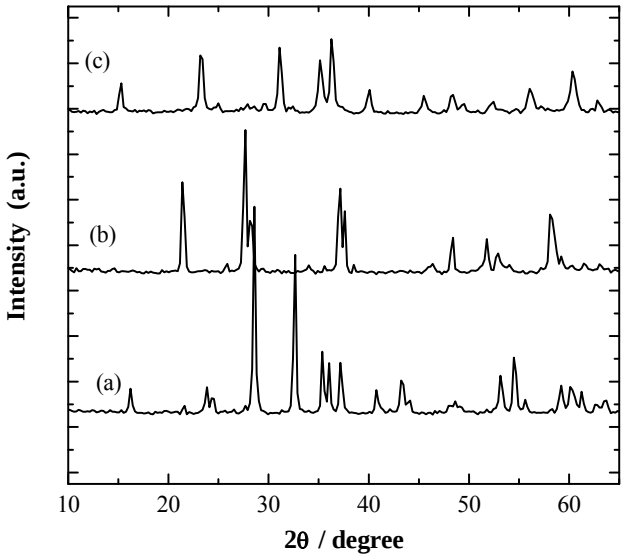

Figure 1. XRD patterns of (a) TaON, (b) Ta_2O_5, and (c) Ta_3N_5 powder.

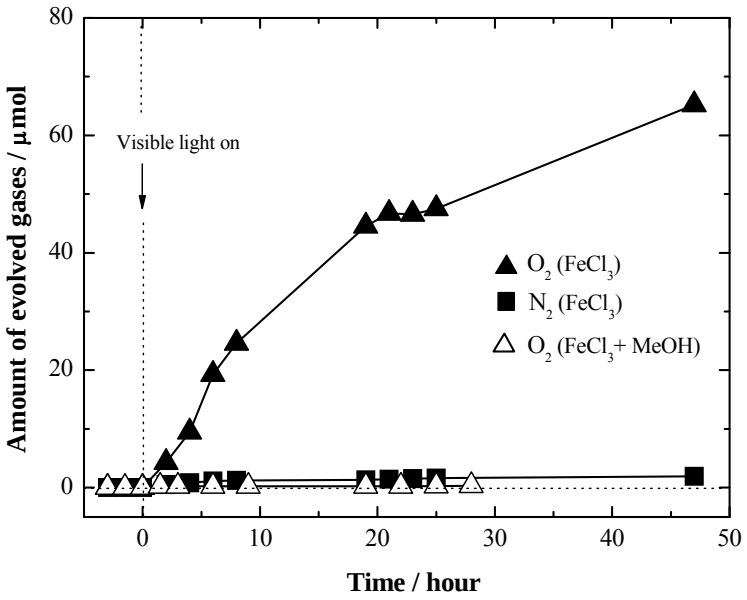

Figure 2. Photocatalytic O_2 and N_2 evolution from an aqueous suspension of TaON powder with 2 mM $FeCl_3$ (pH 2.3) under visible-light ($\lambda \geq 420$ nm) irradiation. The curve marked by open triangles is for the O_2 evolution when methanol (0.5 w%) was added to the above suspension.

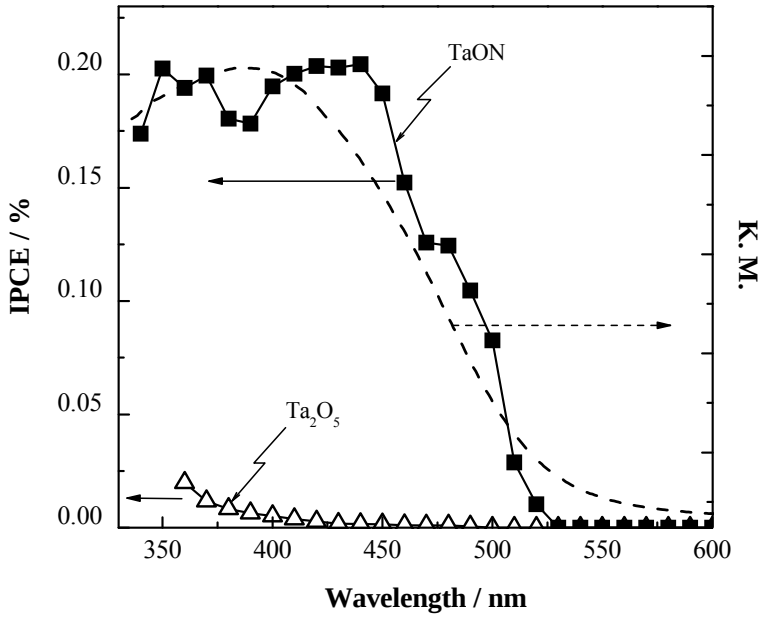

Figure 3. Photocurrent action spectra (IPCE vs. wavelength) for particulate TaON and Ta_2O_5 thin film electrodes, observed in 0.1 M $HClO_4$ at an applied potential of 0.7 V vs. Ag/AgCl. The broken line indicates an observed UV-vis diffuse reflectance spectrum of TaON powder.

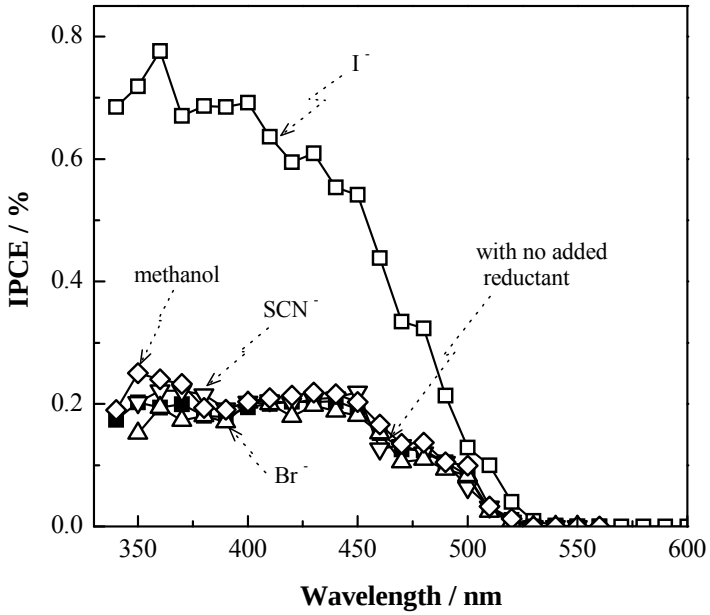

Figure 4. Effect of addition of 6 M MeOH, 0.5 mM I^-, 0.5 mM SCN^-, and 0.5 mM Br^- to the electrolyte on the IPCE vs. λ for a TaON thin film electrode in 0.1 M $HClO_4$. The curve marked by closed squares indicates the IPCE vs. λ in 0.1 M $HClO_4$ with no added reductant. The electrode potential was 0.7 V vs. Ag/AgCl.

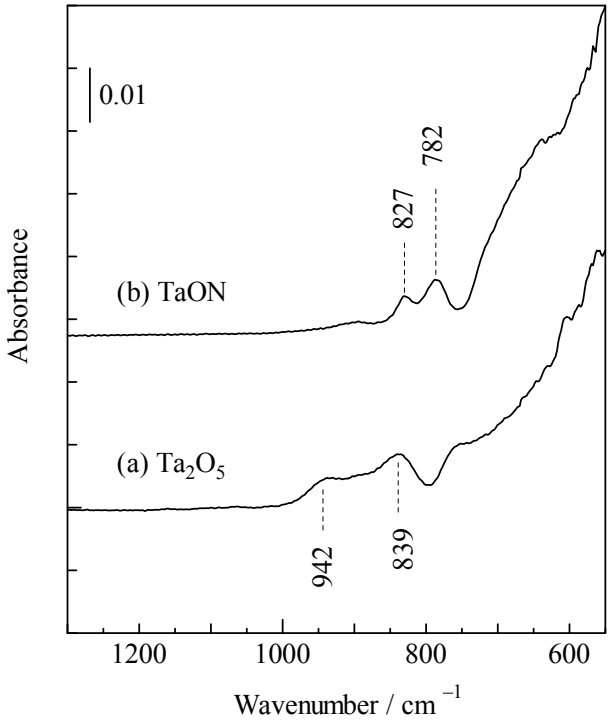

Figure 5. MIR-IR spectra for (a) Ta_2O_5 and (b) TaON particulate films in air.

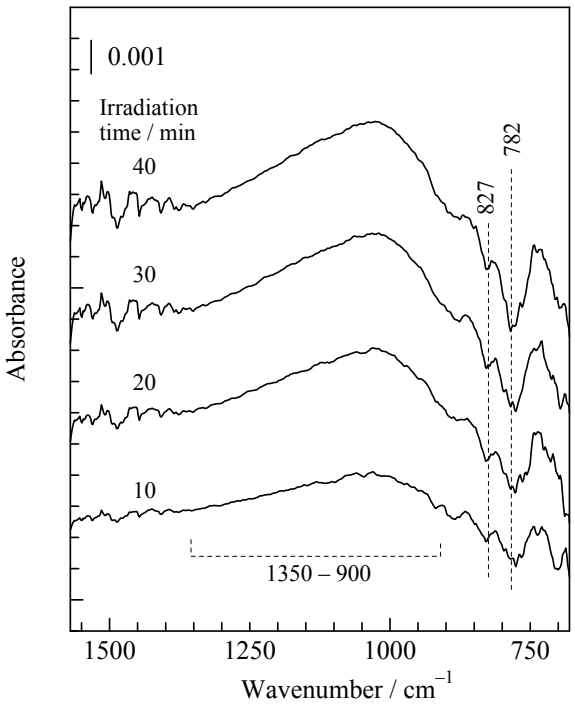

Figure 6. Photoinduced MIR-IR spectra for a TaON particulate film in contact with pure water (pH 7), recorded in 10, 20, 30, and 40 min after the start of visible-light ($\lambda \geq 420$ nm) irradiation. A TaON before irradiation was taken as the reference.

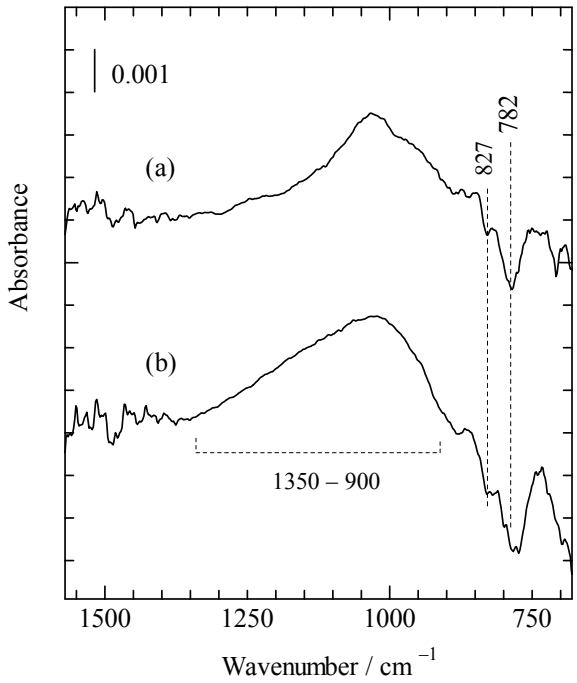

Figure 7. Photoinduced MIR-IR spectra for a TaON film in contact with (a) $H_2{}^{18}O$ and (b) $H_2{}^{16}O$, observed after 20-min visible-light irradiation.

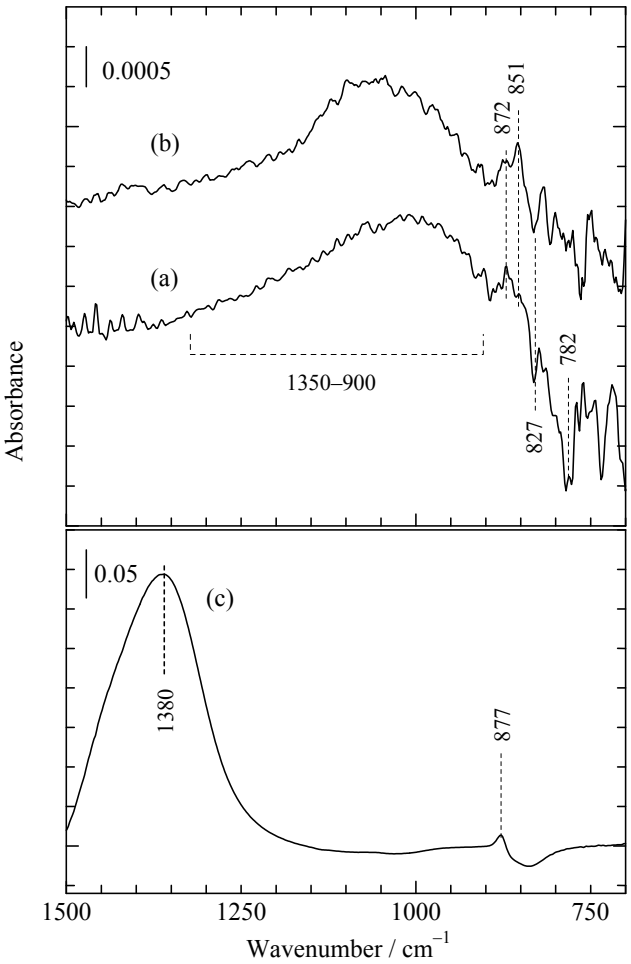

Figure 8. Photoinduced MIR-IR spectra for a TaON film in contact with (a) $H_2{}^{16}O$ and (b) $H_2{}^{18}O$, both containing 10 mM Fe^{3+}, observed after 10-min visible-light irradiation. Spectrum (c) is an MIR-IR spectra for an aqueous solution of 10% HOOH.

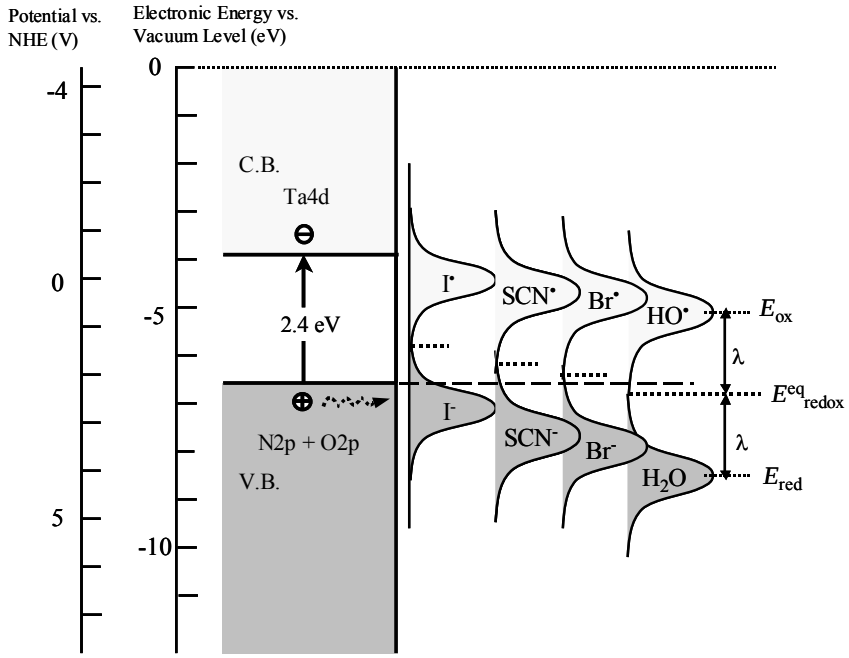

Figure 9. Schematic illustration of the energy bands for TaON at pH 0[16] together with state density distributions for one-electron transfer redox couples estimated from reported reorganization energies (λ)[46]. The minus sign with a circle, electron; the plus sign with a circle, hole; E_{eq}, the equilibrium redox potentials for one-electron-transfer redox couples, reported[45].

Nucleophilic attack mechanism

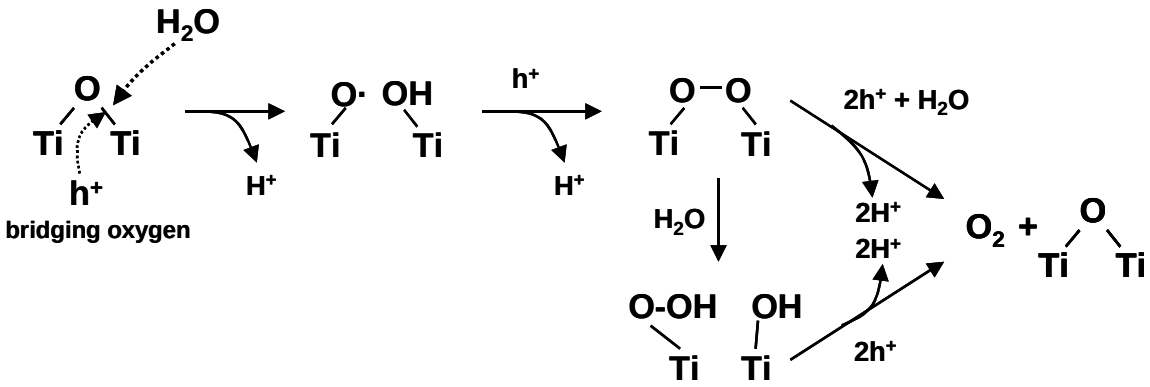

Scheme 1. Reaction Scheme for the Oxygen Photoevolution Reaction on TiO_2 (Rutile) in Contact with an Aqueous Solution of pH of 1 to about 12.[19,20]

General Conclusions

Although the water photoxidation at the surface of TiO_2 or related metal oxides have been studied intensively, the reported mechanisms are rather scattered, and detailed molecular mechanisms have still remained unclear. In the present work, the author has studied the mechanisms of the water photoxidation on TiO_2 electrodes and nanoparticles, with an emphasis placed on the *in situ* direct spectroscopic detection of surface primary intermediates as well as the preparation of atomically well-defined surfaces. It has been concluded by in situ FTIR and PL measurements that the water oxidation is not initiated by the conventional mechanism of an electron-transfer type reaction, but by the new mechanism of a Lewis-acid-base type reaction. This conclusion has also been confirmed by the study on the water photoxidation on visible-light responsive photocatalysts, N-doped TiO_2 and TaON.

As to the *in situ* spectroscopic studies on photocatalytic reaction intermediates, the author has developed a multiple internal reflection infrared (MIR-IR) absorption spectroscopy (***Chapter 1***), and succeed in detecting directly surface peroxo species, Ti-O-O-Ti and Ti-O-OH, as primary intermediates of the water photoxidation at a particulate TiO_2 film (***Chapter 2***). Detailed investigations of the effect of solution pH, presence of an electron acceptor and donor, isotopic exchange of water ($H_2{}^{16}O \rightarrow H_2{}^{18}O$) on the MIR-IR spectra have reveled that the water photoxidation is not initiated by the oxidation of a surface OH group by a photogenerated hole (i.e. electron-transfer type oxidation), but by a nucleophilic attack of a H_2O molecule to a surface-trapped hole at a surface lattice O site, accompanied by bond breaking (i.e. Lewis acid-base type oxidation).

This conclusion has been confirmed by *in situ* PL measurements for atomically well-defined n-TiO_2(rutile) single crystal electrodes (***Chapter 3***). The author has succeeded in

preparing the atomically smooth and stable (100) and (110) n-TiO_2(rutile) single crystal surfaces by a method of immersion of commercially available single crystal wafers in 20% HF, followed by annealing at 600°C in air, and reveled that the PL band peaked at 840 nm from the (100) face is much higher in intensity than that from the (110) face. The crystal-face dependence of the PL band is in good agreement with our previous finding that the intense PL band appeared from the (100) faces exposed in the photoetched n-TiO_2(rutile) electrodes, and confirms that the photoxidation mechanism on the (100) face is different from that on the (110) face.

The key of this work is the finding that the water photoxidation cannot proceed by the electron-transfer type reaction, but by the Lewis acid-base type reaction. This implies that the energetics and kinetics proposed thus far for the water oxidation should be reconsidered, because the probability of occurrence for the water oxidation by the Lewis acid-base type reaction mechanism has no direct relation with the redox potential such as E^{eq}_{redox} for H_2O/•OH, contrary to the electron-transfer-type oxidation mechanism. This has actually been confirmed experimentally by the study on the water photoxidation on visible-light responsive photocatalysts, such as N-doped TiO_2 and TaON (***Chapter 4 and 5***). Thus, the mechanism obtained in this work will be important to understand the photocatalytic activity of TiO_2 and other materials and also to search for new active and stable visible-light responsive photocatalysts.

List of Publications:

(1) *In Situ FTIR Studies of Primary Intermediates of Photocatalytic Reactions on Nanocrystalline TiO_2 Films in Contact with Aqueous Solutions*

Ryuhei Nakamura, Akihito Imanishi, Kei Murakoshi and Yoshihiro Nakato*

Journal of American Chemical Society (Article), **2003**, 125, 7443-7450.

(2) *Primary Intermediates of Oxygen Photoevolution Reaction on TiO_2 (Rutile) Particles, Revealed by in Situ FTIR Absorption and Photoluminescence Measurements*

Ryuhei Nakamura, and Yoshihiro Nakato*

Journal of American Chemical Society (Article), **2004**, 126, 1290-1298.

(3) *Mechanism for Visible Light Responses in Anodic Photocurrents at N-doped TiO_2 Film Electrodes*

Ryuhei Nakamura, Tanaka Tomoaki, and Yoshihiro Nakato*

The Journal of Physical Chemistry B (Letter), **2004**, 106, 5893-5896.

(4) *Crystal-Face Dependences of Surface Band Edges and Hole Reactivity, Revealed by Preparation of Essentially Atomically-Smooth and Stable (110) and (100) n-TiO_2 (Rutile) Surfaces*

Ryuhei Nakamura, Naomichi Ohashi, Akihito Imanishi, Takeo Osawa, Yuji Matsumoto, Hideomi Koinuma and Yoshihiro Nakato*

The Journal of Physical Chemistry B* (Letter),** 2005, 109, 1648-1651.***

(5) *Oxygen Photoevolution on Tantalum Oxynitride Photocatalysts under Visible-light*

Irradiation: How Does Water Photoxidation Proceed on an Oxynitride Surface?

Ryuhei Nakamura, Tanaka Tomoaki, and Yoshihiro Nakato*

The Journal of Physical Chemistry B (Article), **2005**, *in press.*

The papers not included in the present thesis:

(6) *Preparation of Platinum Nanoparticles in Ethyl Acetate in the Presence of Poly (amidoamine) dendrimers with a Methyl Ester Terminal Group*

Kunio Esumi*, Ryuhei Nakamura, Akihiro Suzuki, and Kanjiro Torigoe

Langmuir (Article), **2000**, 16, 7842-7846.

(7) *In-Situ Observation of the Photoenhanced Adsorption of Water on TiO_2 Films by Surface-Enhanced IR Absorption Spectroscopy*

Ryuhei Nakamura, Kazuhiro Ueda, Shinri Sato*

Langmuir (Communication), **2001**, 17, 2298-2300.

(8) *Study of Photocatalytic Reactions over Semiconductor Surfaces by Surface-Enhanced IR Absorption Spectroscopy*

Shinri Sato* and Ryuhei Nakamura

Photochemistry (Review), **2002**, 33, 68-74.

(9) *In-situ IR Observation of Surface Species during the Photocatalytic Decomposition of Acetic Acid over TiO_2 film*

Shinri Sato*, Kazuhiro Ueda, Yasuhiro Kawasaki, and Ryuhei Nakamura

The Journal of Physical Chemistry B (Article), **2002**, 106, 9054-9058.

(10) *Surface-Enhanced IR Absorption of Pt and Its Application to In-Situ Analysis of Surface Species*

Ryuhei Nakamura and Shinri Sato*

Langmuir (Article), **2002**, 18, 4433-4436.

(11) *Oxygen Species Active for Photooxidation of n-Decane over TiO_2 Surfaces*

Ryuhei Nakamura and Shinri Sato*

The Journal of Physical Chemistry B (Article), **2002**, 106, 5893-5896.

(12) *A Nano-Modified Si/TiO_2 Composite Electrode for Efficient Solar Water Splitting*

Susumu Takabayashi, Ryuhei Nakamura, and Yoshihiro Nakato*

Journal of Photochemistry and Photobiology A: Chemistry (Article), **2004**, 166 107–113.

(13) *Visible Light Sensitization of TiO_2 Photocatalysts by Wet-method N Doping*

Shinri Sato*, Ryuhei Nakamura, and Shinji Abe

Applied Catalysis A (Article), **2005**, *in press*.

(14) *Surface Asymmetrization of Metal-Oxide Photocatalysts for Efficient Water Splitting*

Ryuhei Nakamura, Tomoaki Okamura, Yuki Ura, Akihito Imanishi, Yoshihiro Nakato* submitted to *Science.*

(15) *Ordered Nano-Groove Arrays on TiO_2 Formed via Photoetching Induced Symmetry Breaking*

Shuji Nakanishi, Satoshi Fukushima, Takatoshi Tanaka, Ryuhei Nakamura, Tomoyuki Nagai, Kazuhiro Fukami, and Yoshihiro Nakato* submitted to *Science.*

Patents

(16) 2004-065299

(17) 2004-359355

Acknowledgements

The author would like to express his sincerest gratitude to Professor Yoshihiro Nakato for his continuous guidance, discussions, and suggestions through this work, and for providing him with many opportunities to have various experiences. The author grateful to Professor Kei Murakoshi (Hokkaido University) for his invaluable discussions, assistance and understanding. The author also would like to thank Associate Professor Akihiro Imanishi and Dr. Shuji Nakanishi for his continuous encouragements.

The author is extremely indebted to Associate Professor Shinri Sato (Hokkaido University) for his guidance toward his understanding of photocatalysis and in situ FTIR spectroscopy. His guidance and discussions are greatly appreciated. The contribution of Dr. Liu Haimei, Messrs Yuki Ura, Tomoaki Tanaka, Naomichi Ohashi, and Tomoaki Okamura are greatly acknowledged for their cooperation relating his dissertation. The author also would like to thank to Messrs Ken-ichi Okazaki and Susumu Takabayashi for their continuous encouragements.

Furthermore, the author wishes to thank Assistant Noriko Wada and all the members of Prof. Nakato's laboratory..

Finally, the author wish to thank his parents, and his wife for their support and encouragements for his Ph.D. dissertation.

Ryuhei Nakamura

Osaka, January 2005